Effect of global climate change projections on fatigue lifetime of permanently moored floating offshore structures

Zou, Tao

DOI
10.4233/uuid:5da2a711-c5ef-4d0f-8f0d-6fd109ec1d34

Publication date
2018

Document Version
Final published version

Citation (APA)
Zou, T. (2018). *Effect of global climate change projections on fatigue lifetime of permanently moored floating offshore structures.* [Dissertation (TU Delft), Delft University of Technology].
https://doi.org/10.4233/uuid:5da2a711-c5ef-4d0f-8f0d-6fd109ec1d34

Important note
To cite this publication, please use the final published version (if applicable).
Please check the document version above.

Effect of global climate change projections on fatigue lifetime of permanently moored floating offshore structures

Tao ZOU

Effect of global climate change projections on fatigue lifetime of permanently moored floating offshore structures

Dissertation

for the purpose of obtaining the degree of doctor
at Delft University of Technology
by the authority of the Rector Magnificus, prof.dr.ir. T.H.J.J. van der Hagen
chair of the Board for Doctorates
to be defended publicly on
Friday, 7 September 2018 at 12:30 o'clock

by

Tao ZOU

Master of Engineering in Harbor, Coastal and Offshore Engineering, Ocean University of China, China

Born in Fushun, Liaoning, China

This dissertation has been approved by the promotor.

Composition of the doctoral committee:

Rector Magnificus,	chairperson
Prof.dr.ir. M.L. Kaminski	Delft University of Technology, promotor

Independent members:

Prof.dr. H. Li	Ocean University of China, China
Prof.dr. F. Dias	University College Dublin, Ireland
Dr. E. Bitner-Gregersen	DNV GL, Norway
Dr. K. Ewans	Mezocean Research, New Zealand
Prof.dr.ir. M. Veljkovic	Delft University of Technology
Prof.dr.ir. A.P. van 't Veer	Delft University of Technology
Prof.dr.ir. C. van Rhee	Delft University of Technology (reserve)

This research was financially supported by:

TU Delft Delft University of Technology

国家留学基金管理委员会 CHINA SCHOLARSHIP COUNCIL

ISBN: 978-94-9301-431-2

Printed by: Gildeprint, Enschede

An electronic copy of this dissertation is available at http://repository.tudelft.nl/

To my family

Summary

The design of floating offshore structures requires long-term wave data to estimate their fatigue lifetimes, because waves loadings are considered as the main source of fatigue damage. These sea-state data are mainly obtained through past measurements and assumed to be representative of the wave climate which the offshore structure is expected to encounter.

This assumption however includes a lot of uncertainties induced by the climate change. The service lifetime of floating offshore structures is usually more than 20 years. The climate change may significantly affect the properties of sea states. If the wave climate is changed, the fatigue assessment at design stage may overestimate or underestimate the cumulative fatigue damage during service life. Therefore, the effect of climate change on the long-term wave loading and consequently on the fatigue assessment should be considered.

Over the last decades, the importance of climate change has been increasingly discussed, and the effect of climate change has become an increasing subject for debate by industry and academia. But the research on this field is still at the initial stage and requires further improvement. The global or regional trends of wind data and wave data have already been evaluated by different researchers. Most of these trends are qualitative, and the rest are the decadal or even centurial trends based on linear extrapolation. This kind of trends is not applicable to fatigue assessment. A more detailed and reliable trend should be projected in order to identify the effect of climate change on fatigue life of offshore structures. In short, there are still many issues to address as follows:

- Past climate trends are not necessarily indicative of future climate trends.
- The physics and regional characteristics of climate change are not reflected or modelled explicitly in fatigue assessment.
- Moderate sea states contribute most to fatigue failures.
- The trend of sea states should not necessarily be linear or quadratic.

The above-mentioned considerations formulate the following main research question:

How can the fatigue design of floating offshore structures account for the future effects of climate change?

Before addressing the main question, there are three key questions which have to be considered.

1. Why does the climate change affect wave conditions and consequently affect fatigue damage of offshore floating structures?

2. How can these physical processes in the climate system be numerically simulated?

3. To what extent the climate change affects wave conditions and fatigue damage?

In this thesis, the climate scenario "Representative Concentration Pathways" was selected to describe the future climate conditions with an increasing radiative forcing level. Then, the future wave conditions in the North Sea and in the Sable field (off the southern coast of South Africa) were simulated by coupling climate models to wave models. At last, the annual fatigue damage was calculated for an Floating Production, Storage and Offloading unit.

It is concluded that the effect of climate change on sea states and fatigue damage is region-dependent. In the Sable field, both the significant wave height and annual fatigue damage are increasing over time, but the effect of human activities on them is not pronounced. In the North Sea, however, the sea states are becoming calmer with lower significant wave height and fatigue damage. The decreasing trends of wave height and fatigue damage are so significant that the effect of human activities is clearly detected. In addition, the trend of wave height is not representative of the trend of annual fatigue damage. The changes of other wave characteristics (such as wave period and wave direction) are also important to fatigue damage.

Contents

Summary ..... **vii**

INTRODUCTION **1**

1.1 Climate change 2

1.2 Historical overview of research on offshore engineering 4

1.2.1 The effect of climate change on sea states 4

1.2.2 The effect of climate change on ultimate strength of offshore structures 5

1.3 Problem statement 6

1.4 Research questions 8

1.5 Thesis objective and methodology 9

1.6 Thesis structure 9

References 11

CLIMATE CHANGE AND WAVE INDUCED FATIGUE DAMAGE **15**

2.1 Introduction on the Earth's climate system 16

2.2 Mechanics of climate change 18

2.3 Wave scatter diagrams and time series of sea states 19

2.4 Floating Production, Storage and Offloading (FPSO) units 22

2.5 Wave-induced fatigue damage 23

2.6 Relations between climate change and fatigue damage 25

2.7 Conclusions 25

References 26

THE PROJECTION OF CLIMATE CHANGE IMPACT **29**

3.1 Climate scenarios 30

3.2 Climate models 32

3.3 Wave models 34

3.4 The comparison of climate models and validation of wave models 39

3.5 Projection of climate change impact on wave conditions 44

3.5.1 Offshore South Africa 45

3.5.2 North Sea 46

3.6 Projection of climate change impact on fatigue damage 48

3.6.1 Offshore South Africa 51

3.6.2 North Sea 53

3.7 Conclusions 56
References 56
DETECTIONS OF NATURAL VARIABILITY AND HUMAN INDUCED CLIMATE CHANGE 61
4.1 Natural variability of climate system 62
4.2 Human-induced climate change 63
4.3 Control simulations and natural variability 65
4.3.1 6 hours sampling time increment 65
4.3.2 One year sampling time increment 68
4.4 Detection of human-induced climate change 70
4.4.1 Detection of human-induced climate change on significant wave height 70
4.4.2 Detection of human-induced climate change on cubic weighed wave height 77
4.4.3 Detection of human-induced climate change on fatigue damage 80
4.4.4 Comparison between the trends of wave height and fatigue damage 82
4.5 Conclusions 85
References 86
SENSITIVITY ANALYSIS FOR OFFSHORE FLOATING STRUCTURES 89
5.1 Uncertainty and sensitivity analysis 90
5.2 Category of model input parameters 91
5.3 Sensitivity analysis 91
5.3.1 Climate models 91
5.3.2 Wave model parameters 95
5.3.3 Wave properties 101
5.4 Conclusions 106
References 106
CONCLUSIONS AND RECOMMENDATIONS 109
6.1 Overview of methodology 110
6.2 Main conclusions 110
6.3 Validations and development 112
6.4 Recommendation for future work 113
References 113
Acknowledgements 115
Curriculum Vitae 117

1

INTRODUCTION

1.1 Climate change

Climate change is one of the greatest threats to our society. A great deal of evidence has been found to support its existence. For instance, according to the Intergovernmental Panel on Climate Change (IPCC) report [1], many indicators of climate change have been observed in the past decades. These indicators include changes in surface temperature, atmospheric water vapor, precipitation, glaciers, sea level, ocean and land ice. The most direct impact of climate change is global warming. The global surface temperature has been rising since the late nineteenth century, which has consequently affected other climate indicators. What makes things worse is that the temperature has been rising at an increasing rate during the past decades. The rate of global warming over the past 50 years (0.13°C per decade) is approximately twice the rate it was over the last century [2].

Global warming and its associated impacts are also affecting human activities significantly. For example, sea level rise is a central part of the Earth's response to global warming. As the temperature increases, the largest amount of extra heat in the climate system is stored in the ocean, and the melting of land ice (glaciers and ice sheets) becomes the primary contributor to the change in sea level. Global sea level has been rising at an average rate of 1.7 mm/year since 1901 (Fig.1.1a) [3], and the rate of sea level rise has also sped up in recent years. A rising sea level will significantly affect human society, because a large fraction of the world's population and its primary farmlands are located in coastal areas. It is an extremely serious threat to those low-lying countries or areas, such as the Netherlands (Fig.1.1b). About 20% of the Dutch land is below the sea level, and most Dutch people live less than one meter above it. Fortunately, the Netherlands has been actually dealing with this sea level issue since the 1950s through the Delta program. In this program, a series of dams and barriers have been constructed to resist storms and rising water levels (Fig.1.2). Unfortunately, the effect of climate change on human activities goes still further beyond these phenomena.

As the primary emitter of greenhouse gases (GHGs), the fossil fuel industry is often to blame for the adverse environmental effects. In fact, the industry is both a contributor to and a sufferer of climate change. According to climate observations and modelling, no clear trend has been detected in the frequency of tropical storms. But the frequency of tense tropical storms is showing an increasing trend [4, 5]. The increase of tense storms has caused safety concerns in nearshore industrial infrastructures, such as nuclear power plants. Most of these plants are located nearshore, because the operation of reactors requires vast amounts of cool water. Many other kinds of factories have similar needs. Due to the high cost of construction, the design of industrial structures should, in the future, take into account the effect of climate change. In addition, offshore industry is especially sensitive to climate change, because offshore structures are directly subjected to harsher environmental loadings. I will discuss the effect of climate change on offshore engineering in the next section.

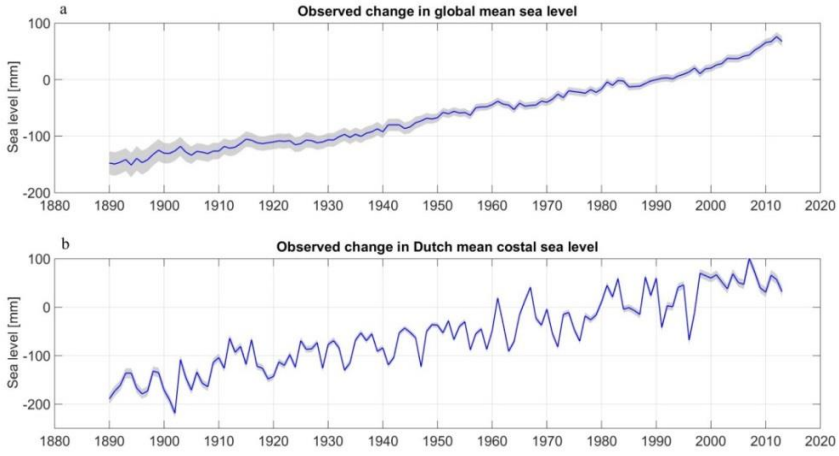

Figure 1.1: Observed change in sea level: (a) the global sea level from 1890 to 2013 is reconstructed from coastal and island tide gauge data. The mean sea level is calculated relative to the level of 1990. (b) the Dutch sea level is the mean value from six observing stations along the Dutch coast. It is calculated relative to the reference level of Amsterdam Ordnance Datum (Normaal Amsterdams Peil, NAP).

Figure 1.2: Maeslantkering. Maeslant barrier is constructed as a part of the Delta program. It is designed to resist against once-in-10,000 years storms. From "Wikimedia Commons", by Eszter Simonfi, 2010 (https://commons.wikimedia.org/wiki/File:Maeslantkering.jpg). Licensed under CC BY-SA 3.0.

1.2 Historical overview of research on offshore engineering

In offshore engineering, offshore structures are designed and constructed for exploration and production of oil and natural gas in a marine environment. These include fixed platforms and floating structures (Fig.1.3). Offshore engineering started in the late 1800s. In the last century, hundreds of offshore platforms were constructed in shallow waters, but the focus of offshore industry now has moved from shallow waters into deep seas. Fixed platforms are not recommended for deep oceans, because their cost increases exponentially with water depth. Instead, floating structures are widely applied to exploit natural resources in the deep oceans. In such situations, floating structures encounter harsh environmental loads, such as wind, waves, and currents. Among them, waves are considered the dominant loading, because they usually contribute most to structural damage [6]. Ocean waves are superposition of many wave components with different amplitudes, frequencies, directions and phases. The wave spectrum is used to describe the distribution of wave energy over different frequencies on the sea surface. In offshore engineering, wave conditions are represented by sea states. These sea states are specified by one or more wave spectra with given wave height, wave period, mean propagation direction, and directional spreading factor. Since the lifecycle of offshore structures consists of design, manufacture, operation (service), and demolition stages, designers try to ensure that the structural strength of their creations can resist all wave conditions which they will encounter in the transportation, installation and operation stages. Most ocean waves are generated by wind, and wind fields are originally caused by the uneven distribution of global solar radiation. With the emission of GHGs, the distribution of global solar radiation is altered, which contributes to the climate change. Therefore, it is necessary to evaluate the impact of climate change on wind fields and subsequently on wave conditions in the design stage of offshore structures.

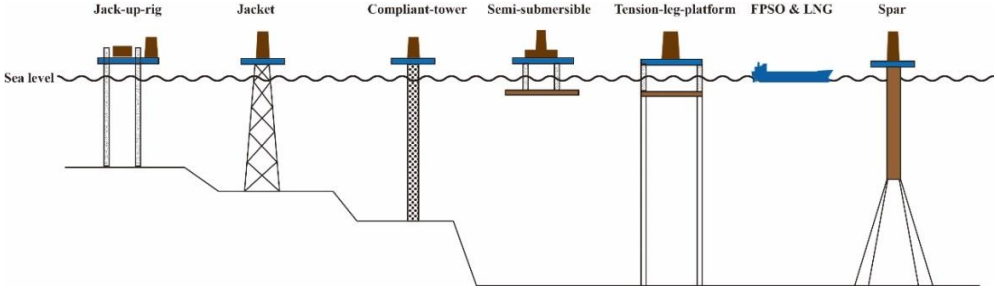

Figure 1.3: Different offshore structures

1.2.1 The effect of climate change on sea states

Many studies on the change of wind and wave conditions due to the climate change focus on wave height and wind speed [7-26]. There are basically three ways to evaluate the trend of sea states. The first approach is to fit a linear or quadratic trend to long-term observations, or hindcasting, over a small or large spatial scale [27-29]. The reliability of the trend is highly dependent on the quality of the observed data. Wave conditions are measured by voluntary observing ships (VOSs), or by instruments such as buoy, radar and satellite. Buoys are considered the most reliable instrument for measuring sea states. However, most long-term buoy data are only available in sea areas around Europe, the United States, and other developed countries [9]. The number of buoys over the globe is still limited. In addition, buoys

can only measure one spot, rather than the entire sea area. They are hence more useful for validating the sea states measured or simulated by other approaches. Altimeters in satellites, for instance, can cover large or even global scales. According to 23 years of satellite measurements (1985-2008), the global mean wind speed has been increasing, while the mean wave height did not show any significant trend. For extreme conditions with 99% percentile, however, there is a clear trend of increasing wave height at high latitudes [29]. The disadvantage of satellite measurements is that they cannot provide all the necessary information about sea states. A hindcast is required to fill in the missing information, and a validation is also required to improve its reliability.

The second approach employs statistics. For example, a joint distribution $f(H, T)$ is normally constructed to describe the correlation between wave height H and wave period T [27]. Then, a three-parameter Weibull distribution with the scale, shape and location parameters is often recommended to represent the marginal distribution of wave height, and the conditional distribution of wave period is defined as log-normal. The long-term linear or quadratic trend of wave height is considered by modifying the location and scale parameters in the Weibull distribution [30]. This trend is estimated based on long-term observations or hindcasting over a small or large spatial scale. The reliability of this approach is, however, highly dependent on the quality of environmental data which are used to fit the parameters. The rate of climate change in the future is mainly estimated based on the past measurements, disregarding the change of climate trends over time.

The third approach to analyzing the trends of sea states is numerical wave modelling. Nowadays, numerical wave models are in its third generation, such as ocean wave model (WAM) [31], simulating waves nearshore model (SWAN) [32], and WaveWatch-III model [33]. These models are all driven by the data of wind forces, and can numerically simulate wind-wave interactions, nonlinear wave-wave interactions, and energy dissipation [34]. Wave models are usually coupled to global climate models (GCMs), as GCMs can provide the time series of wind field data over a large spatial scale. The future effect of climate change on global or regional sea states is projected based on climate scenarios [7, 16, 20, 35-39]. These scenarios are defined as plausible descriptions of a possible future climate condition of the world, including GHG concentrations and global solar radiation. The projection of future climate is not a prediction or forecast. Instead, each climate scenario corresponds to one future possibility, depending on human activities and natural variabilities. Further details of climate scenarios and climate projection are discussed in Chapter 3. There is still no sufficient evidence to show which climate model should be recommended to simulate the sea states in the deep ocean, but WaveWatch-III is becoming more and more widely-used in projecting the wave conditions in the recent years [20, 23-26, 40].

1.2.2 The effect of climate change on ultimate strength of offshore structures

After identifying the effect of climate change on the sea states, it would be of great interest to analyze its effect on ships and offshore structures. One primary failure mode of offshore structures is due to insufficient ultimate strength, a term that refers to the structure maximum resistance against extreme loading. In these cases, such extreme loading conditions usually correspond to extreme sea states. A great number of studies, therefore, focus on the effect of climate change on extreme sea states [41-45], and research on ultimate strength is basically based on the conclusions of these studies. Since this kind of ultimate strength research does

not aim to study the specific mechanics of structural response, more attention has so far been paid to the change of sea states [27, 41, 42, 44]. Offshore structures have several key spots where are more sensitive to external loadings; the stress or damage on the other spots is less significant. Therefore, there is no need to conduct a comprehensive structural analysis of the whole offshore structure to detect the effect of climate change on structures. Instead, a simplified structural analysis of one key spot or small area is sufficient for scientific purposes.

In ultimate strength analysis, the structural response to extreme sea states is usually calculated by linear transfer functions [37, 41, 42]. By considering a linear or quadratic trend of climate change impact, the modified joint distribution of wave height and wave period is used to calculate the extreme sea states within a certain temporal interval (*e.g.,* 100 years). The conclusions indicate that the change of wave load is one of the most important environmental factors in ultimate strength analysis, and that a higher wave height would result in a higher probability of structural failures [41].

1.3 Problem statement

The ongoing research on the effect of climate change on floating offshore structures is at a preliminary stage. Despite the important insight, there are still a number of outstanding major issues to be addressed, as discussed below.

- **Past climate trends are not necessarily indicative of future climate trends.**

  As discussed in section 1.2.1, statistics are widely used to estimate the trend of wave conditions. Both statistical theories are based on long-term observations (or hindcasts) and empirical assumptions. Past climate trends are assumed to be meaningful representations of future climate trends. With the emission of GHGs, however, the rate of climate change is also growing [5]. In addition, sea states do not show exact linear or quadratic trends in reality. Instead, they fluctuate over time due to natural variability, as shown in Fig.1.4.

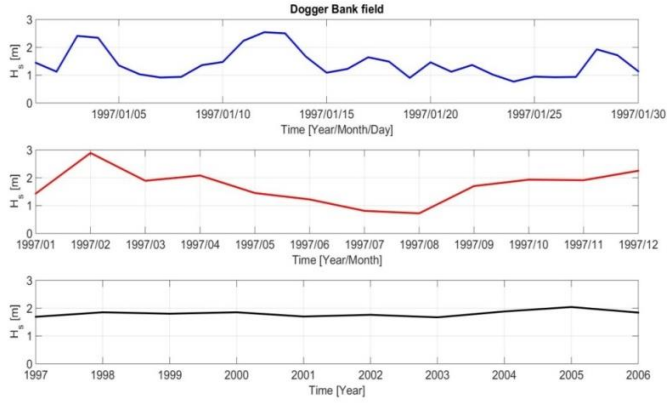

Figure 1.4: Averaged significant wave height (H_s) measured in Dogger Bank field (55.3°N, 2.5°E). The durations of the averages in the subplots are daily, monthly and yearly.

- **The physics and regional characteristics of climate change are not reflected or modelled explicitly.**

  Climate change is a complex phenomenon. Its effect on the sea states involves changes in solar radiation, atmospheric circulation, wave generation, wave propagation and geographic characteristics. These physical processes can hardly be properly considered in the statistical approach. Some joint distributions have been developed to account for the impact of GHG emissions or the physical limitations of waves [43, 46], but they cannot cover all the aspects of the physical processes involved in climate change.

With the introduction of higher-tensile steels, offshore structures have improved their capacity for resisting extreme wave conditions. In the meantime, however, fatigue cracks have emerged as another primary mode of structural failure. When offshore floating structures are operating in seas, wave-induced stresses are considered as the main source of fatigue damage [47]. The varying stresses on structural members and joints initiate fatigue cracks, and these cracks may subsequently grow into the thickness, eventually causing a fatigue failure. It is challenging to project the future effect of climate change on fatigue damage for the following reasons.

- **Moderate sea states contribute most to fatigue failures.**

  Fatigue damage is a long-term cumulative process. Unlike structural failures due to insufficient ultimate strength, fatigue failures usually occur due to moderate wave conditions, because the occurrence of moderate wave conditions is much higher than that of extreme conditions, as shown in Fig.1.5. For a structure, the fatigue design should ensure that its fatigue strength can resist these wave conditions in the operation stage. The lifecycle of an offshore structure may be over 40 years in time. It is, hence, necessary to project the effect of climate change on all short-term sea states in the operation stage. The fatigue design may otherwise overestimate or underestimate the fatigue damage.

- **The trend of sea states should not necessarily be linear or quadratic.**

  The rate of climate change varies year by year. Since all the short-term sea states may contribute to the cumulative fatigue damage, it is necessary to identify the specific effect of climate change on each short-term sea state instead of the average effect. The commonly-used assumption of linear or quadratic trend is not proper here, as it may lead to miscalculations of fatigue damage.

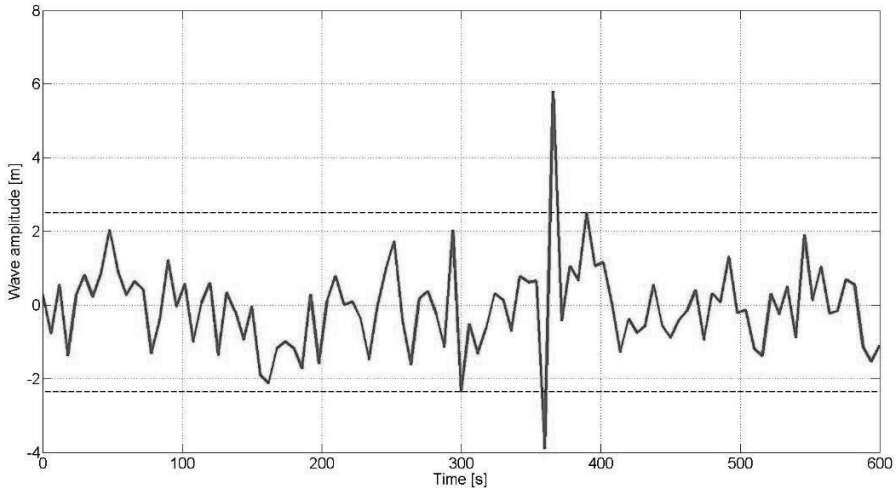

Figure 1.5: Extreme and moderate wave conditions

1.4 Research questions

The cost of offshore structures for design and construction is generally very high. Owners are therefore extremely motivated to maximize the lifetime of their structures. The service life of offshore structures can reach 30 years or even longer. During the operation, offshore structures will inevitably suffer from the effect of climate change. With this regard, it is important to consider the effect of climate change during the design stage. Designers need to "predict" or project all the relevant sea states that the offshore structures may encounter in their operation stage, because all these sea states may contribute to fatigue cracks. As discussed in section 1.3, there are still many questions to answer in order to project the future effect of climate change on sea states and structures. This dissertation therefore aims to answer the following main research question:

How can the fatigue design of offshore floating structures account for the future effects of climate change?

To address this main question, the following three key sub-questions are to be discussed.

1. **Why does the climate change affect wave conditions and consequently affect fatigue damage of offshore floating structures?**

   Before projecting the future effect of climate change, we have to explain the physical process by which wave conditions are affected by the climate change. Then, we need to introduce the wave-induced fatigue damage of floating offshore structures and its relation with the climate change. These explanations and introductions compose the theoretical framework for this thesis, and provide the rationale to investigate the main research question.

2. **How can these physical processes in the climate system be numerically simulated?**

   The relevant physical processes include the atmospheric circulation, the interaction between wind field and water surface, and the wave spectral evolution. These processes, however, require a huge amount of computation to simulate. Fortunately, with the recent developments in computing technologies, computing power has exponentially improved. Many climate and ocean wave models are presented to numerically simulate physical processes in the climate system, and thus to project the effect of climate change on wave conditions and fatigue damage.

3. **To what extent the climate change affects wave conditions and fatigue damage?**

   Even though wave conditions and fatigue damage are affected by climate change, the extent of this impact will determine how much attention people pay to it. In addition, climate change is not entirely human-induced; natural variability is also a cause. It is therefore crucial to understand to what extent the effect of climate change is attributable to human activities.

In the following chapters, all these key questions are discussed. The conclusions can help designers account for the effect of climate change in the fatigue design of offshore structures

1.5 Thesis objective and methodology

The main objective of this study is to present a methodology to project the effect of climate change on future fatigue damage to offshore floating structures. This methodology is outlined in Fig.1.6. There are basically three steps in the methodology. In the first step, designers have to select the proper climate scenario to represent the future climate conditions including greenhouse gas emission and solar radiation level. Then, the non-linear circulation of the global climate system including the atmospheric circulation is simulated by the climate models based on the climate scenario. In the second step, wave models are used to simulate the wave conditions in the sea area where the floating offshore structure is designed to operate. The driving force of wave models is the surface wind field which can be obtained from the simulation of climate models. In the third step, the future fatigue damage of floating offshore structures is calculated based on the time series of these wave conditions.

In Chapter 3, this methodology will be discussed in more detail and demonstrated via case studies. Its detailed procedures will be concluded in Chapter 6

1.6 Thesis structure

The thesis structure is outlined in Fig.1.7. It consists of four main parts represented by Chapters 2 to 5. Below is a short introduction to each chapter.

Chapter 2 explains the composition of climate system and the mechanics of climate change, linking the impact of the latter to fatigue damage. A typical offshore floating structure, the Floating Production Storage and Offloading (FPSO) unit, is the target structure for fatigue.

calculations. Finally, the physics of wave-induced fatigue damage to FPSOs is introduced. This chapter aims to answer the first key question: "How does climate change affect wave conditions, which in turn affect fatigue damage to offshore structures?"

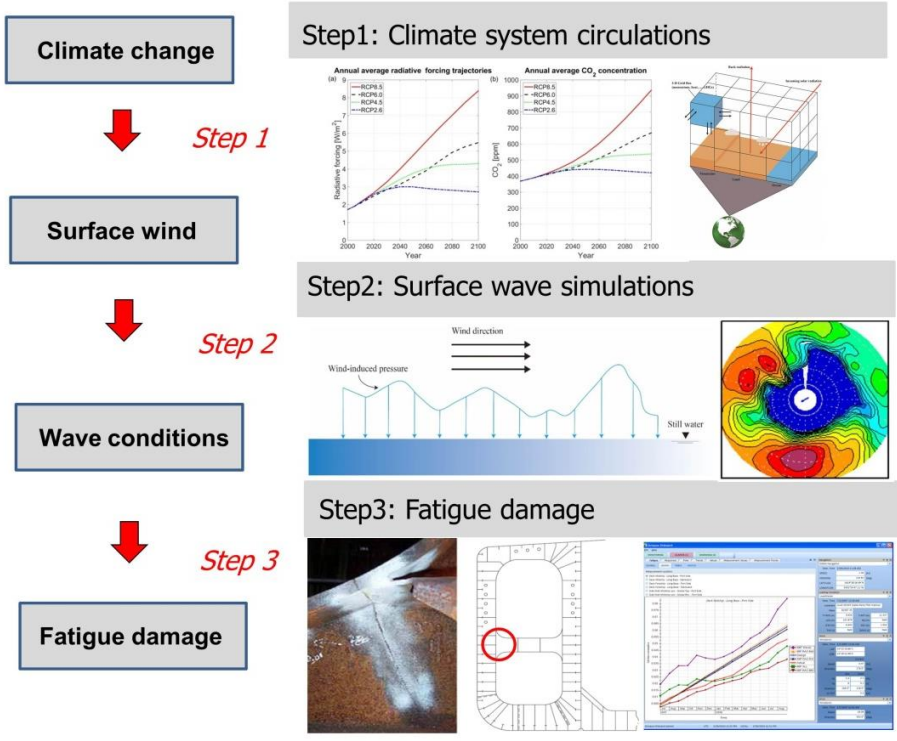

Figure 1.6: Outline of fatigue assessment method with allowance for climate change.

In Chapter 3, climate scenarios are introduced. Physical processes in the climate system are numerically modelled by climate and wave models, and the effect of climate change on fatigue damage to FPSOs is projected. This chapter seeks to demonstrate my methodology via case studies, and to answer the second key question: "How can we simulate physical processes in the climate system, such as atmospheric circulations, wave generations and propagations?"

Chapter 4 investigates the effect of natural variability on wave conditions and fatigue damage by means of control (climatological) simulations. Since climate change results from both natural variability and human activity, the effect of the latter on wave conditions and fatigue damage is also measured and evaluated. Chapter 4 thus addresses the third key question: "Is there a considerable climate change impact on wave conditions and fatigue damage?"

In Chapter 5, some uncertainty factors are discussed, because this methodology includes a considerable number of uncertainties. In addition, sensitivity analysis is conducted to evaluate

the significance of these uncertainties for fatigue calculations.

Finally, Chapter 6 summarizes the conclusions and main findings of this thesis. Suggestions and research limitations are discussed for future studies.

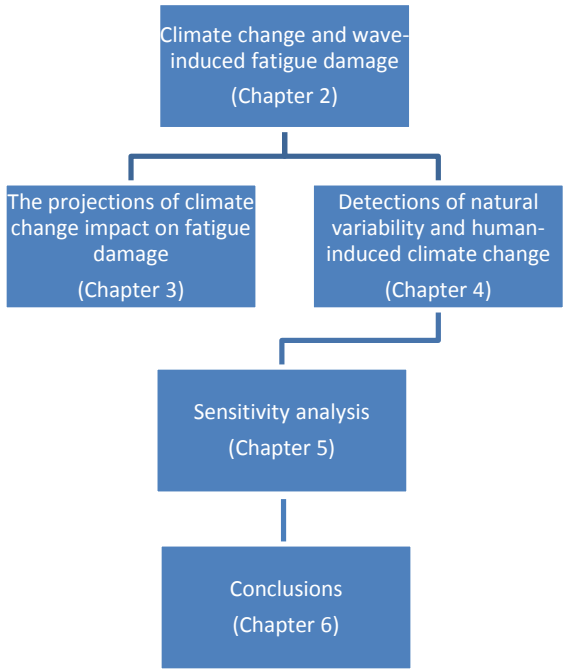

Figure 1.7: Thesis structure

References

[1] IPCC. *Climate Change 2013: The Physical Science Basis. Contribution of Working Group I to the Fifth Assessment Report of the Intergovernmental Panel on Climate Change*. Cambridge, United Kingdom and New York, NY, USA: Cambridge University Press; 2013.

[2] Dessler A. *Introduction to modern climate change*. 2nd ed. New York, USA: Cambridge University Press; 2016.

[3] Church JA, White NJ. Sea-Level Rise from the Late 19th to the Early 21st Century. *Surveys in Geophysics*. 2011;32:585-602.

[4] Knutson TR, McBride JL, Chan J, Emanuel K, Holland G, Landsea C, et al. Tropical cyclones and climate change. *Nature Geoscience*. 2010;3:157-163.

[5] IPCC. *Climate Change 2014: Impacts, Adaptation, and Vulnerability. Part A: Global and Sectoral Aspects. Contribution of Working Group II to the Fifth Assessment Report of the Intergovernmental Panel on Climate Change [Field, C.B., V.R. Barros, D.J. Dokken, K.J. Mach, M.D. Mastrandrea, T.E. Bilir, M. Chatterjee, K.L. Ebi, Y.O. Estrada, R.C. Genova, B. Girma, E.S. Kissel, A.N. Levy, S. MacCracken, P.R. Mastrandrea, and L.L. White (eds.)]*. Cambridge, United Kingdom and New York, NY, USA: Cambridge University Press; 2014.

[6] DNV GL AS. Environmental conditions and environmental loads. 2010.

[7] Wang XL, Zwiers FW, Swail VR. North Atlantic Ocean wave climate change scenarios for the twenty-first century. *Journal of Climate*. 2004; 17:2368-2383.

[8] Baehr J, Keller K, Marotzke J. Detecting potential changes in the meridional overturning circulation at 26˚N in the Atlantic. *Climatic Change*. 2008; 91:11-27.

[9] Dee DP, Uppala SM, Simmons AJ, Berrisford P, Poli P, Kobayashi S, et al. The ERA-Interim reanalysis: configuration and performance of the data assimilation system. *Quarterly Journal of the Royal Meteorological Society*. 2011; 137:553-597.

[10] Charles E, Idier D, Delecluse P, Deque M, Le Cozannet G. Climate change impact on waves in the Bay of Biscay, France. *Ocean Dynamics*. 2012; 62:831-848.

[11] Dobrynin M, Murawsky J, Yang S. Evolution of the global wind wave climate in CMIP5 experiments. *Geophys Res Lett*. 2012; 39.

[12] Woollings T, Gregory JM, Pinto JG, Reyers M, Brayshaw DJ. Response of the North Atlantic storm track to climate change shaped by ocean-atmosphere coupling. *Nature Geoscience*. 2012; 5:313-317.

[13] Colle BA, Zhang ZH, Lombardo KA, Chang E, Liu P, Zhang MH. Historical Evaluation and Future Prediction of Eastern North American and Western Atlantic Extratropical Cyclones in the CMIP5 Models during the Cool Season. *Journal of Climate*. 2013; 26:6882-6903.

[14] Gallagher S, Tiron R, Dias F. A Detailed Investigation of the Nearshore Wave Climate and the Nearshore Wave Energy Resource on the West Coast of Ireland. *Proceedings of the Asme 32nd International Conference on Ocean, Offshore and Arctic Engineering - 2013 - Vol 8*. 2013.

[15] Hemer MA, Fan YL, Mori N, Semedo A, Wang XLL. Projected changes in wave climate from a multi-model ensemble. *Nat Clim Change*. 2013; 3:471-476.

[16] Hemer MA, Katzfey J, Trenham CE. Global dynamical projections of surface ocean wave climate for a future high greenhouse gas emission scenario. *Ocean Modelling*. 2013; 70:221-245.

[17] Woolf D, Wolf J. Impacts of climate change on storms and waves. *MCCIP Science Review*. 2013.

[18] Wang XL, Yang F, Swail VR. Changes in global ocean wave heights as projected using multimodel CMIP5 simulations. *Geophys Res Lett*. 2014; 41:1026-1034.

[19] Dobrynin M, Murawski J, Baehr J, Ilyina T. Detection and attribution of climate change signal in ocean wind waves. *Journal of Climate*. 2015; 28:1578-1591.

[20] Erikson LH, Hegermiller CA, Barnard PL, Ruggiero P, van Ormondt M. Projected wave conditions in the Eastern North Pacific under the influence of two CMIP5 climate scenarios. *Ocean Modelling*. 2015; 96:171-185.

[21] Guo L, Perrie W, Long Z, Toulany B, Sheng J. The Impacts of Climate Change on the Autumn North Atlantic Wave Climate. *Atmosphere-Ocean*. 2015; 53:491-509.

[22] Atan R, Goggins J, Nash S. A Detailed Assessment of the Wave Energy Resource at the Atlantic Marine Energy Test Site. *Energies*. 2016.

[23] Gallagher S, Gleeson E, Tiron R, McGrath R, Dias F. Wave climate projections for Ireland for the end of the 21st century including analysis of EC-Earth winds over the North Atlantic Ocean. *Int J Climatol*. 2016;36:4592-4607.

[24] Gallagher S, Gleeson E, Tiron R, McGrath R, Dias F. Twenty-first century wave climate projections for Ireland and surface winds in the North Atlantic Ocean. *Advances in Science and Research*. 2016;13:75-80.

[25] Hemer MA, Trenham CE. Evaluation of a CMIP5 derived dynamical global wind wave climate model ensemble. *Ocean Modelling*. 2016;103:190-203.

[26] Casas-Prat M, Wang XL, Swart N. CMIP5-based global wave climate projections including the entire Arctic Ocean. *Ocean Modelling*. 2018;123:66-85.

[27] Vanem E, Bitner-Gregersen EM. Stochastic modelling of long-term trends in the wave climate and its potential impact on ship structural loads. *Applied Ocean Research*. 2012;37:235-248.

[28] Gulev SK, Grigorieva V. Variability of the winter wind waves and swell in the North Atlantic and North Pacific as revealed by the voluntary observing ship data. *Journal of Climate*. 2006;19:5667-5685.

[29] Young IR, Zieger S, Babanin AV. Global trends in wind speed and wave height. *Science*. 2011;332:451-455.

[30] Bitner-Gregersen EM, Haver S. Joint Environmental Model For Reliability Calculations. International Society of Offshore and Polar Engineers.

[31] Komen GJ, Cavaleri L, Donelan M, Hasselmann K, Hasselmann S, Janssen P. *Dynamics and modelling of ocean waves*: Cambridge university press; 1996,

[32] Booij LHH, R.C. Ris. The SWAN wave model for shallow water. Coastal Engineering. Orlando, USA1996. p. 668-676.

[33] Tolman H. the WAVEWATCH III Development Group (2014). User Manual and System Documentation of WAVEWATCH III version 4.18. *Tech Note 316, NOAA/NWS/NCEP/MMAB*. 2014.

[34] Janssen PAEM. Progress in ocean wave forecasting. *Journal of Computational Physics*. 2008; 227:3572-3594.

[35] Boldingh Debernard J, Petter RØEd L. Future wind, wave and storm surge climate in the Northern Seas: a revisit. *Tellus A*. 2008; 60:427-438.

[36] Grabemann I, Weisse R. Climate change impact on extreme wave conditions in the North Sea: an ensemble study. *Ocean Dynamics*. 2008; 58:199-212.

[37] Mori N, Yasuda T, Mase H, Tom T, Oku Y. Projection of Extreme Wave Climate Change under Global Warming. *Hydrological Research Letters*. 2010; 4:15-19.

[38] Semedo A, Weisse R, Behrens A, Sterl A, Bengtsson L, Günther H. Projection of Global Wave Climate Change toward the End of the Twenty-First Century. *Journal of Climate*. 2013; 26:8269-8288.

[39] Moss RH, Edmonds JA, Hibbard KA, Manning MR, Rose SK, van Vuuren DP, et al. The next generation of scenarios for climate change research and assessment. *Nature*. 2010; 463:747-756.

[40] Gleeson E, Gallagher S, Clancy C, Dias F. NAO and extreme ocean states in the Northeast Atlantic Ocean. *Advances in Science and Research*. 2017; 14:23-33.

[41] Vanem E, Bitner-Gregersen EM. Modelling Long-Term Trends in Significant Wave Height and its Potential Impacts on Ship Structural Loads. 2013.

[42] Bitner-Gregersen EM, Vanem E, Gramstad O. Design for safety in a changing climate. The 6th International Maritime Conference on Design for Safety. Hamburg, German. 2016.

[43] Vanem E. A Stochastic Model for Long-Term Trends in Significant Wave Height With a CO_2 Regression Component. 2012.

[44] Bitner-Gregersen EM, Horte T, Skjong R. Potential Impact of Climate Change on Tanker Design. 2011; 805-813.

[45] Bitner-Gregersen EM, Eide L. Climate change and effect on marine structure design. *DNVRI Position Paper*. 2010.

[46] Repko A, Van Gelder PHAJM, Voortman HG, Vrijling JK. Bivariate description of offshore wave conditions with physics-based extreme value statistics. *Applied Ocean Research*. 2004; 26:162-170.

[47] Paik JK, Thayamballi AK. *Ship-Shaped Offshore Installations: Design, Building, and Operation*. Noew York, US: Cambridge University Press; 2007.

2

CLIMATE CHANGE AND WAVE INDUCED FATIGUE DAMAGE

As explained in Chapter 1, there is more and more evidence that the earth's climate is changing. In the offshore industry, the climate change has become an increasingly important topic. Many studies investigated the effect of climate change on extreme sea states, because these sea states in combination with ultimate limit states define structural safety in terms of ultimate strength. In contrast, fatigue failure is a long-term cumulative process, and fatigue damage is attributed mainly to moderate sea sates. The offshore structures are subjected to these moderate sea states more often, and the stresses induced by these sea states are already high enough to result in considerable fatigue damage. Hence, more research on fatigue damage is required.

This chapter discusses the relationship between climate change and fatigue damage of offshore floating structures from a physical point of view. At first, I introduce the mechanics of climate change in sections 2.1 and 2.2. At second, the spectral fatigue assessment based on wave scatter diagrams or time series of sea states is introduced in section 2.3-2.5. At last, the relationship between climate change and fatigue damage is discussed in section 2.6.

2.1 Introduction on the Earth's climate system

Weather and climate are closely related. According to the report from the Intergovernmental Panel on Climate Change (IPCC) [1]::

"The weather is the fluctuating state of the atmosphere around us, characterized by the temperature, wind, precipitation, clouds, and other weather elements."

"Climate refers to the average weather in terms of the mean and its variability over a certain time-span and a certain area."

Weather and climate are hence both the indicators of atmospheric states. The difference between them is the time scale. Weather is the condition of atmosphere over a short period of time, and climate is the averaged condition of atmosphere over a relatively long period of time. But they also have one thing in common: both of them vary in time. Basically, climate change refers to the statistically significant variations of the mean atmospheric state over decades or even longer. Besides, the climate change also shows a spatial variation. The latitude, waters, vegetation and other geographical factors all affect the climate in one place, because the atmosphere interacts with these factors [2].

The Earth's climate system is an interactive system which consists of five components: the atmosphere, the cryosphere, the hydrosphere, the land and the biosphere, as shown Fig. 2.1. The circulation of climate system and the interactions between its components are mainly forced by solar radiation.

The atmosphere is the key component in the climate system, as it can significantly affect the solar radiation before it reaches the other climate components. The primary components of atmosphere are nitrogen and oxygen (N_2 and O_2) which account for about 90% volume mixing ratio. The remaining components are, for example, carbon dioxide (CO_2), methane (CH_4), nitrous oxide (N_2O), ozone (O_3), and water vapor; most of them are called greenhouse gases (GHGs), because they have a strong ability to absorb and emit infrared radiation. The atmospheric circulation is basically driven by solar radiation and the rotation of the earth. Due to the uneven distribution of solar heat over the globe, three convection cells (the Hadley cell, the Ferrel cell, and the Polar cell) are formed which transfer energy from the equator to the poles, as shown in Fig. 2.2. In addition, the atmosphere may also circulate in the other

directions due to the difference of surface temperature.

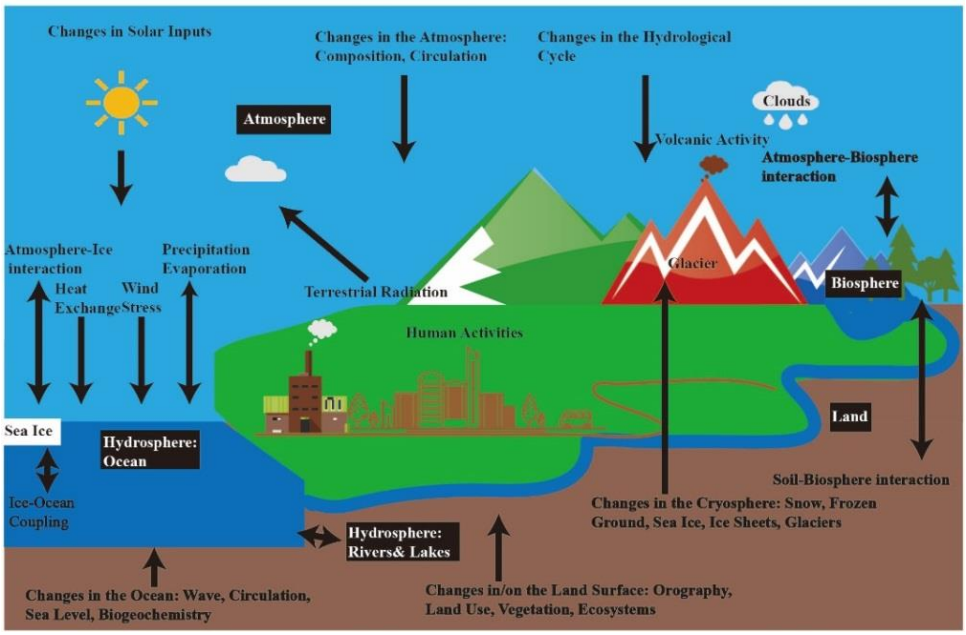

Figure 2.1: Schematic view of the components of the climate system, their processes and interactions [3]

The atmosphere is the key component in the climate system, as it can significantly affect the solar radiation before it reaches the other climate components. The primary components of atmosphere are nitrogen and oxygen (N_2 and O_2) which account for about 90% volume mixing ratio. The remaining components are, for example, carbon dioxide (CO_2), methane (CH_4), nitrous oxide (N_2O), ozone (O_3), and water vapor; most of them are called greenhouse gases (GHGs), because they have a strong ability to absorb and emit infrared radiation. The atmospheric circulation is basically driven by solar radiation and the rotation of the earth. Due to the uneven distribution of solar heat over the globe, three convection cells (the Hadley cell, the Ferrel cell, and the Polar cell) are formed which transfer energy from the equator to the poles, as shown in Fig. 2.2. In addition, the atmosphere may also circulate in the other directions due to the difference of surface temperature.

In the process of circulation, the atmosphere may interact with other climate components as swell. These climate components are interrelated by non-linear interactions. For example, when wind blows over still water, it may generate instability at their interfere which results in very small waves [4]. These small waves in return affect the airflow of the lower atmosphere and lead to an uneven distribution of wind-induced pressure over the water surface, see Fig. 2.3. The air pressure on the windward side of the wave crest is higher than the pressure on the leeward side. As a result, wind energy is transferred into waves. As the waves grow, the energy transfer also becomes more effective further accelerating the growth of waves [5].

Hence, it is predominantly the uneven distribution of air pressure that generates the waves, rather than the wind friction [6]. Since this study focuses on wave conditions, the other interactions are not introduced. There are many chemical and biological processes in the atmospheric circulation and the climate interactions. From the physical point of view however, they are all flux of mass, heat, and momentum. In climate models, these processes are usually numerically simulated based on the energy conservation, as discussed in Chapter 3.

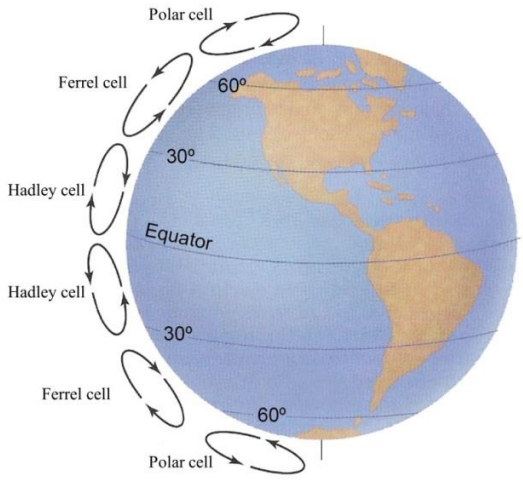

Figure 2.2: Global wind belts: the Hadley cell, the Ferrel cell, and the Polar cell

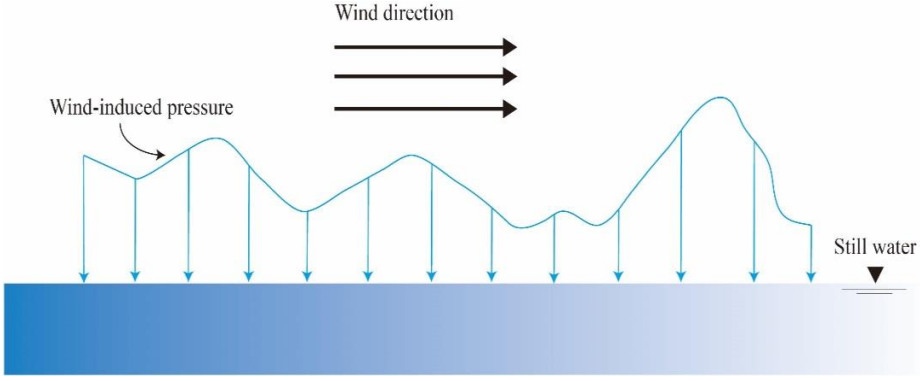

Figure 2.3: The wind-induced pressure across the still water surface

2.2 Mechanics of climate change

The solar radiation is the original driving force of the Earth's climate system, as shown in Fig. 2.1. The Sun sends energy into the Earth via solar radiation, and the Earth emits energy back into the space via infrared radiation. In an equilibrium condition, the solar radiation into the Earth is equal to the infrared radiation out to the space. The break of this equilibrium condition may lead to the imbalance of energy and subsequently result in externally-induced climate change. This imbalance may be induced by many factors, such as the

Milankovitch Effect (change of the Earth's orbit and rotation) or the greenhouse effect. For offshore engineering, more attention is paid on the emission of GHGs, since the other external forcing factors have much longer time-scales (from hundreds to thousands of years). In the remainder of this chapter, externally-induced climate change is merely represented by the human-induced part, because the emission of GHGs is highly affected by human activities and policies.

In addition, those climate components have different response time to external forcing, which may result in the internally-induced climate change. For instance, the response time of atmosphere to the change of solar radiation is from days to months. Differently, due to the huge capacity of heat, the ocean component has a much longer response time (decades or even longer) in temperature, heat content, salinity, sea level, circulation or other factors. In short, the climate components may respond to external forcing differently on a wide range of space- and time-scales [1]. Moreover, even the external radiative forcing has no change, the internally-induced climate change may also occur due to the non-linear interactions between the climate components.

The effect of climate change is the combination of natural variability and human-induced climate change. The natural variability originates from the natural mechanics of climate system, and its occurrence is beyond control and hard to predict. In contrast, the effect of human-induced climate change is mainly induced by human activities. The investigation on the effect of human activities can help decision-makers to improve their policy and lower the potential risk induced by the climate change. It is hence necessary to detect the effect of human-induced climate change from observed or projected climate change [7, 8]. However, it is challenging to evaluate to what extent climate change is attributed to the human activity, because its impact may be counterbalanced by the natural variability.

Based on the mechanics of climate change, the circulation of the climate system has already been modelled by many different research groups, but none of these models incorporated the simulation of wave conditions directly [9]. Instead, some studies usually calculated the wind speed, storm tracks or other climate indices, such as the North Atlantic Oscillation (NAO) or sea level pressure (SLP), to represent the wave climate [10, 11], because these indices are all closely correlated to the waves [12-14]. Another alternative way is by coupling the climate models to the wind-driven wave models [7-9, 11, 14-21], but this approach also includes a lot of uncertainties induced in the process of wind field simulations and wave simulations [14, 22]. I will further discuss the simulations of large-scale wave conditions and its uncertainties in Chapter 3 and 5.

2.3 Wave scatter diagrams and time series of sea states

Offshore floating structures are exposed to marine environment and subjected to wind, wave, and current. Among these, waves are the primary source of fatigue damage [23]. Wave loadings produce fluctuating stress in structures, which result in accumulated fatigue damage. In design stage hence, it is important to identify all the relevant wave conditions that an offshore structure will encounter in its service life.

In fatigue assessment, sea states are commonly defined as the statistical description of wave conditions over 3 or 6 hours. According to classification notes [24, 25], sea states in the fatigue design are represented by wave scatter diagrams, as shown in Fig. 2.4. Each block in the scatter diagram stands for one sea state with its significant wave height (H_s), zero-crossing

period (T_z) and probability of occurrence. The sea states in scatter diagrams are typically characterized based on observations, measurements or hindcast.

Tz [s]	3.5	4.5	5.5	6.5	7.5	8.5	9.5	10.5	11.5	12.5	13.5	14.5	15.5	16.5	17.5	18.5	Sum
Hs [m]																	
0.5	1.3	133.7	865.6	1186	634.2	186.3	36.9	5.6	0.7	0.1	0	0	0	0	0	0	3050
1.5	0	29.3	986	4976	7738	5569.7	2375.7	703.5	160.7	30.5	5.1	0.8	0.1	0	0	0	22575
2.5	0	2.2	197.5	2158.8	6230	7449.5	4860.4	2066	644.5	160.2	33.7	6.3	1.1	0.2	0	0	23810
3.5	0	0.2	34.9	695.5	3226.5	5675	5099.1	2838	1114.4	337.7	84.3	18.2	3.5	0.6	0.1	0	19128
4.5	0	0	6	196.1	1354.3	3288.5	3857.5	2685.5	1275.2	455.1	130.9	31.9	6.9	1.3	0.2	0	13289
5.5	0	0	1	51	498.4	1602.9	2372.7	2008.3	1126	463.6	150.9	41	9.7	2.1	0.4	0.1	8328
6.5	0	0	0.2	12.6	167	690.3	1257.9	1268.6	825.9	386.8	140.8	42.2	10.9	2.5	0.5	0.1	4806
7.5	0	0	0	3	52.1	270.1	594.4	703.2	524.9	276.7	111.7	36.7	10.2	2.5	0.6	0.1	2586
8.5	0	0	0	0.7	15.4	97.9	255.9	350.6	296.9	174.6	77.6	27.7	8.4	2.2	0.5	0.1	1309
9.5	0	0	0	0.2	4.3	33.2	101.9	159.9	152.2	99.2	48.3	18.7	6.1	1.7	0.4	0.1	626
10.5	0	0	0	0	1.2	10.7	37.9	67.5	71.7	51.5	27.3	11.4	4	1.2	0.3	0.1	285
11.5	0	0	0	0	0.3	3.3	13.3	26.6	31.4	24.7	14.2	6.4	2.4	0.7	0.2	0.1	124
12.5	0	0	0	0	0.1	1	4.4	9.9	12.8	11	6.8	3.3	1.3	0.4	0.1	0	51
13.5	0	0	0	0	0	0.3	1.4	3.5	5	4.6	3.1	1.6	0.7	0.2	0.1	0	21
14.5	0	0	0	0	0	0.1	0.4	1.2	1.8	1.8	1.3	0.7	0.3	0.1	0	0	8
15.5	0	0	0	0	0	0	0.1	0.4	0.6	0.7	0.5	0.3	0.1	0.1	0	0	3
16.5	0	0	0	0	0	0	0	0.1	0.2	0.2	0.2	0.1	0.1	0	0	0	1
Sum	1	165	2091	9280	19922	24879	20870	12898	6245	2479	837	247	66	16	3	1	100000

Figure 2.4: Unidirectional non-seasonal scatter diagram for North Atlantic. The data source is from DNV classification note [24].

Observations and measurements

Wave conditions can be observed by either visual observers or instruments. In fact, visual observations are the most traditional way to obtain wave data, however they are often not optimally reliable, since eyes tend to concentrate on the nearest and steepest waves. The reliability of visual observations is highly dependent on the observers. On the other hand, there are several techniques to measure wave conditions instrumentally, though no one is generally appropriate for all sea areas. Among them, buoys are considered as the most reliable instrument. Wave conditions are recorded by buoys with 3-6 hours interval. For each record, at least 200 waves should be measured in order to reduce the scatter of waves. The optimal recording duration is 15-35 minutes based on experience [26]. It is assumed that the spectrum measured in this interval is representative of the wave conditions in 3-6 hours. Besides, satellite techniques are rapidly developing, and can provide a large spatial-scale measurement of wave conditions of wave conditions. These satellite measurements however, still require further improvement, as the recorded wave spectra are not yet desirably reliable. Satellite measurements usually need further validations by wave numerical models or in situ measurements [27].

Hindcast

Due to the limitations of wave observations, it is possible that the historical wave data at a certain sea area are not available. Instead, wave hindcasting can be carried out to simulate wave conditions over historical time periods based on wind field data. Wind-driven wave models are usually used to reproduce these sea states by simulating the evolution of wave spectra [28].

Although wave scatter diagrams are recommended by many classification societies, they are not exactly representative of ocean waves. This is mainly because some information of wave properties is eliminated when constructing scatter diagrams, such as wave directions, wave directional spreading and the sequence of sea states. The structural response of vessels changes with the variation of wave directions. The sequence of sea states can also affect the

wave-induced fatigue damage of the vessel. In modern industry, the consideration of time-series of sea states are highly recommended in order to improve the accuracy of fatigue calculations, as exemplified in Table 2.1. The significant wave height, zero crossing period, mean wave direction (θ), and directional spreading coefficient (s) for each wave system (wind waves and swells) are all listed in Table 2.1.

Table 2.1: An example of sea state time-series

Date and time	Wind wave				Swell			
	H_s	T_z	θ	s	H_s	T_z	θ	s
[yyyy-mm-dd-hh]	[m]	[s]	[deg]	-	[m]	[s]	[deg]	-
2006-01-01-00	0.67	3.82	121	8	1.53	9.20	357	15
2006-01-01-06	1.83	5.40	98	9	1.44	8.66	6	20
2006-01-01-12	2.58	6.16	109	11	1.01	8.22	8	15
	…	…	…	…	…	…	…	…
2006-12-31-18	0.84	4.45	255	8	1.90	7.10	225	15

In reality, the wave spectra are more complicated than the idealized ones. Since waves are superposition of many different wave components, they may include multiple peaks in their spectra, as shown in Fig. 2.5. Therefore, the reliability of fatigue calculations can be improved if the wave spectra are partitioned into wave systems (normally, one wind wave and several swells) for which the fatigue consumption is calculated separately. The wave spectral partitioning methodology with automated swell tracking and storm source identification capabilities is widely used in wave models [29, 30] where each sea state consisting of multiple wave systems is represented by multiple single-peak wave spectra.

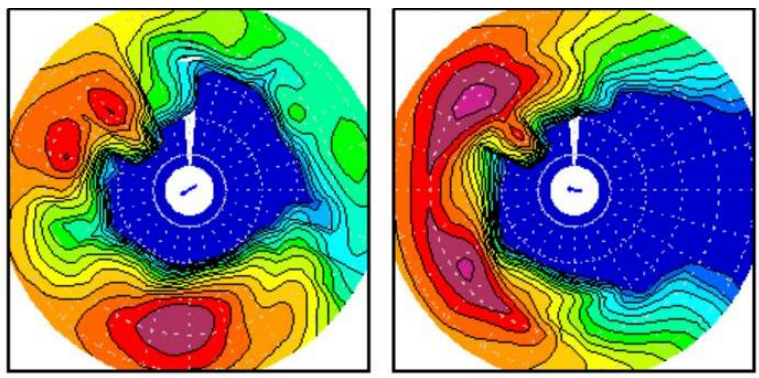

Figure 2.5: Examples of multiple-peaks wave spectra. The radial coordinate: wave period; The angular coordinate: wave heading; The contour lines: wave energy.

It is believed that these partitioned sea states still need further improvement since they are all constructed based on the sea states obtained in the past. It is assumed that past sea states can be representative of future sea states. There might be decades passed between the wave observations and the service of offshore structures. Furthermore, the sea states in the future will probably be affected by natural variability or human-induced climate change and become significantly different from the sea states in the past [31]. Therefore, it is first necessary to consider the climate change impact on sea states and consequently on fatigue damage in the design of offshore structures.

2.4 Floating Production, Storage and Offloading (FPSO) units

The first submerged oil wells were drilled from platforms in the Grand Lake St. Marys around 1891. Since then, a large number of oil fields in shallow waters have been discovered and exploited by fixed platforms. Nowadays, with the decrease of output in shallow oil fields, the interest of offshore industry is moving into deep waters. As the cost of fixed platforms increases exponentially with water depth, more floating offshore structures are required.

Floating Production, Storage, and Offloading units (FPSOs) are one of the most popular offshore floating structures, as shown with an example in Fig. 2.6. They are designed for exploitation, processing, and storage of gas and oil in the marine environment. Their advantages are as follows:

- The manufacture of FPSOs is cost effective. They are ship-shaped structures, and many of them are converted from tankers, which can hugely reduce the capital expenditure.
- An FPSO is a practical solution to short-life oil fields or remote sea areas, because they are easy to install and the oil can be transferred by shuttle tankers instead of laying pipelines.
- It is easy to recycle FPSOs after installations. Once the oil production is exhausted or an extreme sea state is coming, FPSOs can be easily removed to other places.

Figure 2.6: The Floating Production, Storage and Offloading unit. From "Wikimedia Commons", by Edersguerri, 2011 (https://commons.wikimedia.org/wiki/File:3AFPSO_OSX-1.jpg). Licensed under CC BY-SA 3.0.

Due to their ship-like shapes, the structural response of FPSOs are more sensitive to the change of wave directions than many other floating platforms' response. The relative wave direction to the heading of vessel is highly affected by the mooring system. There are two primary types of mooring systems for FPSOs: spread mooring and turret mooring, as demonstrated in Fig. 2.7. Spread mooring systems fix vessels to the seabed with multiple mooring lines connected to the hull. In turret mooring system, a turret is integrated into a vessel. This turret is fixed to the seabed by mooring lines and allows the vessel to rotate around it.

The directionality of wave conditions influences the way a floater is moored at a site. When wave systems are coming from predominantly one direction, the spread mooring system is recommended. In this way, the mean geographical direction of the floater is fixed and aligned with the predominant direction of wave systems, though the floater can still change its direction by a few degrees depending on the rotational stiffness of the mooring system. In the other case, i.e. when wave systems come from varying directions, the turret mooring system is a better choice. This is because the floater can rotate into the proper heading direction by determining the angle of the zero yaw moment around the turret from environmental loadings [32].

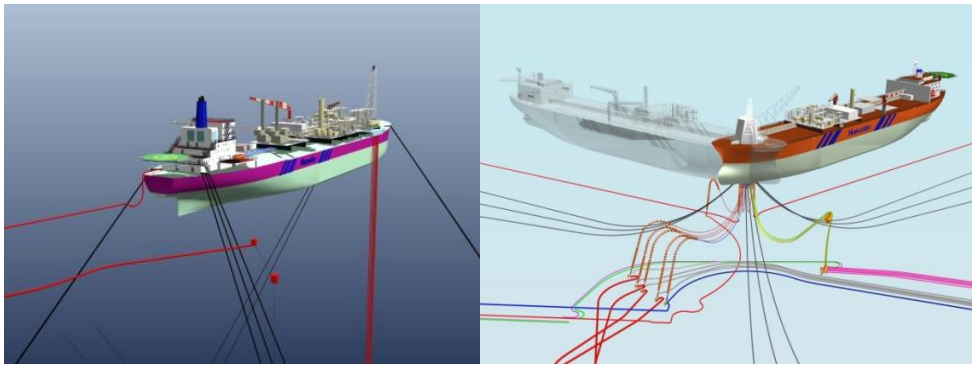

Figure 2.7: Spread moored floater (left) and turret moored floater (right) (www.bluewater.com). Copy right by Bluewater. Reprinted with permission.

2.5 Wave-induced fatigue damage

Offshore floating structures are generally subject to loads induced by wind, wave, and current. Wave-induced stresses are considered as the main source of fatigue damage. The varying stresses in structural members and joints initiate fatigue cracks. These cracks, when propagating, may subsequently cause a fatigue failure, see Fig. 2.8.

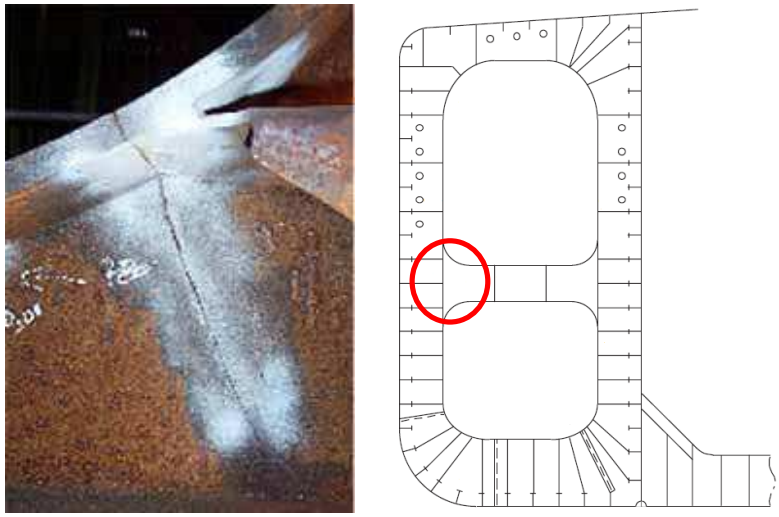

Figure 2.8: Fatigue cracks in structural joints (https://www.twi-global.com/)

For offshore structures, fatigue damage is usually calculated based on the spectral approach, and the fatigue resistance is represented by S-N curves [24]. If the long-term stress range distribution is defined as the sum of the Rayleigh distribution from each short-term stress range corresponding to each sea state, the cumulative fatigue damage with one slope S-N curve is given by:

$$\mathrm{D} = \frac{\omega_0 T_d}{a} \Gamma\left(1+\frac{m}{2}\right) \sum_{n=1}^{N_{load}} p_n \sum_{i=1,j=1}^{\substack{all\ seastates \\ all\ headings}} r_{ijn} \left(2\sqrt{2m_{0ijn}}\right)^m \tag{2.1}$$

where D is accumulated fatigue damage, ω_0 is the average long-term zero-crossing frequency, a and m are the S-N curve parameters, T_d is the design life of the structure, Γ is the gamma function, N_{load} is the total number of load conditions, p_n is the fraction of the design life in load condition n, r_{ijn} is the relative number of stress cycles in short-term condition i, j, and m_{0ijn} is the zero spectral moment of stress response process.

The stress response spectrum and spectral moments in linear models are defined as

$$S_\sigma(\omega|H_s, T_z, \theta) = |H_\sigma(\omega|\theta)|^2 \cdot S_\eta(\omega|H_s, T_z) \tag{2.2}$$

$$m_n = \int_\omega \sum_{\theta-90^\circ}^{\theta+90^\circ} f(\theta)\omega^n \cdot S_\sigma(\omega|H_s, T_z, \theta) d\omega \tag{2.3}$$

where $H_\sigma(\omega|\theta)$is the transfer function which represents the relation between unit wave amplitude and response, $S_\eta(\omega|H_s, T_z)$ is the wave spectrum, and $f(\theta)$ is the wave spreading function. If the wave spectrum in one sea state is partitioned into wind wave and swell systems, the total fatigue damage D_{tot} can be calculated empirically as Eq. (2.4):

$$D_{tot}^{\frac{2}{3}} = D_{ww}^{\frac{2}{3}} + D_{swell}^{\frac{2}{3}} \tag{2.4}$$

D_{ww} and D_{swell} are the fatigue damages induced by wind waves and swells respectively and independently.

2.6 Relations between climate change and fatigue damage

Climate change is a long-term cumulative process, and changes the wave conditions slowly and gradually. The lifecycle of an offshore structure may be over 30 years. The annual fatigue damage during this period is expected to be influenced where wave conditions are sensitive to climate change. According to sections 2.1-2.5, I can clarify the relation between climate change and fatigue damage from a physical point of view, as illustrated in Fig. 2.9.

- Due to the natural variability and the human-induced climate change, the climate circulation changes in time. The atmosphere makes the most rapid response to the climate change. The surface wind field, as the part of lower atmosphere, is also changed.
- Most ocean surface waves are generated by wind. The climate change therefore leads to different wave conditions.
- The waves are one of the primary sources of fatigue damage for offshore floating structures. As a result, fatigue damage may be affected by the climate change.

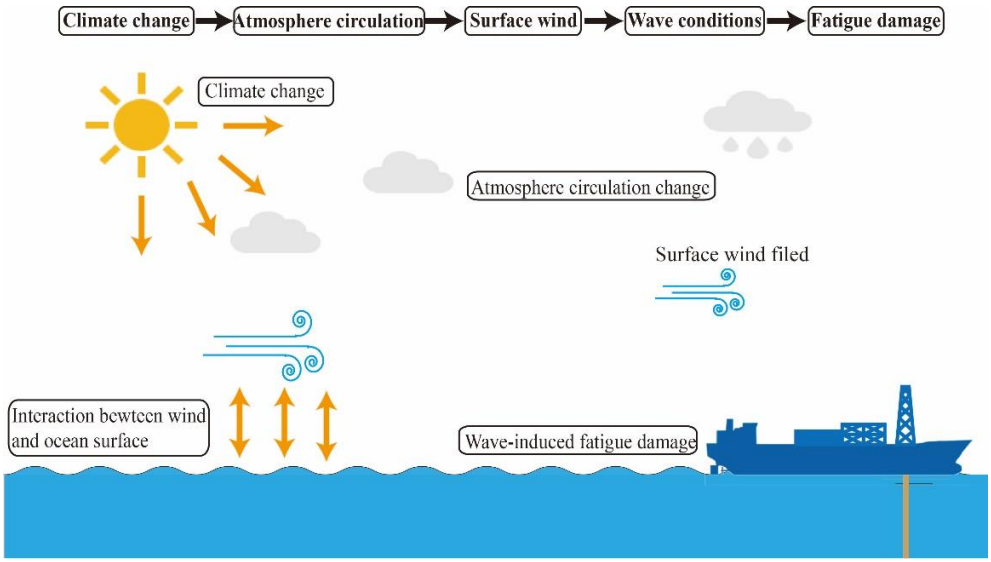

Figure 2.9: The relation between climate change and fatigue damage from a physical point of view

2.7 Conclusions

In this chapter, I briefly described the relation between climate change and fatigue damage of offshore floating structures from a physical point of view. The climate system consists of five components: the atmosphere, the cryosphere, the hydrosphere, the land, and the biosphere. The original driving force for all of them is the solar radiation. The atmosphere is the key component to investigate the climate change, because it makes the most rapid response to climate change compared to the other ones. Climate change is attributed to external forcing change and internal forcing change. The external forcing change refers to the change of the

radiation forcing, which is highly affected by GHG emission. Hence, the external forcing change is also called human-induced climate change in this study. Alternatively, the internal forcing change is induced by the different response time and the non-linear interactions between various climate components (*i.g.,* natural variability).

It is necessary to consider the effect of climate change in the fatigue design of floating offshore structures. When facing climate change, the atmospheric circulation and its interaction with the ocean surface respond rapidly, compared to the other climate components. Most ocean waves are generated by wind fields, and they contribute the most to the fatigue damage of floating structures, such as FPSOs. The lifecycle of FPSOs may be as long as 30 years. The wave conditions measured in the past may not necessarily be representative of the future wave conditions that FPSOs will encounter in their service life.

The fatigue damage is usually calculated based on the spectral approach, and the constructions of scatter diagrams or time series of sea states are required to represent the wave conditions. When making fatigue analysis for turret moored FPSOs which are of interest to this thesis, the relative wave directions should be taken into account, because the vessel may rotate around its moored line. If we want to consider climate change in the fatigue design stage of turret moored FPSOs, the wave load data should be updated accordingly.

References

[1] Houghton JT, Ding Y, Griggs DJ, Noguer M, van der Linden PJ, Dai X, et al. Climate Change 2001: The Scientific Basis. Contribution of Working Group I to the Third Assessment Report of the Intergovernmental Panel on Climate Change. Cambridge, United Kingdom and New York, NY, USA: IPCC; 2001; 881.

[2] Feddema JJ, Oleson KW, Bonan GB, Mearns LO, Buja LE, Meehl GA, et al. Atmospheric science: The importance of land-cover change in simulating future climates. *Science*. 2005; 310:1674-1678.

[3] Solomon S, Qin D, Manning M, Chen Z, Marquis M, Averyt KB, et al. Climate Change 2007: The Physical Science Basis. Contribution of Working Group I to the Fourth Assessment Report of the Intergovernmental Panel on Climate Change. IPCC; 2007.

[4] Lamb H. *Hydrodynamics*. 6th ed. New York: Dover Publications; 1932.

[5] Miles JW. On the generation of surface waves by shear flows. *Journal of Fluid Mechanics*. 1957; 3:185-204.

[6] Holthuijsen LH. *Waves in Oceanic and Coastal Waters*: Cambridge University Press; 2007.

[7] Dobrynin M, Murawsky J, Yang S. Evolution of the global wind wave climate in CMIP5 experiments. *Geophys Res Lett*. 2012; 39.

[8] Gallagher S, Gleeson E, Tiron R, McGrath R, Dias F. Wave climate projections for Ireland for the end of the 21st century including analysis of EC-Earth winds over the North Atlantic Ocean. *Int J Climatol*. 2016; 36:4592-4607.

[9] Hemer MA, Trenham CE. Evaluation of a CMIP5 derived dynamical global wind wave climate model ensemble. *Ocean Modelling*. 2016; 103:190-203.

[10] Wang XL, Zwiers FW, Swail VR. North Atlantic Ocean wave climate change scenarios for the twenty-first century. *Journal of Climate*. 2004; 17:2368-2383.

[11] Wang XL, Yang F, Swail VR. Changes in global ocean wave heights as projected using multimodel CMIP5 simulations. *Geophys Res Lett*. 2014; 41:1026-1034.

[12] Atan R, Goggins J, Nash S. A Detailed Assessment of the Wave Energy Resource at the Atlantic Marine Energy Test Site. *Energies*. 2016; 9.

[13] Santo H, Taylor PH, Eatock Taylor R, Stansby P. Decadal variability of wave power production in the North-East Atlantic and North Sea for the M4 machine. *Renewable Energy*. 2016; 91:442-450.

[14] Woolf D, Wolf J. Impacts of climate change on storms and waves. *MCCIP Science Review*. 2013.

[15] Casas-Prat M, Wang XL, Swart N. CMIP5-based global wave climate projections including the entire Arctic Ocean. *Ocean Modelling*. 2018; 123:66-85.

[16] Gallagher S, Gleeson E, Tiron R, McGrath R, Dias F. Twenty-first century wave climate projections for Ireland and surface winds in the North Atlantic Ocean. *Advances in Science and Research*. 2016; 13:75-80.

[17] Guo L, Perrie W, Long Z, Toulany B, Sheng J. The Impacts of Climate Change on the Autumn North Atlantic Wave Climate. *Atmosphere-Ocean*. 2015; 53:491-509.

[18] Charles E, Idier D, Delecluse P, Deque M, Le Cozannet G. Climate change impact on waves in the Bay of Biscay, France. *Ocean Dynamics*. 2012; 62:831-848.

[19] Erikson LH, Hegermiller CA, Barnard PL, Ruggiero P, van Ormondt M. Projected wave conditions in the Eastern North Pacific under the influence of two CMIP5 climate scenarios. *Ocean Modelling*. 2015; 96:171-185.

[20] Hemer MA, Fan YL, Mori N, Semedo A, Wang XLL. Projected changes in wave climate from a multi-model ensemble. *Nat Clim Change*. 2013; 3:471-476.

[21] Hemer MA, Katzfey J, Trenham CE. Global dynamical projections of surface ocean wave climate for a future high greenhouse gas emission scenario. *Ocean Modelling*. 2013; 70:221-245.

[22] Gleeson E, Gallagher S, Clancy C, Dias F. NAO and extreme ocean states in the Northeast Atlantic Ocean. *Advances in Science and Research*. 2017; 14:23-33.

[23] Paik JK, Thayamballi AK. *Ship-Shaped Offshore Installations: Design, Building, and Operation*. Noew York, US: Cambridge University Press; 2007.

[24] DNV GL AS. Fatigue Assessment of Ship Structures. 2014.

[25] Shipping ABO. Guidance notes on spectral-based fatigue analysis for floating offshore structures 2005.

[26] WMO. *Guide to Wave Analysis and Forecasting*: World Meteorological Organization; 1998.

[27] Janssen PAEM, Abdalla S, Hersbach H, Bidlot J-R. Error Estimation of Buoy, Satellite, and Model Wave Height Data. *Journal of Atmospheric and Oceanic Technology*. 2007; 24:1665-1677.

[28] Tolman HL, Balasubramaniyan B, Burroughs LD, Chalikov DV, Chao YY, Chen HS, et al. Development and implementation of wind-generated ocean surface wave modelsat NCEP. *Weather and forecasting*. 2002; 17:311-333.

[29] Hanson JL, Phillips OM. Automated Analysis of Ocean Surface Directional Wave Spectra. *Journal of Atmospheric and Oceanic Technology*. 2001; 18:277-293.

[30] Hanson J. LA, Aalberts P., Kaminski M.L. Wave Measurements for the Monitas System. Texas, USA. 2010; 1-12.

[31] Bitner-Gregersen EM, Eide L. Climate change and effect on marine structure design. *DNVRI Position Paper*. 2010.

[32] van der Cammen JJ, Hoogeland M, Koning J. Comparison of Measured and Calculated Vessel Heading of a Turret-Moored FPSO. 12th Offshore Symposium. Houston, Texas, USA. 2003.

3

THE PROJECTION OF CLIMATE CHANGE IMPACT

Some sections of this chapter have been published in Journal of Ocean Dynamics, 2016 [1].

In Chapter 2, the mechanics of climate change was introduced, and the relationship between the climate change and fatigue damage was discussed. The fatigue design of the Floating Production Storage and Offloading (FPSO) units requires wave scatter diagrams or time series of sea states including all the relevant sea states which FPSOs will encounter in their service life, as discussed in section 2.3. As the lifetime of FPSOs could be more than 30 years, the climate change may considerably affect the future sea states and the long-term cumulative fatigue damage.

In this chapter, a methodology to project the effect of climate change on fatigue damage will be presented, as shown in Fig. 3.1. The driving forces of climate change are introduced in section 3.1. In Chapter 2, I have preliminarily introduced the climate system and the mechanics of wave generation. In section 3.2 and 3.3, I will demonstrate the modelling of climate system and wave conditions. Finally, the future sea states and future annual fatigue damages are projected by coupling climate models to wave models in section 3.4-3.6.

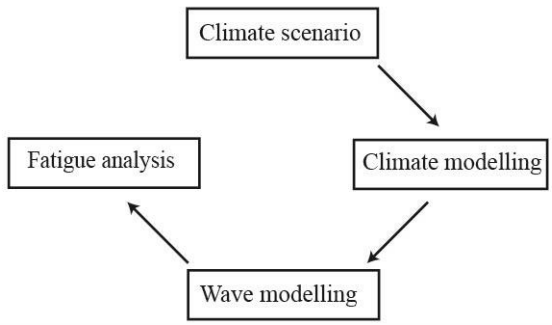

Figure 3.1: Outline of fatigue analysis method with allowance for climate change

3.1 Climate scenarios

Climate scenarios are used to describe the historical and future climate with respect to a wide range of variables including socio-economic change, technological development, energy composition, land use, and emissions of greenhouse gases (GHGs) and air pollutants [2]. According to the Intergovernmental Panel on Climate Change (IPCC), climate scenarios are described as:

"In climate change research, scenarios describe plausible trajectories of different aspects of the future that are constructed to investigate the potential consequences of anthropogenic climate change. Scenarios represent many of the major driving forces - including processes, impacts (physical, ecological, and socioeconomic), and potential responses that are important for informing climate change policy."

The climate scenarios were initially constructed using a sequential approach, as shown in Fig. 3.2a. The emissions and socio-economic scenarios were developed first to describe the storyline of GHG concentrations and radiative forcing. As a result, a variety of climate scenarios were presented, and plenty of climate projections were conducted based on different sequential climate scenarios. However, it was hardly possible to compare one projection to another, due to their different storylines.

In 2007, IPCC claimed that new climate scenarios were needed to run the new generation of climate models [3, 4]. In contrast with the previous sequential approach, the parallel approach was applied to construct new climate scenarios, see Fig. 3.2b. This parallel approach began with the construction of radiative forcing trajectory and GHG concentrations directly. Then, the circulation of climate system is projected by climate models. Based on the result of projections, the climate change impacts are analyzed which in return affects the improvement of climate models. In addition, with this parallel approach, the constructions of emission and socio-economic scenarios are not prerequisites for climate modelling anymore.

According to the previous climate scenarios [5, 6], the radiative forcing until the end of 2100 would reach a level ranging from 2.5 W/m^2 to 9 W/m^2 . Hence, four parallel climate scenarios were selected to cover this range in IPCC, as shown in Fig. 3.3a. All these four climate scenarios are termed "Representative Concentration Pathways (RCPs)". Each of them represents a large set of sequential climate scenarios, as listed in Table 3.1.

RCPs provide the trajectories of all the radiative forcing components over time, including the emissions of GHGs (for instance, the CO_2 concertation in Fig. 3.3b), air pollutants, and land use. The trajectories cover both the historical and future period from 2000 to 2100, and all the RCPs have been harmonized for a smooth transition between the historical and future periods. The radiative data in RCPS have the spatial resolution of approximately 60 kilometers and the temporal resolution of one year. The temporal resolution can be modified to monthly, daily or even 6-hourly by considering the seasonal cycle and the historic radiative data.

Although RCPs include the future data, they should not be viewed as accurate predictions of the future climate. Instead, each of them only represents one possibility of the future based on a set of prior expectations. Therefore, we use the term "projections" instead of "predictions" to represent all the simulations for the future conditions. In addition, the RCPs are not associated with unique socio-economic factors and emission scenarios. Each RCP can result from different combinations of economic, technological, demographic, policy, and institutional futures. The parallel approach makes the climate scenarios more flexible and allows researchers to focus on the impact, adaptation, vulnerability, and mitigation of climate change.

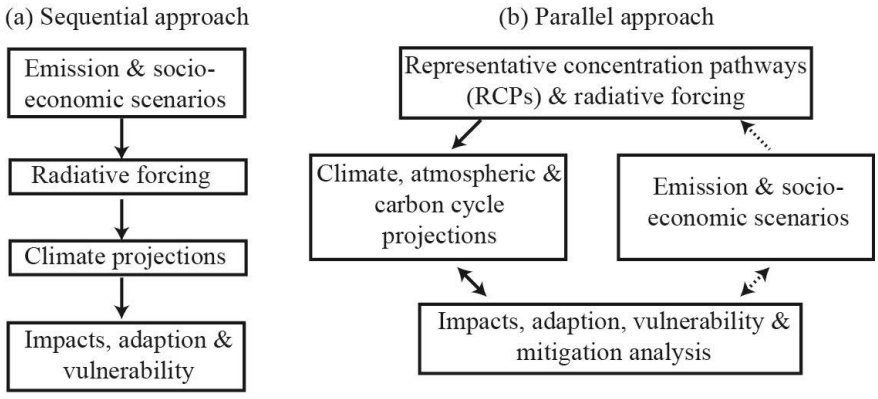

Figure 3.2: Approaches to the development of global scenarios: (a) sequential approach; (b) parallel approach. [3]

In this thesis, the climate scenario for all the climate simulations is defined as RCP8.5 which is characterized by increasing GHGs and radiative forcing level. In fact, the radiative forces of four RCPs are not significantly different before 2020 as seen in Fig. 3.3. RCP8.5 is associated with the highest emission of GHG and it will result in the most significant impact of climate change than the other RCPs [7, 8].

Table 3.1: The descriptions of RCPs

Name	Description
RCP8.5	Rising radiative forcing pathway leading to 8.5 W/m2 in 2100.
RCP6	Stabilization without overshoot pathway to 6 W/m2 at stabilization after 2100
RCP4.5	Stabilization without overshoot pathway to 4.5 W/m2 at stabilization after 2100
RCP2.6	Peak in radiative forcing at ~ 3 W/m2 before 2100 and decline

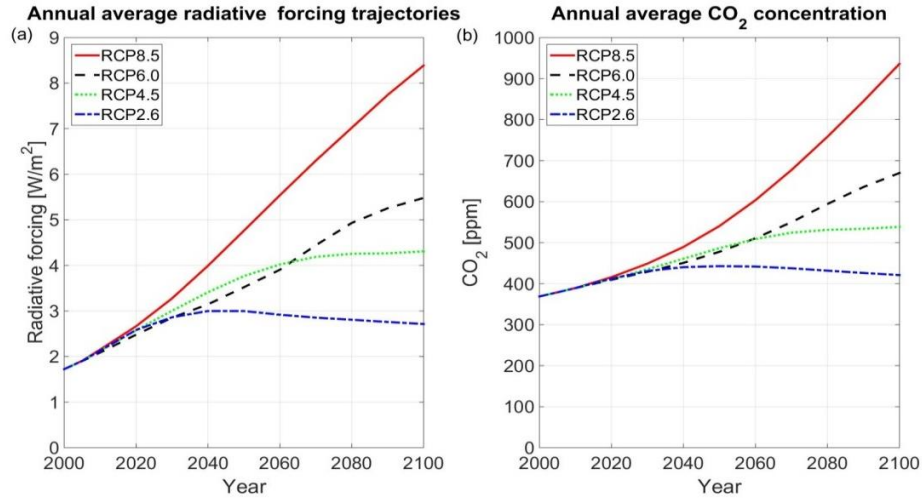

Figure 3.3: Radiative forcing and CO_2 concentration trajectories of RCPs

3.2 Climate models

According to section 2.1, the circulation of atmosphere is originally induced by the uneven distribution of solar radiation and temperature over the globe. When the global solar radiation changes as projected by climate scenarios, climate models are designed to simulate its impact on the atmosphere circulation and the interactions with other climate components.

The modelling technology of the climate system has been highly developed since last century. In 2008, the fifth phase of the Coupled Model Intercomparison Project (CMIP5) was proposed with the aim to examine climate "predictability" and to explore the ability of models

to "predict" climate on decadal time-scales [9]. The meeting involved about 20 climate research groups around the world with their different climate models. Basically, all the state-of-the-art global climate models (GCMs) are constructed by the fundamental physical laws (such as conservation of mass, energy and momentum) with many specific developments [10]. These models were designed to simulate the circulation of climate system for different specific purposes and may differ in parametrizations and numerical formulations. GCMs usually include atmospheric and ocean components. According to their design objective, some of them also include sea ice and land components as shown in Fig. 3.4 [11]. Many factors may affect the radiative forcing as discussed in section 2.2. For offshore engineering, more attentions should be paid on the emission of GHGs, because the greenhouse effect has a shorter time-scale (from decades to centuries). As there is a range of climate models in CMIP5, as listed in Table 3.2, it is hardly possible to give a detailed description of all these models. In the following part of this section, I only introduce the atmosphere model, because it is the key component in this study.

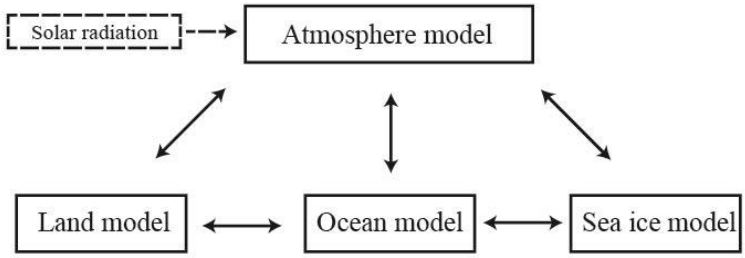

Figure 3.4: Climate component models. There are four climate components in the climate system. The emission of greenhouse gases affects the solar radiation and results in the climate change.

Table 3.2: Climate models in CMIP5

Model Name	Institute
ACCESS1.0	CSIRO (Commonwealth Scientific and Industrial Research
ACCESS1.3	Organization, Australia), and BOM (Bureau of Meteorology, Australia)
BCC-CSM	Beijing Climate Center, China Meteorological Administration
CMCC-CESM	Centro Euro-Mediterraneo per I Cambiamenti Climatici
CMCC-CM	
HadGEM2-A	Met Office Hadley Centre
INM-CM4	Institute for Numerical Mathematics
MRI-CGCM3	Meteorological Research Institute
NorESM1-M	Norwegian Climate Centre
…	…

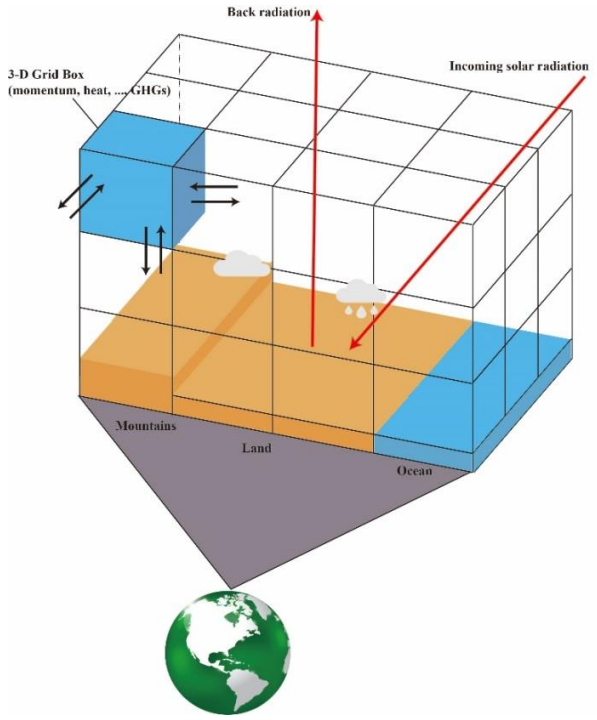

Figure 3.5: Illustration of an atmosphere model. The multiple vertical layers and horizontal grid result in multiple 3-D grid boxes [12].

An atmosphere model, also called atmospheric general circulation model (AGCM), is numerically designed to simulate a wide range of key atmospheric processes, such as the exchanges of momentum, heat, water, and other tracers [13]. These processes are described by integrating a variety of dynamical, chemical, or even biological equations derived from the fundamental physical laws including the fluid motion of air; conservation of mass, energy, and other properties; and gas laws covering the expansion and contraction of air. There are various variables in the equations, including temperature, pressure and surface wind speed [14]. The modelling atmosphere is divided into multiple vertical layers and horizontally meshed by grids along latitude and longitude lines, see Fig. 3.5. In the atmosphere models, the atmospheric momentum, heat, water, CO_2 and other atmospheric components are transferred both horizontally and vertically. For each 3D grid box, the flows of energy and mass are numerically simulated in consistence with the neighbouring grid boxes.

3.3 Wave models

Most ocean waves are generated by surface winds. With climate models, the atmospheric circulation in each layer is numerically simulated. The surface wind field, as part of the lower layer of atmosphere, is also modelled. Then, in order to describe the evolution of wave spectrum in each sea state, wind-driven wave models are designed to numerically simulate wind-wave interactions, nonlinear wave-wave interactions, and energy dissipation over a large or even global scale [15]. The driving force of wave models is the surface wind field. By

coupling climate models to wave models, it is feasible to simulate the climate change impact on ocean waves. In other words, the response of ocean surface to climate scenarios (*i.g.,* ocean waves) can be simulated by wave models. If the radiative forcing is changed, the wave simulations would also be affected.

The wave conditions are represented by wave spectra in wave modelling. Nowadays, the most widely used wind-driven wave models are ocean wave model (WAM), simulating waves nearshore model (SWAN), and WaveWatch-III (WW3) model. These models have been widely applied in coastal engineering [16], wave energy harvesting [17], wave forecasting and hindcasting [18]. All these wave models are constructed based on energy conservations. The wave spectra over a sea area are simultaneously calculated on Cartesian x,y-grids (the Eulerian approach), as demonstrated in Fig. 3.6.

In an idealized case where a constant wind (constant in space and time) is blowing over deep open water, the wave energy is locally balanced for each cell as:

$$change\ of\ energy\ in\ cell = net\ import\ of\ energy + local\ generation\ of\ energy$$

Since the group wave speed in deep water is independent of geographical locations, the spectral energy balance equation is as follows:

$$\frac{\partial E(k,\theta;x,y,t)}{\partial t} + c_{g,x}\frac{\partial E(k,\theta;x,y,t)}{\partial x} + c_{g,y}\frac{\partial E(k,\theta;x,y,t)}{\partial y} = S(k,\theta;x,y,t) \tag{3.1}$$

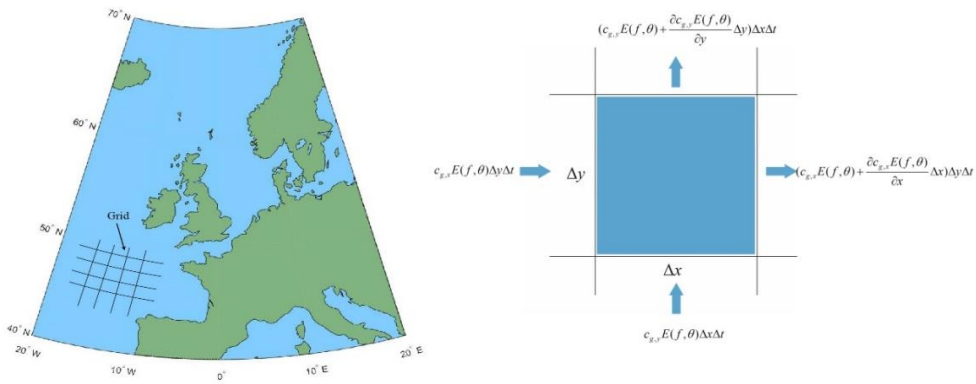

Figure 3.6: The energy propagation through one cell of the grid

In marine environment, ocean currents may also affect wave energy balance and make it no longer conserved, but wave action $\mathrm{N}(k,\theta;X,t) = \mathrm{E}(k,\theta;X,t)/\sigma$ is still conserved [19, 20]. If we consider the influence of ocean current U, the energy balance equation should be transferred into the spectral action balance equation as:

$$\frac{\partial N}{\partial t} + \nabla_x \cdot \dot{\boldsymbol{X}} N + \frac{\partial}{\partial k}\dot{\boldsymbol{k}} N + \frac{\partial}{\partial \theta}\dot{\boldsymbol{\theta}} N = \frac{S}{\sigma} \tag{3.2}$$

$$\dot{X} = \boldsymbol{c_g} + \boldsymbol{U} \tag{3.3}$$

$$\dot{\boldsymbol{k}} = -\frac{\partial \sigma}{\partial d}\frac{\partial d}{\partial s} - \boldsymbol{k}\cdot\frac{\partial \boldsymbol{U}}{\partial s} \tag{3.4}$$

$$\dot{\theta} = -\frac{1}{k}\left[\frac{\partial\sigma}{\partial d}\frac{\partial d}{\partial r} + \boldsymbol{k}\cdot\frac{\partial \boldsymbol{U}}{\partial r}\right] \tag{3.5}$$

$$\mathrm{S} = S_{in} + S_{nl} + S_{ds} + S_{bot} + S_{db} \tag{3.6}$$

where $\mathrm{N}(k,\theta;X,t)$ is the wave action density spectrum, $\mathrm{N}(k,\theta;X,t) = \mathrm{E}(k,\theta;X,t)/\sigma$, $\mathrm{E}(k,\theta;X,t)$ is wave variance spectrum, X stands for the geographical variables (x, y in Cartesian grids or λ, φ in longitude-latitude grids), $\boldsymbol{\sigma}$ is radian frequency, $\boldsymbol{U}$ and $\boldsymbol{c_g}$ are the vectors of current and wave group given by group speed c_g and wave direction θ, $\boldsymbol{k}$ is wave number vector, d is mean water depth, s is a coordinate in the direction θ, and r is a coordinate perpendicular to s. S is the source function. Eq. (3.2) represents the dispersion relation. In deep water, the source function includes three parts: wind-wave generation (S_{in}), nonlinear wave-wave interaction (S_{nl}) and dissipation by wave breaking (S_{ds}). In shallow water, wave-bottom interactions (S_{bot}) and depth-induced breaking (S_{db}) are also considered, as described in Eq. (3.5).

The lifecycle of waves consists of generation by wind, nonlinear wave-wave interactions, and dissipation. In these processes, the wave energy is transferred in/out and redistributed over spectrum [21]. When wind blows over sea water, the wind energy is transferred into waves. The wave energy transferred from wind mainly concentrate on the spectra peak frequency and on its high-frequency part, as shown in Fig. 3.7. As the waves propagate in deep water, the wave energy is redistributed from one wave component to another by resonance in Fig. 3.8. Two pairs of wave components fulfil the resonance conditions: $\vec{k}_1 + \vec{k}_2 = \vec{k}_3 + \vec{k}_4$ and then interact with each other. The wave energy is neither transferred in or out in this process. But a significant fraction of energy is transferred from middle frequency to the low-frequency part, and a small fraction is moved to high-frequency part of spectrum in Fig. 3.9. The last process is dissipation (white-capping) which is least understood. It is widely accepted the dissipation is very sensitive to wave steepness. Some researchers believed that the dissipation can be seen as the mirror-image of wind-induced growth: the wave lose energy by dissipation like an inverse process of the wave generation by wind, see Fig. 3.10 [21]. In summary, waves are receiving energy from winds which occurs on its middle and high frequency parts of spectrum. Then, the wave energy in the middle is transferred towards the low and high frequency sides via wave-wave interactions. They lose net energy in the middle frequency domain due to dissipation, and the net energy on the high frequency part is in equilibrium. As the growth of waves under a constant wind, the spectra are getting more and more energy on the low frequencies, and the peak frequencies are moving downwards (to the low frequency part), as shown in Fig. 3.11.

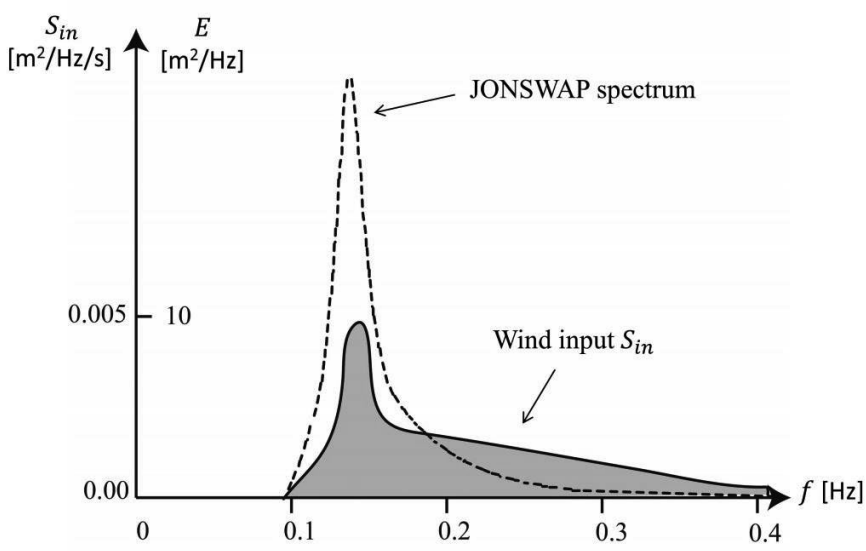

Figure 3.7: The wind input source term in deep water for H_m =3.5 m, T_p =7 s and U_{10}=20 m/s [22, 23]

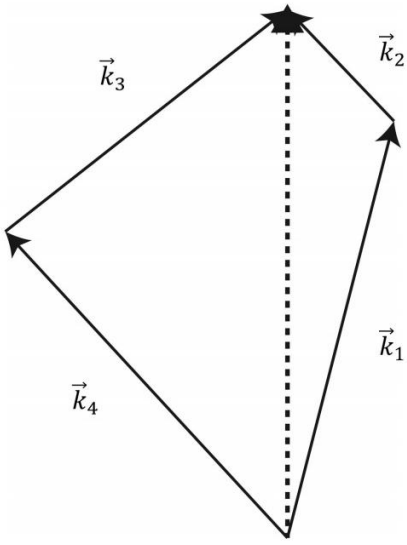

Figure 3.8: Quadruplet wave-wave interactions through resonance. The resonance conditions: $\vec{k}_1 + \vec{k}_2 = \vec{k}_3 + \vec{k}_4$

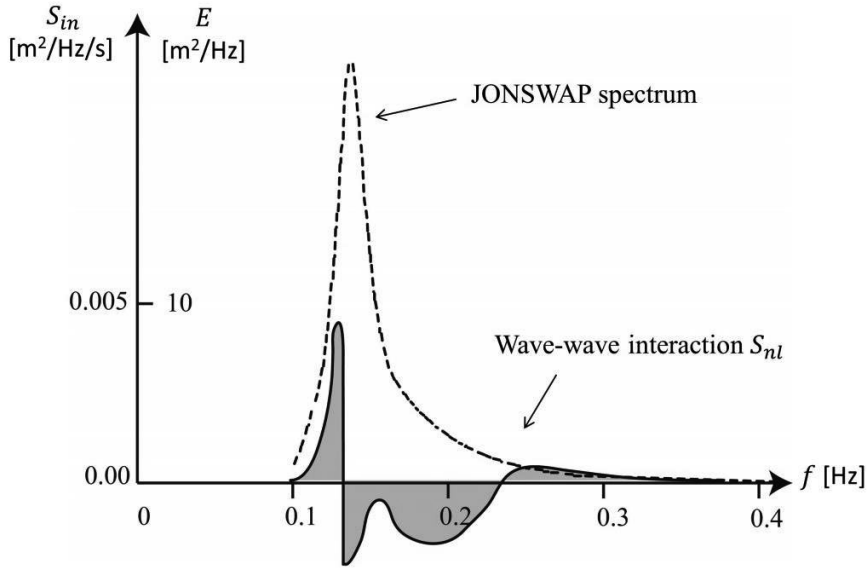

Figure 3.9: The source term for quadruplet wave-wave interactions in deep water for H_m=3.5 m and T_p=7 s [24, 25]

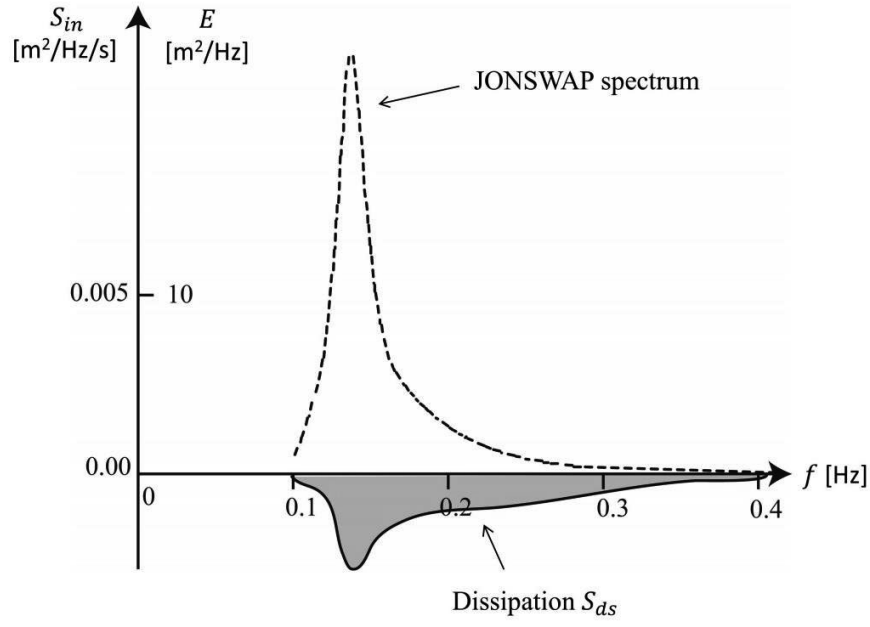

Figure 3.10: The source term for dissipation in deep water for H_m=3.5 m and T_p=7 s [26]

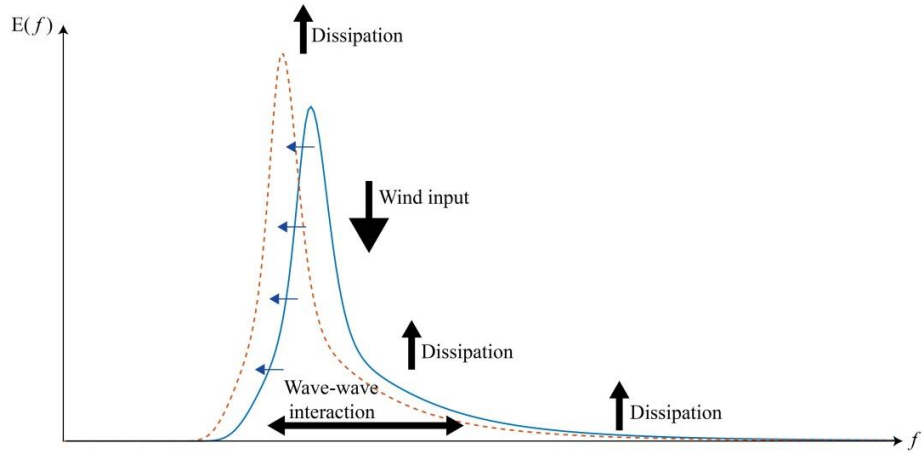

Figure 3.11: The energy flow in the evolution of JONSWAP spectrum [21]

3.4 The comparison of climate models and validation of wave models

Since climate models in CMIP5 were designed for different purposes, a high performance of GCMs for climate simulations does not imply high performance for wind-driven wave simulations [27]. It is hence necessary to compare their abilities to simulate wind fields, and to select the most proper one for fatigue calculations. According to RCP8.5, there are ten climate models available from CMIP5. Among them, ACCESS1.0, ACCESS1.3, CMCC-CM and MRI-CGCM3 are preliminarily selected, because they have finer grid resolutions, as listed in Table 3.3.

Table 3.3: The grid resolutions of climate models

Model Name	Atmospheric Grid Size	
	Latitude	Longitude
ACCESS1.0	1.25°	1.875°
ACCESS1.3	1.25°	1.875°
CMCC-CM	0.75°	0.75°
MRI-CGCM3	1.12°	1.125°

The global wind data simulated by these climate models were obtained from the CMIP5 database. The 10m-height annual wind speed from 2006 to 2015 was compared with ERA-interim dataset. In this study, ERA-interim data[1] are considered as the "true" data due to the lack of measured wind and wave data. ERA-Interim project is a global atmospheric reanalysis project covering the period from 1979 to the present [28, 29]. This project can provide plenty of atmospheric data including 10m-height wind data with 1.0°×1.0° latitude/longitude grid and

[1] More information about ERA-interim is listed in website: https://www.ecmwf.int/en/research/climate-reanalysis/era-interim

6-hourly interval. It is using WAM to simulate the global waves with the same resolution [15]

For offshore structures, they are subjected to local environmental loadings rather than global averaged loadings. Hence, I conducted the comparison of climate models with ERA-interim in a specific oil field, the Sable field located in offshore South Africa (35.21°S, 21.32°E). The annual wind speed (the averaged value of wind speed over each year) from these four climate models was compared with the ERA-interim dataset as shown in Table 3.4 and Fig. 3.12. The averaged wind speed and standard deviation (SD) of these four climate models are all very close to ERA-interim. The maximum difference of wind speed is 0.79 m/s for MRI-CGCM3, and the minimum difference is 0.47 m/s for ACCESS1.3. Compared with ERA-interim, each climate model tends to underestimate or overestimate continuously. CMCC-CM is the only climate model which overestimated the wind speed for the decade. In contrast, the annual wind speeds of the other three models are always below ERA-interim. This result is consistent with the comparison of the cumulative probability distributions in Fig. 3.13. In addition, the wind speed distributions from ERA-interim and the climate models were compared by the quantile-quantile plot (Q-Q plot), see Fig. 3.14. The wind speed distributions of ACCESS1.0 and CMCC-CM are linearly related to the distribution of ERA-interim, because the points in the Q-Q plot are falling in a straight reference line, as shown in Fig. 3.14a and Fig. 3.14d. Similarly, most of the points in Fig. 3.14b and Fig. 3.14c also fall in a straight line, but they start to deviate from the straight line at high values. It indicates that the wind speed distributions of ACCESS1.3 and MRI-CGCM3 have a heavy or light right tail. In addition, the reference line (red line) in Fig. 3.14d is slightly steeper than the 45-degree straight line (black line). Therefore, the CMCC-CM distribution is more dispersed than the distribution of ERA-interim. Conversely, the distributions of the other climate models are less dispersed than ERA-interim.

After comparison, all these four models showed the comparable results. Their performances on wind field simulations are not significantly different. As mentioned above, all these climate models were designed for different spatial regions or research purposes. For further research, it is recommended to design or develop climate models with specific schemes. These schemes should enable the climate models to simulate the surface wind field data with the same distributions of wind speed as the local measurement. In this following study, wind data from CMCC-CM are selected to drive wave simulations, because the grid resolution of CMCC-CM wind data is equal to the grid resolution of the wave simulations in the following sections..

Table 3.4: The comparison of averaged wind speed from 2006 to 2015

	ERA-Interim	ACCESS1.0	ACCESS1.3	CMCC-CM	MRI-CGCM3
Wind speed [m/s]	7.10	6.33	6.63	7.88	6.31
SD [m/s]	0.25	0.23	0.21	0.25	0.28

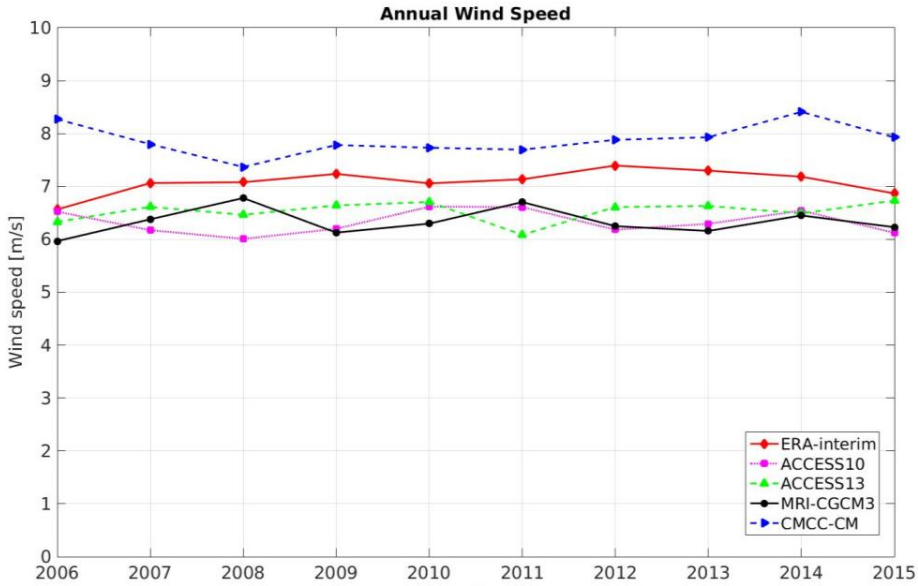

Figure 3.12: The comparison of annual wind speed from 2006 to 2015 at Sable field

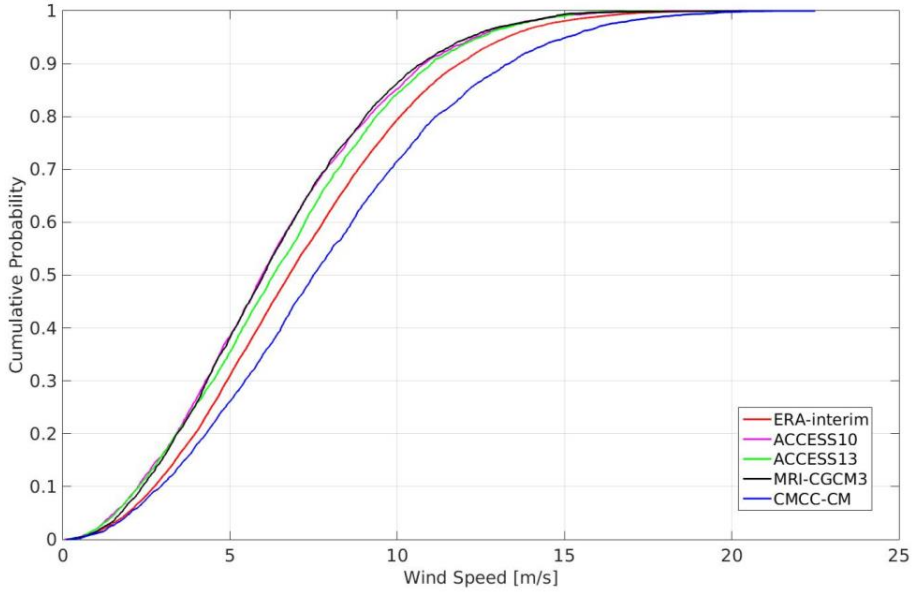

Figure 3.13: The cumulative probability of wind speed at Sable field

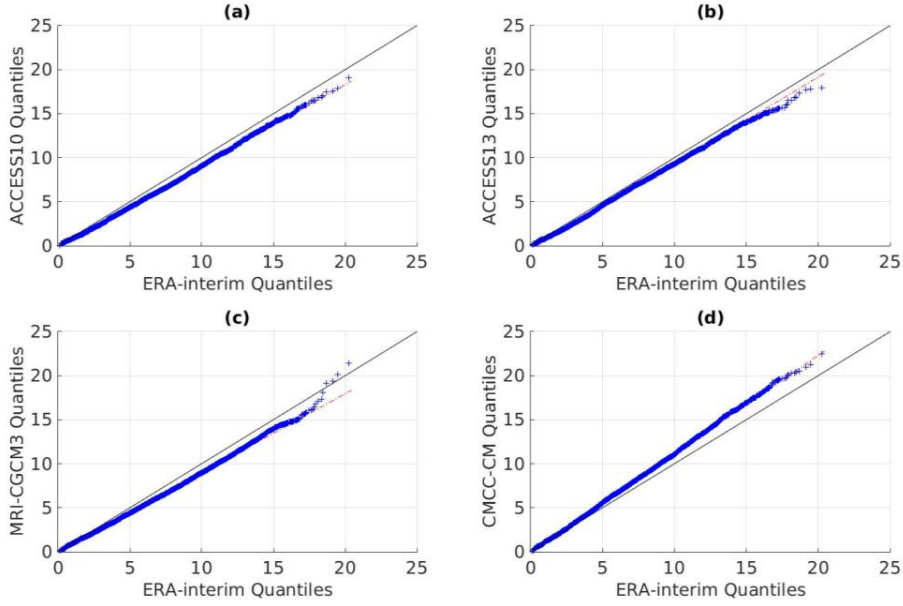

Figure 3.14: Q-Q plot of wind speed data from ERA-interim and climate models

After the comparison of climate models, it is also necessary to validate the wave model's ability to simulate wave conditions. In this study, I use WaveWatch-III to simulate ocean surface. WaveWatch-III is the third generation wave model developed at NOAA/NCEP [30]. A large scale or even global wave simulation is required to simulate all the waves in the Sable field, because the Sable field is located between the Atlantic and Indian Ocean, as shown in Fig. 3.15. Global simulations can ensure that all the swells generated in remote sea areas could propagate into the Sable field. The output of the wave model is 6-hourly JONSWAP wave spectra defined for 24 directions (i.e. every 15°) and 25 frequencies ranging from 0.042 Hz to 0.414 Hz. The JONSWAP is defined as Eqs. (3.7) and (3.8) [31]:

$$E(f) = \frac{5}{16} \cdot H_s^2 f_p^4 \cdot f^{-5} \cdot exp\left[-\frac{5}{4}\left(\frac{f}{f_p}\right)^{-4}\right] \cdot \gamma^{exp\left[-0.5\left(\frac{f-f_p}{\sigma f_p}\right)^2\right]} \tag{3.7}$$

$$f = \frac{2\pi}{T_p} \tag{3.8}$$

where:

$E(f)$: Wave spectrum

H_s : Significant wave height

f_p : Peak wave frequency

T_p : Peak wave period

σ : Spectral width parameter

γ : Non-dimensional peak shape parameter. The average value is 3.3.

The spatial resolution of grids in the model is $0.75° \times 0.75°$ Latitude/Longitude with the global time step 3600 seconds. The wave condition at each spatial grid was partitioned into two wave systems (wind waves and swells). The global topographic and bathymetric data ETOPO1 were obtained from National Centers for Environmental Information, NOAA, U.S. Department of Commerce with the resolution of 1 arc-minute [32].

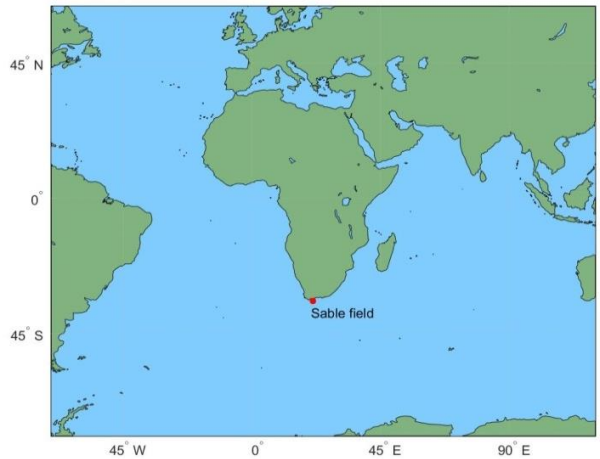

Figure 3.15: The South Atlantic and Indian oceans. The wave modelling area covers a rectangular region of 70°S-60°N/70°W-120°E Latitude/Longitude to consider the remote swells.

The sea states from 2006 to 2015 in the Sable field were simulated based on the wind data from CMCC-CM. The results were compared with ERA-interim wave data. The wave height trajectories of CMCC-CM and ERA-interim are rather close as shown in Fig. 3.16. The averaged significant wave height (the averaged value of significant wave height over years) of CMCC-CM is only 4% higher than the wave height of ERA-interim. Table 3.5 lists the averaged significant wave height ($\overline{H_s}$), SD and coefficient of variation (CV). The slight overestimate of wave height is consistent with the overestimate of wind speed by CMCC-CM.

Table 3.5: Annual significant wave heights from 2006 to 2015 at Sable field

	$\overline{H_s}$ [m]	SD [m]	CV
CMCC-CM	2.67	0.09	0.03
ERA-interim	2.56	0.10	0.04

In the thesis, all the projected climate simulations are conducted by CMCC-CM with one single ensemble under RCP8.5. Hence, there is no assessment of internal model uncertainty in these simulations. In fact, there are a large number of uncertainties involved in the climate and wave simulations. I will further discuss them in Chapter 5.

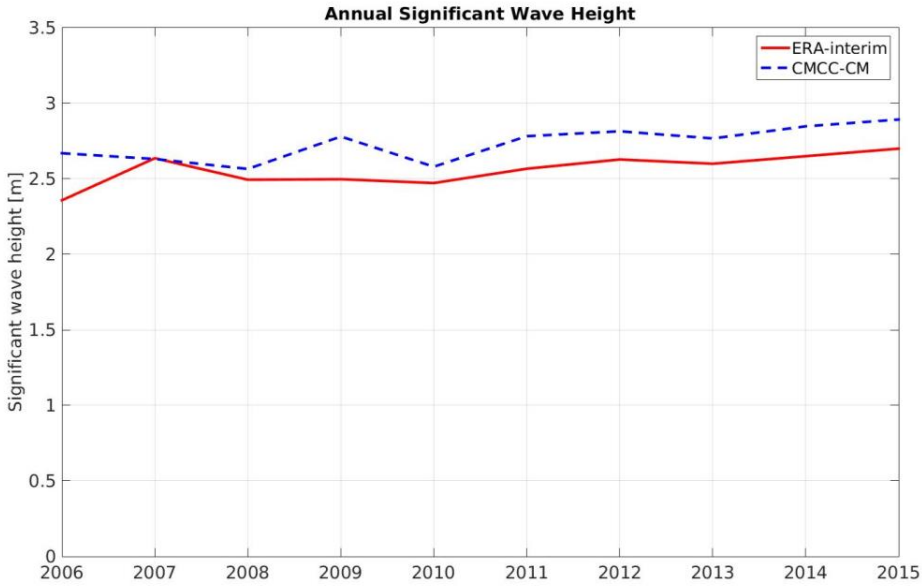

Figure 3.16: The comparison of annual significant wave height from 2006 to 2015

3.5 Projection of climate change impact on wave conditions

According to section 2.1, the effect of climate change is region-dependent. Hence, oil fields in two sea areas are selected to project wave conditions and construct the time series of sea states. One sea area is offshore South Africa; the other is the North Sea. The detailed settings of all the projected simulations in this Chapter are listed in Table 3.6.

Table 3.6: Settings of all the projected simulations

Climate model	CMCC-CM
Climate scenario	RCP8.5
Spatial resolution	0.75°×0.75° (latitude/longitude)
Ensemble	r1i1p1
Time frequency of wind data	6 hours
Wave model	WaveWatch-III (version 4.18)
Spatial resolution	0.75°×0.75° (latitude/longitude)
Time step (global, spatial, directional and source term)	3600 s, 1200 s, 1800 s, 300 s
Bathymetry	ETOPO1
Direction number	24 (i.e. every 15°)
Frequencies range	0.042 Hz to 0.414 Hz

3.5.1 Offshore South Africa

The Sable field is located 95 km off the southern coast of South Africa. Based on RCP8.5, the global surface wind data in the wave modelling area for decades 2011-2020 (present decade), 2051-2060 (near future decade) and 2091-2100 (far future decade) were obtained from CMCC-CM [33]. The gap between these two periods is 30 years, which is equal to the service lifetime of offshore structures.

The wave conditions over the South Atlantic and Indian oceans were projected by WaveWatch-III. This process is called "projected simulations", because the radiative forcing is projected by climate scenarios. The averaged significant wave heights of these three decades are very close to each other, as listed in Table 3.7; the difference is less than 0.01 m. Annual significant wave height of future decades is neither continuously higher or lower than wave height of present decade, as shown in Fig. 3.17. Hence, the annual significant wave height is neither increasing nor decreasing continuously over time in the Sable field.

Table 3.7: Averaged annual significant wave heights in 2011-2020, 2051-2060 and 2091-2100

	$\overline{H_s}$ [m]	SD [m]	CV
2011-2020	2.82	0.07	0.02
2051-2060	2.81	0.09	0.03
2091-2100	2.81	0.07	0.03

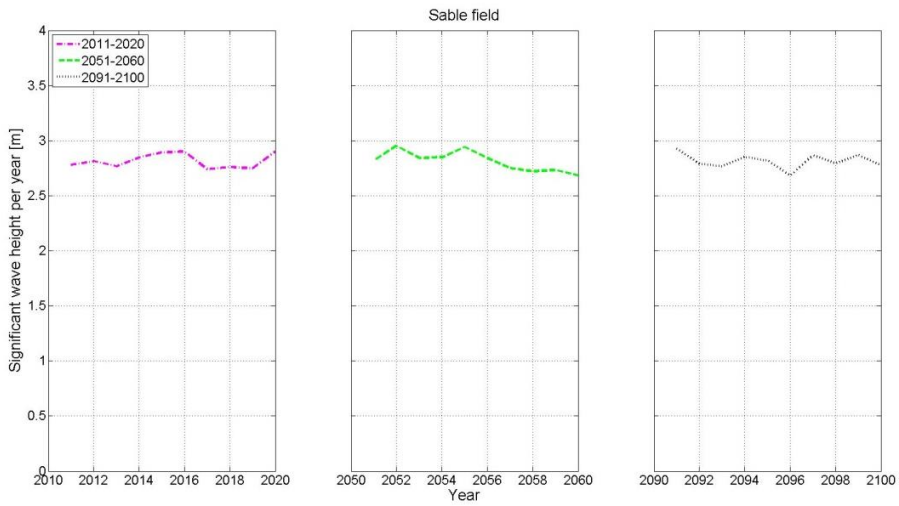

Figure 3.17: The annual significant wave height in 2011-2020, 2051-2060 and 2091-2100

3.5.2 North Sea

The North Sea is a mature oil and gas producing region. The exploitation of the North Sea oil reserves began in the 1970's. Due to its high oil quality and the political stability, a lot of oil fields have been discovered and exploited. With the decrease of output in shallow oil fields however, more oil fields in deep water are exploited, which requires more floating offshore structures. In this study, three North Sea oil fields were selected, Rosebank, Alma/Galia and Pierce, see Fig. 3.18, to evaluate the climate change impact on their wave conditions. The oil fields Alma/Galia (56.2°N; 2.8°E) and Pierce (58°N; 1.45°E) are both in the central North Sea with a water depth of approximately 100 meters. Rosebank oil field (61°N; 4°W) is located North-West of the Shetland Islands with a water depth of approximately 1100 meters.

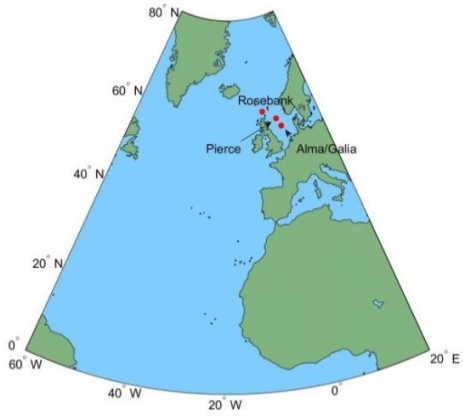

Figure 3.18: The North Atlantic. The wave modelling area covers a rectangular region of 0°-80°N/60°W-20°E Latitude/Longitude to consider the remote swells

With the wind driving force from CMCC-CM, the sea states in the North Atlantic were also projected by WaveWatch-III. Then, the annual H_s in the selected oil fields were calculated. There is a downward trend of annual H_s over time in all three oil fields as shown in Fig. 3.19. The H_s decreased by approximately 0.5 meter from 2011 to 2100. Considering that the North Sea is a wind-wave-dominated sea area, this decrease is in agreement with the earlier findings [7, 34-40]. These earlier findings reveal that the overall wind speed in the North Sea is decreasing with the emission of GHGs over time. Furthermore, the results indicate that the averaged wave height of Rosebank oil field under projected simulations is higher than the other oil fields. As the distance between Alma/Galia and Pierce oil fields is not very far, their averaged wave heights are relatively close to each other, as listed in Table 3.8. Rosebank has the highest wave height, because it is more vulnerable to waves from the Atlantic Ocean.

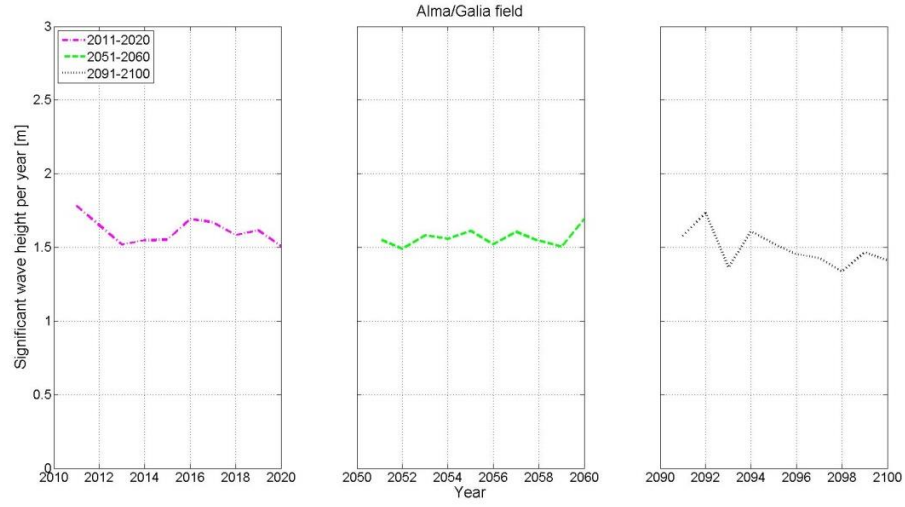
Alma/Galia field
2011-2020
2051-2060
2091-2100
Significant wave height per year [m]
Year

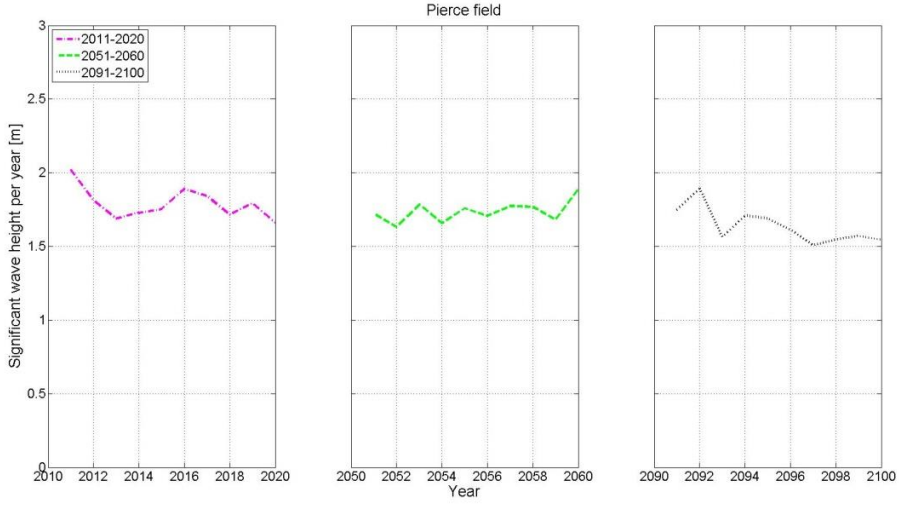
Pierce field
2011-2020
2051-2060
2091-2100
Significant wave height per year [m]
Year

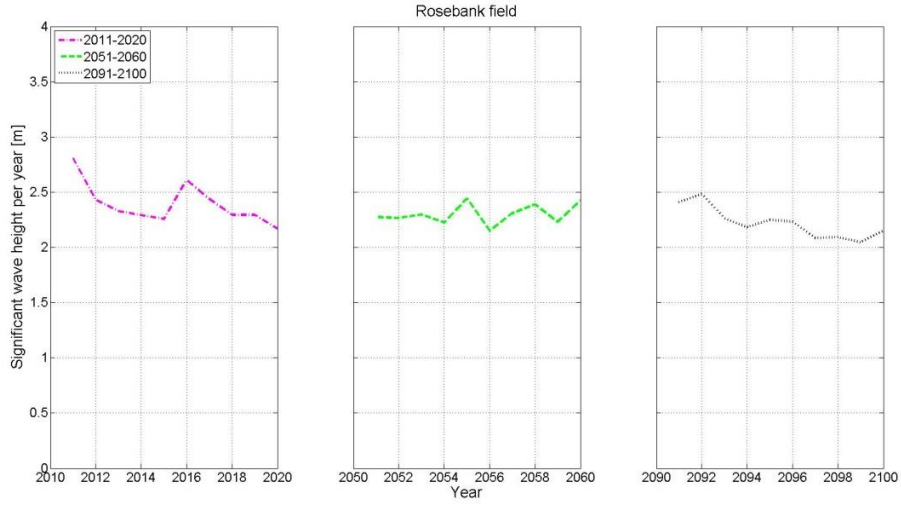

Figure 3.19: Variability of annual significant wave height at the selected oil fields.

Table 3.8: Statistical characteristics of waves under the projected simulations

Oil field	Time	Mean	Standard deviation	*CV**
Unit	-	m	m	-
Rosebank	2011-2020	2.39	0.19	0.08
	2051-2060	2.30	0.09	0.04
	2091-2100	2.22	0.14	0.06
Alma/Galia	2011-2020	1.61	0.09	0.06
	2051-2060	1.57	0.06	0.04
	2091-2100	1.49	0.12	0.08
Pierce	2011-2020	1.79	0.11	0.06
	2051-2060	1.74	0.07	0.04
	2091-2100	1.64	0.12	0.07

***** Coefficient of variation expresses the extent of variability in relation to mean value. A higher *CV* stands for a higher variation.

3.6 Projection of climate change impact on fatigue damage

In section 3.5, the 6-hourly sea states in the Sable field and three oil fields in the North Sea for decades 2011-2020, 2051-2060 and 2091-2100 were simulated by coupling WW3 to

CMCC-CM. In this section, the annual fatigue damages were calculated based on the time series of these sea states. The projections of fatigue damage were carried out for the FPSO-Glas Dowr. Glas Dowr is a converted FPSO owned by Bluewater. The main characteristics of the Glas Dowr FPSO are presented in Table 3.9. The fatigue damages in the main deck of Glas Dowr (at frame 66½ above decks longitudinal #22, see location 1 in Fig. 3.20) were calculated by the conventional spectral fatigue calculation method [31, 41]. The one-slope S-N curve with m=3.0 and log(C) =12.44 (stress in MPa) was used to represent the fatigue resistance of Glas Dowr (The curve IV in Fig. 3.21).

Table 3.9: Main characteristics of the Glas Dowr FPSO[2]

Displacement	121,400 metric tons	Depth	21.2 m
Length	232 m	Midship Draft	12.99 m
Breadth	42 m		

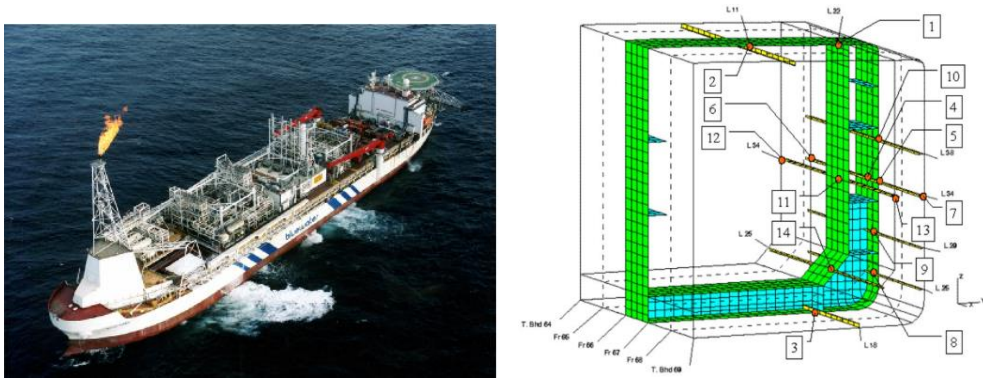

Figure 3.20: FPSO-Glas Dowr and its midship section [42]

In the spectral method, the long-term fatigue damage is the sum of all the short-term fatigue damage corresponding to short-term sea states. The wave spectra in sea states are defined applying JONSWAP spectra, and the wave-induced stress is defined following Rayleigh distributions. Then, the fatigue damage is calculated by Eq. (2.1).

The structural responses to wave loadings are calculated via stress transfer functions, which express the relation between the wave loadings and stress responses at a specific location of vessels[3] (Fig. 3.22). The vessel of FPSO is represented by a simple beam model. There are four loading mechanisms in this simple beam model: overall vertical and horizontal bending of the vessel, and local bending of secondary stiffeners caused by external action of waves and internal tank pressure fluctuations induced by varying motions of the FPSO. Therefore, the response spectrum of vessels can be directly calculated as Eq. (2.2).

[2] The structural characteristics of Glas Dowr was provided by Bluewater

[3] The stress transfer function of FPSO-Glas Dowr at the midship is provided by Bluewater.

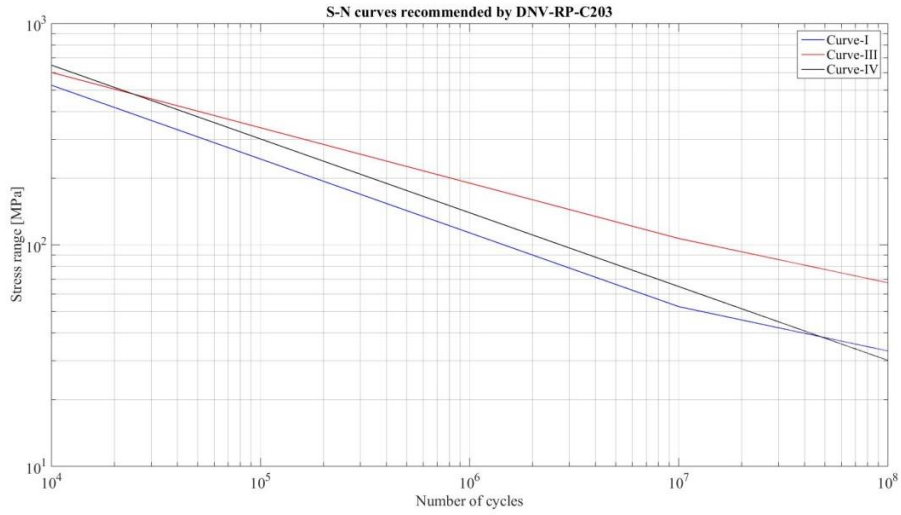

Figure 3.21: S-N curves. They are used to represent the fatigue resistance of structures.

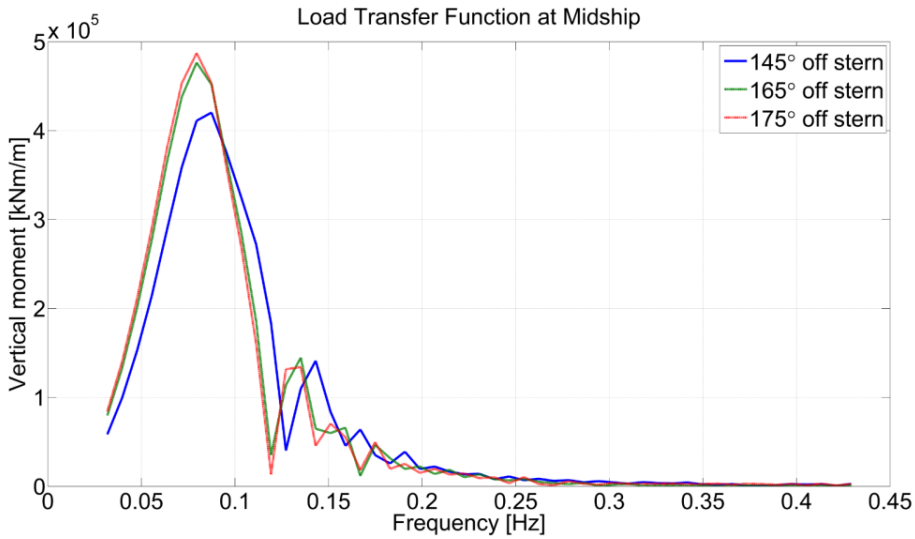

Figure 3.22: Response amplitude operators (RAO, load transfer functions) of midship vertical bending moment

Each sea state consists of one or more wave systems (one wind wave and multiple swells). In this study, each wave system is represented by JONSWAP characterized by significant wave height (H_s), zero-crossing wave period (T_z) and relative wave directions. Since Glas Dowr is a turret moored FPSO, it can rotate the vessel heading to a stable direction against environmental loadings. The relative wave direction was calculated in two steps. First, each wave system was represented by a vector. The mean wave direction θ_m of each vector is

defined as the energy weighted mean direction over all frequencies [43]:

$$\theta_m = \text{atan}\left(\frac{b}{a}\right) \tag{3.9}$$

$$a = \int_0^{2\pi}\int_0^{\infty} \cos(\theta)\, F(\sigma,\theta) d\sigma d\theta \tag{3.10}$$

$$b = \int_0^{2\pi}\int_0^{\infty} \sin(\theta)\, F(\sigma,\theta) d\sigma d\theta \tag{3.11}$$

where $F(\sigma,\theta)$ is the wave spectral density. The length of each vector was proportional to the energy contained in each wave system. In the second step, the heading analysis was conducted by considering the forces from both wind and waves in order to keep the vessel in a stable position [44]. Once the vessel heading is known, the relative wave directions α, β, and γ can be calculated as illustrated in Fig. 3.23.

In section 3.5, I projected the sea states in four oil & gas fields and constructed the time series of sea states for the three decades. In the following sections, the annual fatigue damages are calculated.

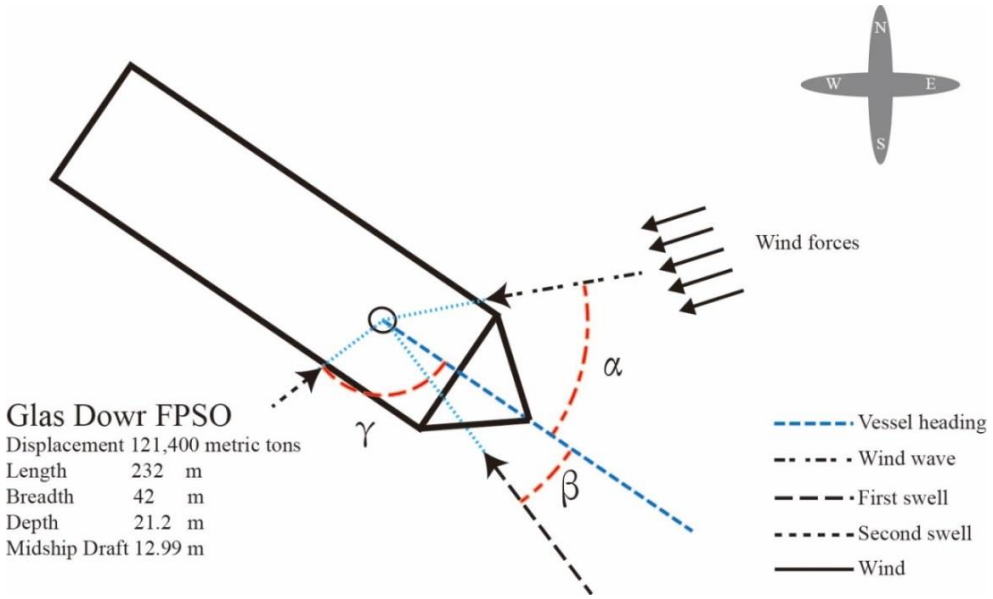

Figure 3.23: Relative directions of wave systems and calculation of the vessel heading. The relative wave directions α, β, and γ are calculated clockwise.

3.6.1 Offshore South Africa

In this section, the annual fatigue damage in the Sable filed was investigated. There is no significant trend of annual fatigue damage as shown in Fig. 3.24. The averaged fatigue damages (the averaged value of annual fatigue damage within a certain period) in the three projected decades (2011-2020, 2051-2060 and 2091-2100) are very close to each other, and there is a slight decreasing trend which can be neglected, as listed in Table 3.10. The coefficient of variation for the annual fatigue damage (0.15, 0.16 and 0.11) is much higher than the coefficient of variation for wave height (0.02, 0.03 and 0.03), because the fatigue

damage is approximately proportional to the third power of significant wave height in linear models. This indicates that the annual fatigue damage has more variability than the annual significant wave height.

In order to validate the projected simulations, fatigue damage based on buoy-measurement was calculated for comparison. The sea state data in the Sable field were measured by buoys from July 2007 to June 2008 [45]. The fatigue damage in these 12 months was calculated as a reference value, see Table 3.10. It is lower than the averaged fatigue damage in the present decade and future decade. However, due to the existence of random natural variability, it does not mean that the methodology overestimates the annual fatigue damage. In fact, the projection of sea states for a particular year should not necessarily match buoy measurements due to both natural variability and the uncertainties in numerical models. The methodology is more useful to evaluate the trend of sea states and the cumulated fatigue damage over a long-term period. In Table 3.10, there is a slight decreasing trend of averaged fatigue damage over time, and the differences of averaged fatigue damage between neighbouring periods are less than half of the standard deviation. Hence, this decreasing trend is not pronounced, and may be induced by the randomness in the modelling.

Table 3.10: Annual fatigue damages in 2011-2020, 2051-2060 and 2091-2100

Period	Averaged fatigue damage $[\times 10^{-3}]$	SD $[\times 10^{-3}]$	CV
2011-2020	8.06	1.18	0.15
2051-2060	7.93	1.30	0.16
2091-2100	7.82	0.82	0.11
Buoy 07/2007-06/2008	6.20	-	-

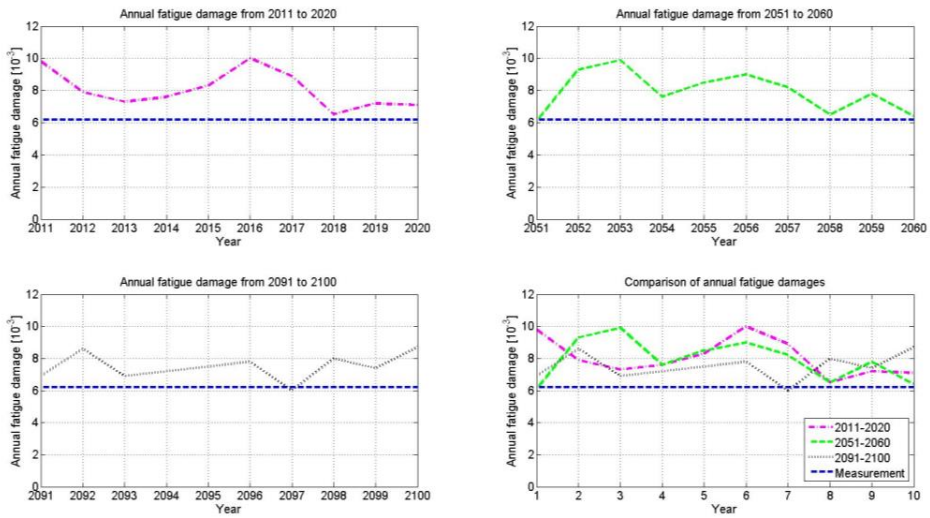

Figure 3.24: Projected annual fatigue damages in the Sable field. The fatigue damages of each decade are represented by different colors. The dotted straight line is the reference value of annual fatigue damage calculated based on the buoy-measurements in 07/2007-06/2008.

3.6.2 North Sea

The annual fatigue damages in the oil fields of North Sea were also calculated using the sea states from projected simulations. All these three oil fields show a decreasing trend of annual fatigue damage over time as shown in Fig. 3.25-3.27 and Table 3.11. This trend is consistent with the trend of significant wave height. Based on the similar trends in these three oil fields, I can preliminarily conclude that the sea states in the North Sea are becoming milder and the annual fatigue damage is decreasing. The sea states in Rosebank are the severest, which result in the highest fatigue damage. The fatigue damages in the other two fields are much lower, because they are less vulnerable to the swells from the North Atlantic. Clearly, the composition of mixed waves (the proportion of wind wave and swells) is dependent on the location. Different compositions may affect both the amount of climate change and its deceasing rate.

The reference value of annual fatigue damage is calculated based on the bouy-measured wave data in Doggerbank (55.343°N/2.5°E), as listed in Table 3.11. These wave data were measured from 1997 to 2006 by every 6 hours. They are part of the WorldWaves database [46].

Table 3.11: Comparison of annual fatigue damage in three oil fields

Oil field	Time	Mean	Standard deviation	CV
Unit	-	$\times 10^{-3}$	$\times 10^{-3}$	-
Rosebank	2011-2020	5.35	1.95	0.36
	2051-2060	4.61	0.78	0.17
	2091-2100	3.88	1.12	0.29
Alma/Galia	2011-2020	0.78	0.40	0.51
	2051-2060	0.81	0.27	0.33
	2091-2100	0.56	0.21	0.38
Pierce	2011-2020	1.36	0.44	0.33
	2051-2060	1.40	0.38	0.27
	2091-2100	1.10	0.27	0.25
Measurement*	1997-2006	2.64	-	-

*The buoy data were measured and provided by Boskalis in Doggerbank field (55.343°N/2.5°E). It is part of the WorldWaves database. It was measured from 1997 to 2006 by every 6 hours.

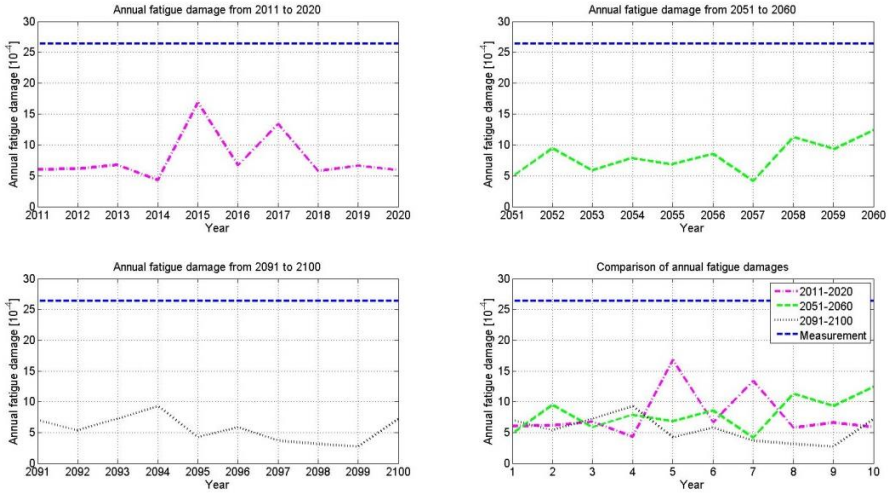

Figure 3.25: Projected annual fatigue damages in the Alma/Galia field. The fatigue damages of each decade are represented by different colors. The blue dotted straight line is the reference value of averaged annual fatigue damage calculated based on the buoy-measurements in the period 1997-2006.

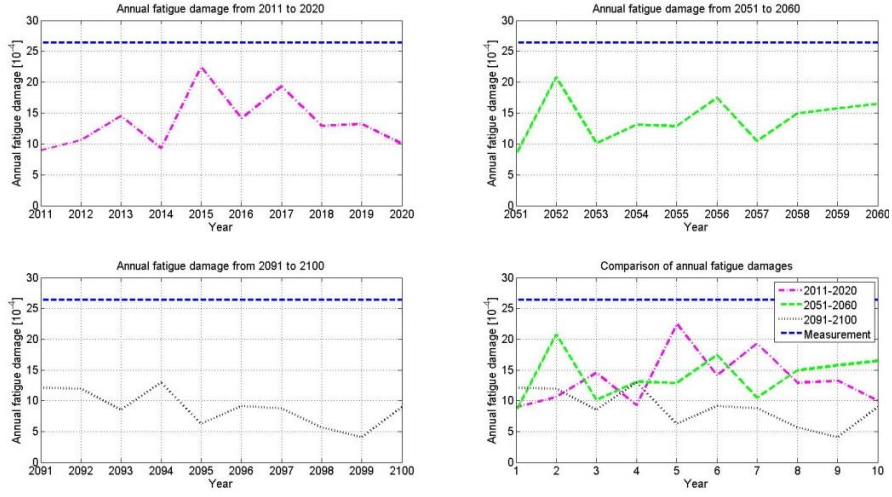

Figure 3.26: Projected annual fatigue damages in the Pierce field. The fatigue damages of each decade are represented by different colors. The blue dotted straight line is the reference value of averaged annual fatigue damage calculated based on the buoy-measurements in the period 1997-2006.

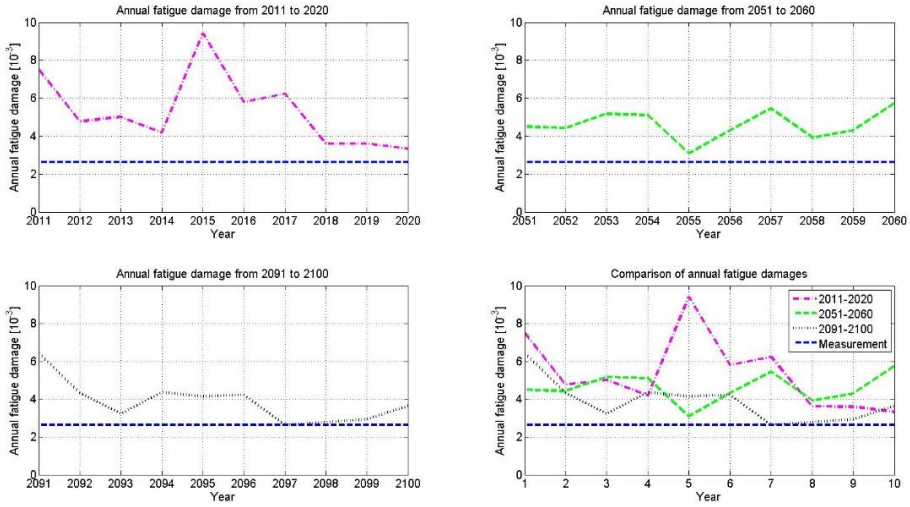

Figure 3.27: Projected annual fatigue damages in the Rosebank field. The fatigue damages of each decade are represented by different colors. The blue dotted straight line is the reference value of averaged annual fatigue damage calculated based on the buoy-measurements in the period 1997-2006.

The averaged annual fatigue damage is plotted as the blue straight lines in Fig. 3.25-3.27. It is between the fatigue damages of Rosebank and the other two fields. The amount of reference fatigue damage is consistent with the discussion above. It is lower than the fatigue of Rosebank, because Doggerbank is also less subjected to swells from the North Atlantic. Its location is close to Alma/Galia and Pierce fields (Fig. 3.28). Their wave climates should be rather similar. The wave data in Doggerbank however were measured ten or twenty years ago. According to the decreasing trend in the North Sea, there is no surprise that the reference annual fatigue damage is higher than the projected damage in the present or future decades.

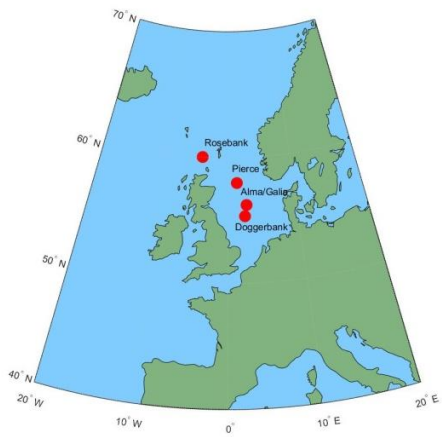

Figure 3.28: The locations of oil fields in the North Sea

3.7 Conclusions

In this Chapter, I demonstrated the methodology which can project the effect of climate change on future fatigue damage. The circulation of climate system and wave conditions were simulated numerically based on the mechanics of climate change. The radiative driving forcing of climate system was projected by the climate scenario RCP8.5, which is characterized by increasing GHGs and radiative forcing level. Climate scenarios are not the accurate predictions of the future climate. Instead, each of them represents one possibility of the future climate condition based on a set of prior expectations. Plenty of climate models were presented to simulate the circulation of climate system and the interactions between climate components, but they were designed for different specific purposes. Hence, before projecting climate and wave conditions, four climate models were compared with ERA-interim data to find out the most suitable model for fatigue assessment. As a result, CMCC-CM was selected to simulate the global surface wind fields in three decadal periods (2011-2020, 2051-2060 and 2091-2100). The wind-driven wave model WaveWatch-III was validated and used to simulate the evolution of wave spectrum over a large spatial scale, including wave generations, propagations, and dissipation. The 6-hourly sea states were projected in four offshore oil fields: one is the Sable field, offshore South Africa; the others are the Rosebank, Alma/Galia and Pierce in the North Sea. The time series of sea states for each year were constructed, and the annual fatigue damage of the FPSO Glas Dowr was finally calculated by spectral approach.

According to the results, there are no continuously increasing or decreasing trends of significant wave height and annual fatigue damage in the Sable field. In contrast, both of them are decreasing in the North Sea with the high emission of GHGs. It is concluded that the effect of climate change on fatigue damage is dependent on geographic locations. The geographic characteristics of each location may significantly affect the evolution of waves. Therefore, in the fatigue design, it is necessary to investigate the climate change impact on sea states in the specific oil field where the offshore structures will operate.

In addition, the effect of climate change is the combination of both human-induced climate change and natural variability. It is still not clear whether the trends of climate change in these oil fields are mainly attributed to GHG emissions or non-linear interactions between climate components. In the next chapter, the control simulations are conducted to detect the contributions of human activities and non-linear interactions to the climate change consequences.

References

[1] Zou T, Kaminski ML. Applicability of WaveWatch-III wave model to fatigue assessment of offshore floating structures. *Ocean Dynamics*. 2016; 66:1099-1108.

[2] van Vuuren DP, Edmonds J, Kainuma M, Riahi K, Thomson A, Hibbard K, et al. The representative concentration pathways: an overview. *Climatic Change*. 2011; 109:5.

[3] Moss RH, Nakicenovic N, O'Neill BC. *Towards New Scenarios for Analysis of Emissions, Climate Change, Impacts, and Response Strategies*. Geneva: IPCC; 2008.

[4] Moss RH, Edmonds JA, Hibbard KA, Manning MR, Rose SK, van Vuuren DP, et al. The next generation of scenarios for climate change research and assessment. *Nature*. 2010; 463:747-56.

[5] Fisher Srt. Issues related to mitigation in the long term context, In Climate Change 2007: Mitigation. Contribution of Working Group III to the Fourth Assessment Report of the Inter-governmental. 2007.

[6] Van Vuuren DP, Riahi K. The relationship between short-term emissions and long-term concentration targets. *Climatic Change*. 2011; 104:793-801.

[7] Gallagher S, Gleeson E, Tiron R, McGrath R, Dias F. Twenty-first century wave climate projections for Ireland and surface winds in the North Atlantic Ocean. *Advances in Science and Research*. 2016; 13:75-80.

[8] Erikson LH, Hegermiller CA, Barnard PL, Ruggiero P, van Ormondt M. Projected wave conditions in the Eastern North Pacific under the influence of two CMIP5 climate scenarios. *Ocean Modelling*. 2015; 96:171-185.

[9] Taylor KE, Stouffer RJ, Meehl GA. An Overview of CMIP5 and the Experiment Design. *Bulletin of the American Meteorological Society*. 2012; 93:485-98.

[10] Solomon S, Qin D, Manning M, Chen Z, Marquis M, Averyt KB, et al. Climate Change 2007: The Physical Science Basis. Contribution of Working Group I to the Fourth Assessment Report of the Intergovernmental Panel on Climate Change. IPCC; 2007.

[11] Wu T, Song L, Li W, Wang Z, Zhang H, Xin X, et al. An overview of BCC climate system model development and application for climate change studies. *Acta Meteorologica Sinica*. 2014; 28:34-56.

[12] Ruddiman WF. *Earth's Climate: Past and Future*: W. H. Freeman; 2001.

[13] Stocker T. *Introduction to Climate Modelling*: Springer-Verlag Berlin Heidelberg; 2011.

[14] Wu T, Yu R, Zhang F. A Modified Dynamic Framework for the Atmospheric Spectral Model and Its Application. *Journal of the Atmospheric Sciences*. 2008;65:2235-2253.

[15] Janssen PAEM. Progress in ocean wave forecasting. *Journal of Computational Physics*. 2008;227:3572-3594.

[16] Booij N, Ris R, Holthuijsen LH. A third-generation wave model for coastal regions: 1. Model description and validation. *Journal of geophysical research: Oceans*. 1999; 104:7649-7666.

[17] Rusu E, Soares CG. Numerical modelling to estimate the spatial distribution of the wave energy in the Portuguese nearshore. *Renewable Energy*. 2009; 34:1501-1516.

[18] Gómez Lahoz M, Carretero Albiach J. Wave forecasting at the Spanish coasts. *Journal of Atmospheric & Ocean Science*. 2005; 10:389-405.

[19] Whitham GB. A general approach to linear and non-linear dispersive waves using a Lagrangian. *Journal of Fluid Mechanics*. 1965; 22:273-283.

[20] Bretherthon FP, R. GCJ. Wavetrains in inhomogeneous moving media. *Proceedings of the Royal Society of London Series A Mathematical and Physical Sciences*. 1968; 302:529-554.

[21] Holthuijsen LH. *Waves in Oceanic and Coastal Waters*: Cambridge University Press; 2007.

[22] Cavaleri L, Rizzoli PM. Wind wave prediction in shallow water: Theory and applications. *Journal of Geophysical Research*. 1981; 86.

[23] Miles JW. On the generation of surface waves by shear flows. *Journal of Fluid Mechanics*. 1957; 3:185.

[24] van Vledder GP. The WRT method for the computation of non-linear four-wave interactions in discrete spectral wave models. *Coastal Engineering*. 2006;53:223-42.

[25] van Vledder GP, Bottema M. Improved Modelling of Nonlinear Four-Wave Interactions in Shallow Water. 2002: 459-472.

[26] Hasselmann K. On the spectral dissipation of ocean waves due to white capping. *Boundary-Layer Meteorology*. 1974; 6:107-127.

[27] Hemer MA, Trenham CE. Evaluation of a CMIP5 derived dynamical global wind wave climate model ensemble. *Ocean Modelling*. 2016; 103:190-203.

[28] Berrisford P, Dee D, Poli P, Brugge R, Fielding K, Fuentes M, et al. The ERA-Interim archive [Version 2.0]. European Centre for Medium Range Weather Forecasts, Shinfield Park. *Reading, Berkshire RG2 9AX, United Kingdom*. 2011.

[29] Dee DP, Uppala SM, Simmons AJ, Berrisford P, Poli P, Kobayashi S, et al. The ERA-Interim reanalysis: configuration and performance of the data assimilation system. *Quarterly Journal of the Royal Meteorological Society*. 2011; 137:553-597.

[30] Tolman H. the WAVEWATCH III Development Group (2014). User Manual and System Documentation of WAVEWATCH III version 4.18. *Tech Note 316, NOAA/NWS/NCEP/MMAB*. 2014.

[31] DNV GL AS. Environmental conditions and environmental loads. 2010.

[32] Amante C, Eakins B. ETOPO1 1 Arc-Minute Global Relief Model: Procedures, Data Sources and Analysis. NOAA Technical Memorandum NESDIS NGDC-24. National Geophysical Data Center, NOAA, USA. 2009.

[33] Scoccimarro E, Gualdi S, Bellucci A, Sanna A, Giuseppe Fogli P, Manzini E, et al. Effects of tropical cyclones on ocean heat transport in a high-resolution coupled general circulation model. *Journal of Climate*. 2011;24:4368-4384.

[34] Dobrynin M, Murawski J, Baehr J, Ilyina T. Detection and attribution of climate change signal in ocean wind waves. *Journal of Climate*. 2015; 28:1578-1591.

[35] Young IR, Zieger S, Babanin AV. Global trends in wind speed and wave height. *Science*. 2011; 332:451-455.

[36] Collins M, Knutti R, Arblaster J, Dufresne J-L, Fichefet T, Friedlingstein P, et al. Long-term Climate Change: Projections, Commitments and Irreversibility. In: Intergovernmental Panel on Climate C, editor. Climate Change 2013 – The Physical Science

Basis: Working Group I Contribution to the Fifth Assessment Report of the Intergovernmental Panel on Climate Change. Cambridge: Cambridge University Press; 2013; 1029-1136.

[37] Gallagher S, Gleeson E, Tiron R, McGrath R, Dias F. Wave climate projections for Ireland for the end of the 21st century including analysis of EC-Earth winds over the North Atlantic Ocean. *Int J Climatol*. 2016;36:4592-4607.

[38] Gleeson E, Gallagher S, Clancy C, Dias F. NAO and extreme ocean states in the Northeast Atlantic Ocean. *Advances in Science and Research*. 2017; 14:23-33.

[39] Hemer MA, Katzfey J, Trenham CE. Global dynamical projections of surface ocean wave climate for a future high greenhouse gas emission scenario. *Ocean Modelling*. 2013; 70:221-245.

[40] Hemer MA, Fan YL, Mori N, Semedo A, Wang XLL. Projected changes in wave climate from a multi-model ensemble. *Nat Clim Change*. 2013; 3:471-476.

[41] Shipping ABO. Guidance notes on SPECTRAL-BASED FATIGUE ANALYSIS FOR FLOATING OFFSHORE STRUCTURES 2005.

[42] Kaminski ML. Sensing and understanding fatigue lifetime of new and converted FPSOs. Offshore Technology Conference. Houston, Texas, USA. 2007.

[43] Longuet-Higgins M, Cartwright DE, Smith ND. Observations of the directional spectrum of sea waves using the motions of a floating buoy. Ocean Wave Spectra, proceedings of a conference, Easton, Maryland: Prentice-Hall; 1963; 111-136.

[44] van der Cammen JJ, Hoogeland M, Koning J. Comparison of Measured and Calculated Vessel Heading of a Turret-Moored FPSO. 12th Offshore Symposium. Houston, Texas, USA. 2003.

[45] Hanson J, Ltibben A, Aalberts P, Kaminski ML. Wave Measurements for the Monitas System. Offshore Technology Conference. Houston, Texas, USA. 2010.

[46] Barstow S, Mørk G, Lønseth L, Schjølberg P, Machado U, Athanassoulis G, et al. WORLDWAVES: Fusion of data from many sources in a user-friendly software package for timely calculation of wave statistics in global coastal waters. The Thirteenth International Offshore and Polar Engineering Conference: International Society of Offshore and Polar Engineers; 2003.

4

DETECTIONS OF NATURAL VARIABILITY AND HUMAN INDUCED CLIMATE CHANGE

Some sections of this chapter have been published in Journal of Ocean Dynamics, 2016 [1].

In the previous chapter, I demonstrated the methodology to project the future sea states and to calculate annual fatigue damages of FPSOs. Then, the effect of climate change on fatigue damage was investigated. However, it is still not clear what the exact cause of climate change and their impact are, because the climate change consists of natural variability and human-induced climate change. The natural variability has a huge amount of randomness, and it may partially mask the effect of human-induced climate change.

In section 2.2, I preliminarily introduced the causes of natural variability and human-induced climate change. The aim of this chapter is to evaluate the range of natural variability and detect the human-induced climate change from the natural variability. At the beginning, the mechanics of the natural variability and the human-induced climate are further discussed in section 4.1 and 4.2. In section 4.3, the control simulations are introduced and conducted to estimate the range of natural variability. At last, the control simulations are compared with the projected ones in order to detect the effect of human activities and the trend of human-induced climate change.

4.1 Natural variability of climate system

Generally, the natural variability is attributed to the external forcing causes and internal non-linear causes. As known, the driving forcing of climate system is originally the solar radiation. With the variation of solar forcing, the atmospheric component may respond fast, and the other climate components would respond relatively slowly. In short, the climate components respond differently to variations of radiative forcing on a wide range of space- and time-scales. Besides, even without the variation of radiative forcing, the natural variability may also occur due to the non-linear interactions and behaviors in the climate system. Some effects of climate change may in turn affect the causes. For instance, with the increase of global temperature, more surface water may be evaporated into the atmosphere. The water vapor is one of primary GHG components. As a result, more water vapor in the atmosphere would intensify the greenhouse effect and increase the global temperature further. In contrast, with the increase of temperature, the land surface is emitting more energy back into the space via infrared radiation, which limits the increase of temperature and reduces the effect of climate change. In meteorology, we call the former as positive feedback, and the latter as negative feedback.

It is hard to predict the effect of natural variability, because there are too many variables involved. The Earth's climate is a complex interactive system, and there is a huge amount of physical or biochemical processes in it. Many of these processes are rather chaotic and sensitive to initial conditions, because even a small perturbation in initial conditions may result in different evolutions of the processes. Furthermore, due to the non-linear interactions, the climate system would keep on varying over time, and never come into an equilibrium state.

In climate modelling, most primary physical processes of climate system can already be simulated. But scientists still cannot accurately predict the effect of natural variability due to its complexity and chaos. Nevertheless, it does not mean the effect of climate change is unpredictable, especially for those long-term cumulative processes. I have already introduced the predictability of climate change in Chapter 3. In section 4.3, we will further discuss how to estimate the effect of natural variability.

4.2 Human-induced climate change

As mentioned above, the circulation of climate system is originally driven by solar radiation. In climate modellings, the original solar radiative forcing level is considered as constant, and the change of the Earth's orbit or rotation is neglected due to their long time-scales (from hundreds to thousands of years). The solar radiation which reaches the earth surface is mainly affected by the greenhouse effect, because the response time of the greenhouse effect is relatively shorter. In offshore engineering, more attentions are paid on the change of wave conditions in decade or century time-scales, as shown in Fig. 4.1.

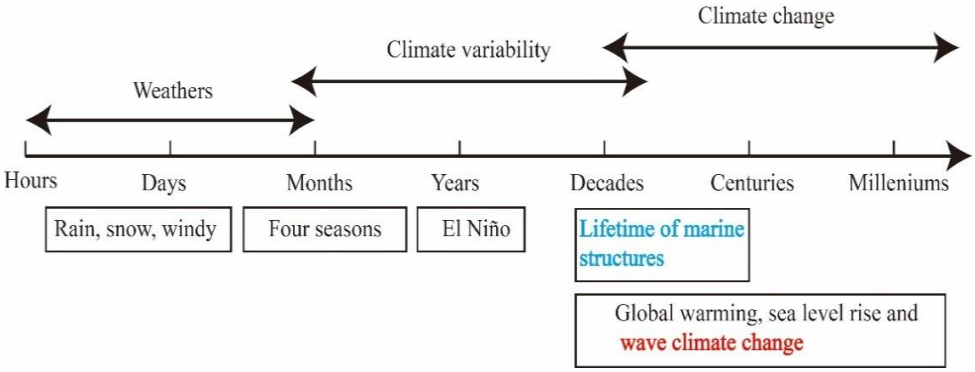

Figure 4.1: Illustration of time scales for weather, climate variability and climate change

Due to the greenhouse effect, the emission of GHGs may affect the global distribution of radiative forcing and eventually cause climate change [2]. Fig. 4.2 demonstrates the mechanics of greenhouse effect through a simplified atmospheric model. There are multiple isothermal layers in the atmosphere. The solar radiation passes through the layers and reaches the ground surface. As a return, the ground sends longwave radiation back into the space. In this process, all the atmospheric layers keep absorbing and re-emitting the equal amount of radiation to both the space (upwards) and the ground surface (downwards).

In Fig. 4.2a, there are three components: solar radiation, atmosphere and ground. When the solar radiation is passing through the atmospheric layers, these atmospheric layers will absorb the solar radiation and send part of it back into the space. When the rest of the solar radiation reaches the ground, its amount is defined as S. In order to keep balance, the ground will also send radiation upwards which is defined as G. G must be higher than S, because the atmosphere will absorb G and re-emit part of G back into the ground. After passing through the atmosphere, the ground radiation finally reaches the space. The amount of this ground radiation is defined as R_1. If the radiation of atmosphere layers is isotropic, they will re-emit the same amount of ground radiation upwards and downwards. For the first layer, it will send radiation upwards R_1 and downwards R_1 ($2\times R_1$ in all) and receive radiation only from the second layer $2\times R_1=R_2$. If the climate system is in energy balance, the energy absorbed by the climate system should be equal to the energy sent out to the space ($R_1=S$). Otherwise, the net energy of the ground will increase or decrease. Then, for the second layer, it re-emits $2\times R_2$ and receive radiation from both the first layer and the third one: $2\times R_2=R_1+R_3$ and $R_3=3\times S$. If R_n stands for the radiation re-emitted by the layer n, the radiation of the layer n can be calculated

as $R_n = n \times S$. It refers only to radiation that has been emitted by the ground, and it does not include the directly absorbed and re-emitted radiation from the Sun. The ground radiation is calculated by $G_a = (n + 1) \times S$.

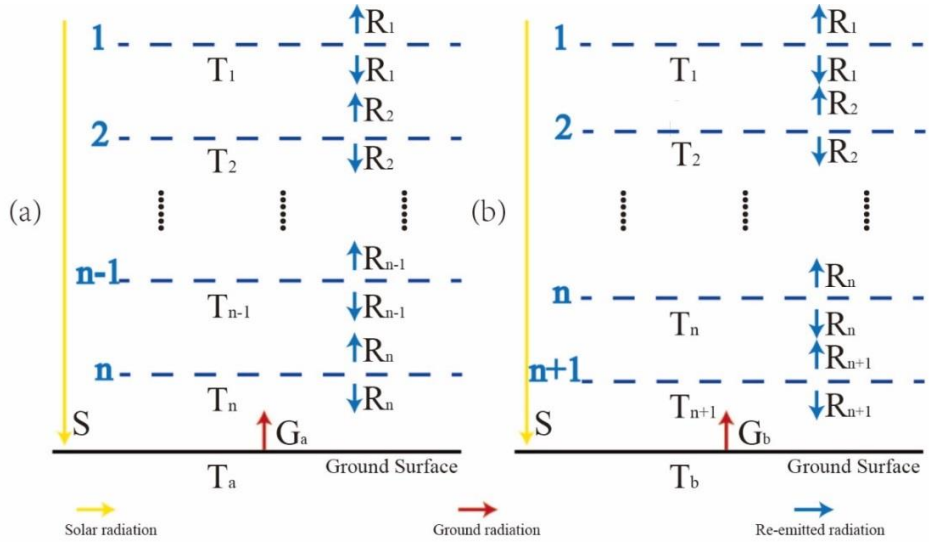

Figure 4.2: The energy flow in a simplified atmosphere model with multiple atmospheric layers; (a) a model with the constant amount of GHGs in the atmosphere; (b) the same model with more GHGs in the atmosphere. The increase of GHGs is represented by an additional atmospheric layer above the ground surface. S is the solar radiation absorbed by the ground. T is the temperature of the layers and the ground.

With the increase of GHGs concentration, the atmospheric layers absorb more longwave radiation from the ground surface and re-emit it back to the earth, which breaks the energy balance of the climate system. In this situation, radiative forcing is defined as the difference between solar radiation absorbed by the Earth and energy radiated back to space (Radiative forcing $= S - R_1$). In simplified atmospheric models, the emission of GHGs can be represented by more atmospheric layers [3]. For example, one more layer is added in Fig. 4.2b to represent the increased concentration of GHGs. Then, the climate system would re-balance itself by radiating more energy from the ground. As a result, the ground radiation $G_b = (n + 2) \times S$. It indicates that the temperature of the ground increases and the climate change occurs.

In RCP climate scenarios, the GHG concentration trajectories until 2100 are projected, and the GHG emission is highly affected by human activities. According to the mechanics of greenhouse effect, the time series of radiative forcing in each layer and ground surface is calculated. Then, the circulation of climate system is simulated via climate models. Based on the GHG concentration trajectories, the effect of human activities on future surface wind field is projected through climate models. It should be noticed that the long-term variation of wind field or the other variables is attributed to both human activities and natural variability. In climate modellings, the human-induced climate change originates from the variation of

radiative forcing (*i.g.,* climate scenarios); the natural variability is induced by the non-linear climate behavior which are simulated by climate models. The reliability of climate projections requires the development of both climate scenarios and climate models.

4.3 Control simulations and natural variability

The effect of climate change is the combination of natural variability and human-induced climate change. In order to further investigate the effect of human-induced climate change on wave conditions and fatigue damage, it is required to separate human-induced climate change from observed or projected climate change. In other words, it is required to evaluate to what extent climate change is attributed to human activities.

In climate models, the effect of human activities is directly represented by GHG emissions (*i.g.,* climate scenarios), and the natural variability is represented by simulating the non-linear interactions and circulations of climate components under a certain radiative forcing level. Therefore, a multiple-member ensemble analysis with the controlled radiative forcing level is used to identify the randomness of natural variability. In the ensemble analysis, the radiative forcing is "controlled", which is constant and equal to the mean forcing level of a preindustrial year (*e.g.*, 1850). Therefore, this ensemble analysis is also called the control simulation below. A long-term (decadal or century) control simulation is conducted under this constant radiative forcing by climate and wave models. As control simulations produce different responses of the climate system to the constant radiative forcing, the simulation time only represents the model time, not the real calendar years. This constant radiative forcing eliminates the effect of human-induced climate change. If the simulations time is long enough, all the possibilities of natural variability can be theoretically identified. The detailed settings of all the control simulations in this Chapter are listed in Table 4.1.

Table 4.1: Settings of all the control simulations

Climate model	CMCC-CM
Climate scenario	pre-industrial control
Spatial resolution	0.75°×0.75° (latitude/longitude)
Ensemble	r1i1p1
Time frequency of wind data	6 hours
Wave model	WaveWatch-III (version 4.18)
Spatial resolution	0.75°×0.75° (latitude/longitude)
Time step (global, spatial, directional and source term)	3600 s, 1200 s, 1800 s, 300 s
Bathymetry	ETOPO1
Direction number	24 (i.e. every 15°)
Frequencies range	0.042 Hz to 0.414 Hz

4.3.1 6 hours sampling time increment

In this section, a 30-member control simulation was conducted under the constant radiative forcing level of the preindustrial year 1850. The ending climate condition of each member simulation is the initial condition for the next member. In 1850, the emission of global GHGs by human activities was limited, and there was hardly any human-induced climate change.

The control simulations were conducted over the same sea area as the projected simulations in Chapter 3, and the continuous sea states in each oil field were simulated. The sea states from each ensemble number stand for one possibility of the sea states in 1850. As a result, there are 1460 (4 sea states per day × 365 days) continuous sea states simulated for each ensemble member with a duration of 1 year., and each sea state stands for the averaged wave condition over 6 hours. These 6-hourly sea states are indexed by two indices: an index $\boldsymbol{n}$ to denote an ensemble number with $\boldsymbol{n}$={1,2,…, 30} and an index $\boldsymbol{m}$ to denote a successive sea state number with $\boldsymbol{m}$ ={1,2,…,1460} [4, 5]. The $\boldsymbol{m}$th sea state in the $\boldsymbol{n}$th ensemble member is represented by the indicator $\boldsymbol{n-m}$. For each oil field, all the 6-hourly sea states in the control simulation were subsampled with different sampling lengths (ranging from 1 to 10 years). The sampling was conducted by shifting the sampling length with a constant time increment of 6 hours (*i.g.,* the length of one sea state) over successive sea states, see Fig. 4.3. Overlapping samples were allowed as shown in Fig. 4.4. As a result, the sample size (the number of sampling unit) for each sampling length was ranging from 42,341 to 29,201. The averaged significant wave height of sampling units in the same sample length was fitted by the normal distribution $N(\boldsymbol{\mu_i}, \boldsymbol{\sigma_i})$, $\boldsymbol{i}$={1,2, ,…, 10} ($\boldsymbol{i}$ is corresponding to each sampling length).

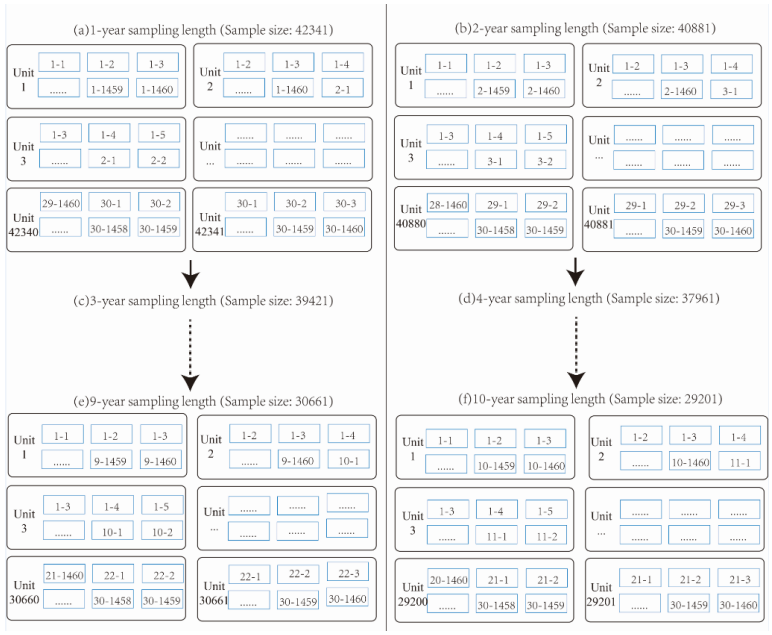

Figure 4.3: Sampling result with 6-hour time increment. Each 6-hourly sea state is represented by the indicator $\boldsymbol{n-m}$ in the blue boxes. The black boxes stand for the sampling units in each sample.

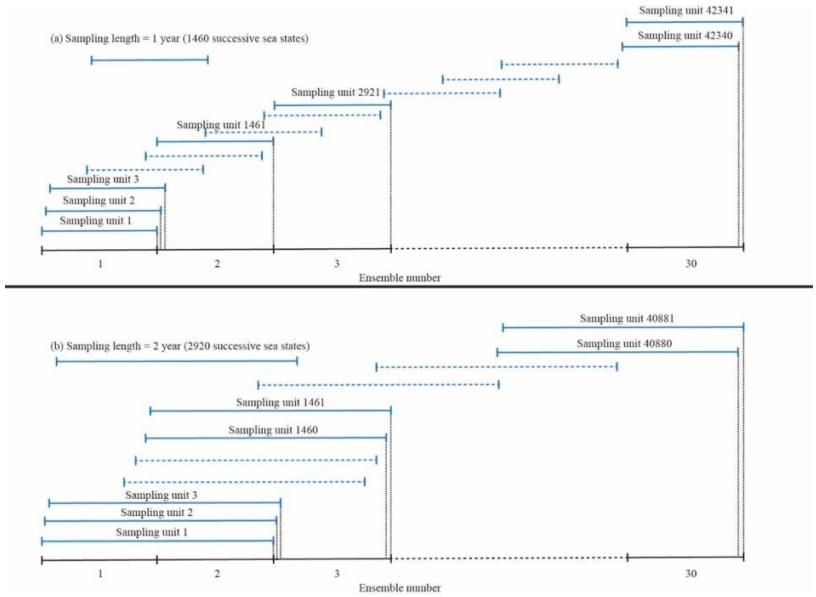

Figure 4.4: Illustration of overlapping samples with 6 hour time increment. Neighboring units overlap with each other by (a) 1459 sea states and (b) 2919 sea states. Most sampling units are not shown to simplify the plot.

After sampling, the sea state data were analyzed, as listed in Table 4.2. In all four oil fields, the averaged significant wave height (μ) is very stable. The average value for each sampling length is not exact the same, but the difference is very small which can be neglected. Differently, the deviation of sampling data is decreasing with sampling length. When the sampling length is 1 years, the sampling data has the highest dispersion which is represented by standard deviation (SD). It indicates that the natural variability may significantly affect the simulations over short periods, and the result of these simulations include a high level of randomness. With the increase of sampling length, the dispersion of significant wave height is getting smaller, because the variation in one year is compensated for by the opposite variation in another year. We can also explain it by assuming that the significant wave height of the 6-hourly sea states is a variable $H_s \sim N(\mu_s, \sigma_s)$. All the sea states are considered unrelated. Then, for each sample unit, the number of sea states N, and their averaged significant wave height is defined as $\overline{H}_s \sim N(\bar{\mu}_s, \bar{\sigma}_s)$. μ_s is very close to $\bar{\mu}_s$, because they are from the same population. The standard deviation of $\overline{\mathrm{H}}_\mathrm{s}$ is the standard deviation of H_s for each individual sea state divided by the square root of sea state number n:

$$\bar{\sigma}_s = \frac{\sigma_s}{\sqrt{n}} \tag{4.1}$$

n is increasing with the length of sampling length. As a result, with the increase of sampling length, the range of natural variability is becoming narrower, and its effect is getting less pronounced. In short, due to the randomness of natural variability, long-term (decades or century) simulations are recommended to improve their reliability.

Table 4.2: The sampling result with 6-hour time increment

Sampling length [year]		1	2	3	4	5	6	7	8	9	10
Sable	μ [m]	2.76	2.76	2.76	2.76	2.76	2.76	2.76	2.76	2.76	2.76
	SD [m]	0.097	0.061	0.045	0.034	0.027	0.022	0.022	0.021	0.019	0.017
Alma/Galia	μ [m]	1.87	1.87	1.87	1.87	1.87	1.87	1.87	1.87	1.87	1.87
	SD [m]	0.107	0.072	0.050	0.039	0.030	0.026	0.027	0.025	0.022	0.020
Pierce	μ [m]	2.06	2.06	2.06	2.07	2.07	2.07	2.07	2.07	2.07	2.07
	SD [m]	0.111	0.076	0.054	0.045	0.034	0.030	0.030	0.029	0.028	0.026
Rosebank	μ [m]	2.73	2.73	2.74	2.74	2.74	2.74	2.74	2.74	2.74	2.74
	SD [m]	0.145	0.092	0.059	0.047	0.034	0.032	0.032	0.028	0.025	0.020

4.3.2 One year sampling time increment

Since the calculations of fatigue damage are more time consuming than simulating sea states, the sea state data from the control simulation were also subsampled with a long-time increment to reduce the amount of fatigue computations. The primary difference was that the constant time increment increased from 6 hours to 1 year as shown in Fig. 4.5 and Fig. 4.6. In this case, the sample size was significantly decreased to 30 for 1-year sample and 21 for 10-year sample. This sampling approach can effectively reduce the calculation time, but it may also induce more uncertainties into the calculations.

With the 1-year time increment, μ and *SD* for each sampling length were not significantly changed, see Table 4.3. If we compare Table 4.2 with Table 4.3, it can be seen that μ is almost the same for both time increments, and *SD* is only changed by at most 10% which is negligible. It indicates that the change of time increment from 6 hours to 1 year does not significantly affect the standard deviation of samples which is important to estimate the range of natural variability. Hence, it is recommended to use the 1-year time increment to sample data for the following fatigue calculations, because it can limit the sample size and reduce the amount of calculations.

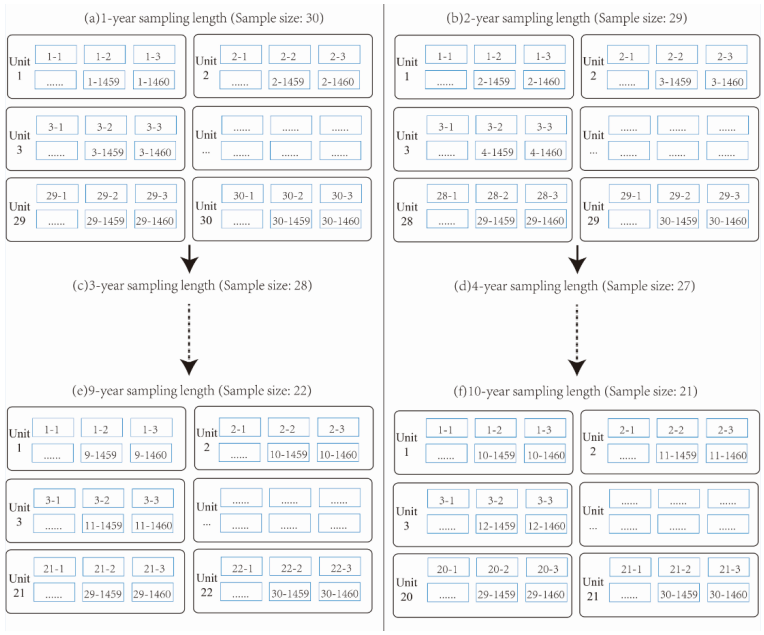

Figure 4.5: Sampling result with 1 year time increment. Each 6-hourly sea state is represented by the indicator $\boldsymbol{n-m}$ in the blue boxes. The black boxes stand for the sampling units in each sample.

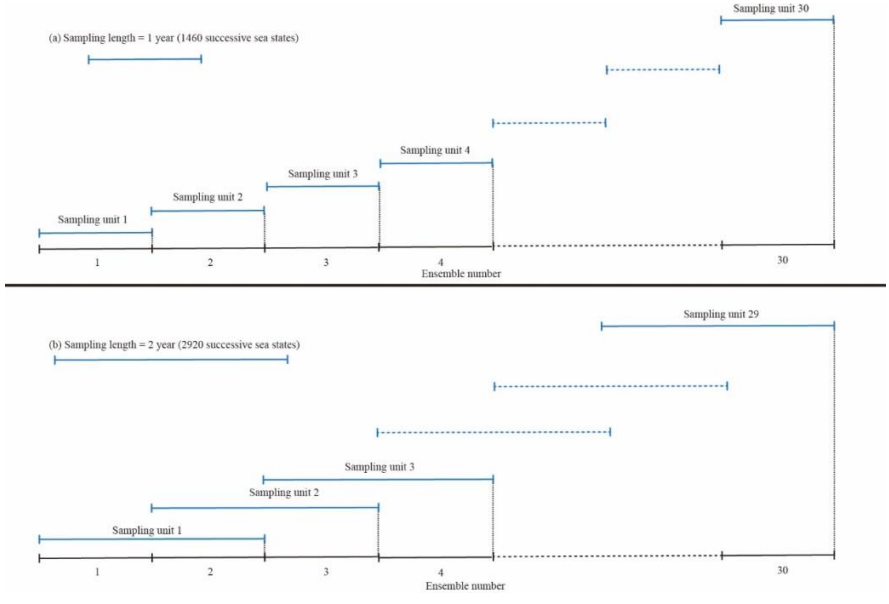

Figure 4.6: Illustration of overlapping samples with 1 year time increment. Neighboring units overlap with each other by (a) 0 sea states and (b) 1460 sea states. Most sampling units are not shown to simplify the plot.

Table 4.3: The sampling result with 1-year time increment

Sampling length [year]		1	2	3	4	5	6	7	8	9	10
Sable	μ [m]	2.78	2.78	2.77	2.77	2.78	2.77	2.77	2.77	2.77	2.77
	SD [m]	0.090	0.066	0.053	0.045	0.039	0.034	0.031	0.029	0.026	0.024
Alma/Galia	μ [m]	1.86	1.87	1.87	1.87	1.87	1.87	1.87	1.87	1.87	1.87
	SD [m]	0.117	0.074	0.054	0.043	0.031	0.027	0.026	0.025	0.023	0.019
Pierce	μ [m]	2.06	2.06	2.06	2.06	2.07	2.07	2.07	2.07	2.07	2.07
	SD [m]	0.121	0.079	0.058	0.046	0.034	0.029	0.029	0.028	0.026	0.024
Rosebank	μ [m]	2.73	2.73	2.73	2.74	2.74	2.74	2.74	2.74	2.74	2.74
	SD [m]	0.154	0.102	0.071	0.049	0.034	0.034	0.032	0.027	0.024	0.021

4.4 Detection of human-induced climate change

Since the variability of sea states in the control simulation was induced by natural variability, the range of natural variability was estimated by confidence intervals. The 0.05 and 0.95 confidence intervals of the normal distribution $N(\boldsymbol{\mu_i}, \boldsymbol{\sigma_i})$, $\boldsymbol{i}$ ={1,2,3,…,10}, were calculated as the lower and upper boundaries of natural variability for each sampling length. In order to detect the human-induced climate change, the projected simulations (as defined in section 3.5.1) under projected climate scenarios are compared with the control simulations. The result of projected simulations includes the effects from both human-induced climate change and natural variability.

In control simulations: climate change = natural variability

In projected simulations: climate change = natural variability + impact of human activities

Please note this is not a linear summation. In the real climate system, natural variability and human activities are non-linearly and dynamically coupled. It is hard (or even impossible) to pinpoint the portion of climate change induced by the natural variability and the portion induced by human activities.

Once the projected climate trajectory exceeds the upper or lower limit of natural variability, the human-induced climate change is considered detected in this thesis, as defined in the work of Baehr *et al.* (2008) and Dobrynin *et al.* (2015) [4, 5]. These projected trajectories are calculated without the consideration of uncertainties, and their confidence intervals will not be plotted as the control simulations. Instead, the uncertainties in the projected simulations will be discussed in Chapter 5.

4.4.1 Detection of human-induced climate change on significant wave height

For each oil field, the 6-hourly sea states in the present, near future and far future decades

(2011-2020, 2051-2060 and 2091-2100) were simulated in the projected simulations based on RCP8.5 in Chapter 3. Then, the annual significant wave height was calculated. For the present decade, the averaging significant wave height $H_{sa}(t)$ for each sampling length $t = \{1; 2; \dots; 10\}$ was calculated as follows:

$$H_{sa}(1) = \overline{H_s}(2011) \tag{4.2}$$

$$H_{sa}(2) = \overline{H_s}(2011\sim\text{-}2012) \tag{4.3}$$

$$H_{sa}(3) = \overline{H_s}(2011\sim\text{-}2013) \tag{4.4}$$

$$\vdots$$

$$H_{sa}(10) = \overline{H_s}(2011\text{-}\sim2020) \tag{4.5}$$

where $\overline{H_s}(p)$ is the averaged significant wave height within the time period $p = \{2011;\ 2011\sim2012;\ 2011\sim2013; \cdots; 2011\sim2020\}$. For the future decades, the averaging significant wave height $H_{sa}(t)$ was calculated in the same way as listed in Eqs. (4.2)-(4.5).

Sable field offshore South Africa

The trajectories of averaging significant wave height $H_{sa}(t)$ in the Sable field were compared to the range of natural variability which is estimated with 6-hour time increment. The human-induced climate change has been detected, as all the trajectories of averaging significant wave height in the present, near future and the far future decades exceed the upper limit of natural variability, see Fig.4.7. The detection period is defined as the earliest year when the projected trajectory exceeds the range of natural variability, and the detection period here is 4 years. Although the impact of human activities is detected, this detection is not so pronounced. The impact of human activities on wave height in the Sable field is not so significant to make a clear detection.

The averaging significant wave heights in these three periods are all above the horizontal straight dotted line which is defined as the averaged significant wave height in the control simulations for each sampling length. It means that climate change results in higher wave height in the Sable field over century time-scales. This conclusion contradicts earlier conclusion that averaged significant wave heights $\overline{H_s}$ in the periods 2011-2020, 2051-2060, and 2091-2100 are close to each other as discussed in section 3.5. Since there is a 30-year gap between the neighboring decades, one possible explanation is that the increased wave height during the 30 years induced by human activities is counterbalanced by the decreased wave height caused by the natural variability. Evidently, the selected periods 2011-2020, 2051-2060, and 2091-2100 are too close to each other. The time gap is too short for exposing significant trend of wave height change in the Sable field. When the sampling length is 1 year, the averaging wave height of the present decade 2091-2100 is the highest, because the significant wave height in 2091 is higher than in 2011 or 2051. With the increase of sampling length, these three projected trajectories gradually converge.

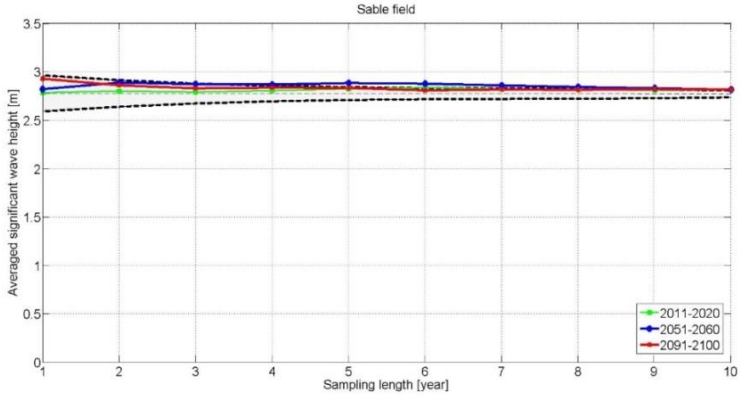

(a)

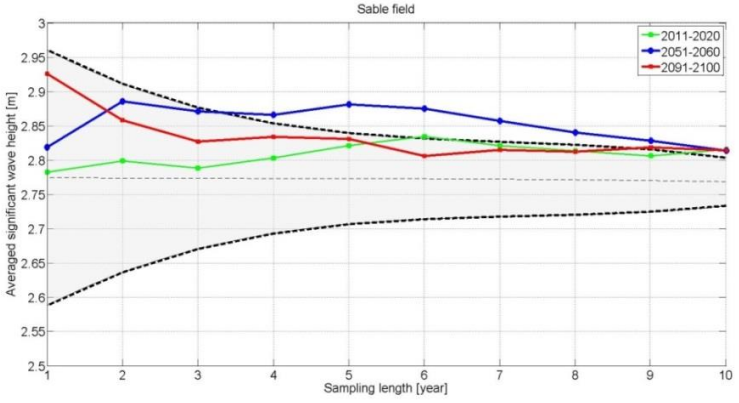

(b)

Figure 4.7: The natural variability of significant wave height with 6-hour time increment and the detection of human-induced climate change in the Sable field. (b) is the zoomed-in plot of (a). The shadowed area represents the range of natural variability calculated by the control simulation with 6-hour time increment. The trajectories are the averaging significant wave heights for the present decade (green line), the near future decade (blue line) and the far future decade (red line), as calculated in Eqs. (4.2)-(4.5). The lower and upper boundaries of natural variability are represented by the black dotted lines. The horizontal straight dotted line is the averaged significant wave height in the control simulations for each sampling length.

North Sea

The trajectories of averaging significant wave height in three oil fields of North Sea were also compared with their ranges of natural variability in Fig. 4.8. All the trajectories exceed the lower boundary of natural variability, and the human-induced climate change is clearly detected. In contrast to the Sable field, the significant wave height in the North Sea is decreased compared to the control simulations. Since we have identified that there is a

downward trend of H_s in the North Sea from 2011 to 2100 in section 3.5.2, it can be concluded that the significant wave height here is decreasing over time due to the effect of human activities. Although all three oil fields are located in the North Sea, the wave height in Rosebank has higher SD which indicates greater randomness of natural variability as listed in Table 4.2. The higher dispersion is attributed to the location of Rosebank, because Rosebank is located in North of Scotland where is more vulnerable to the waves from the North Atlantic.

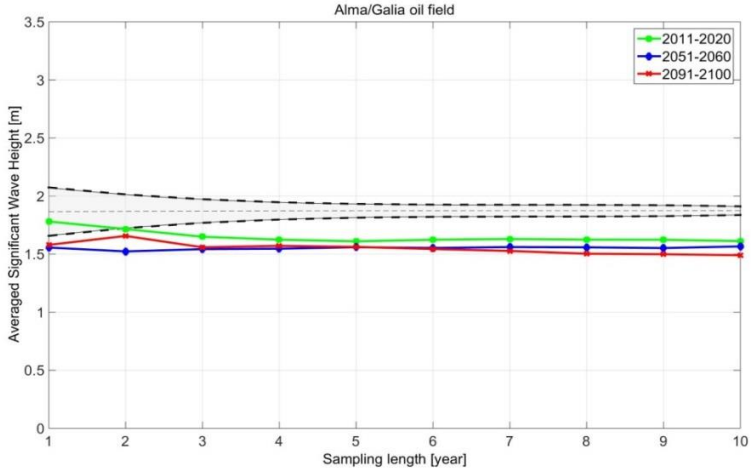

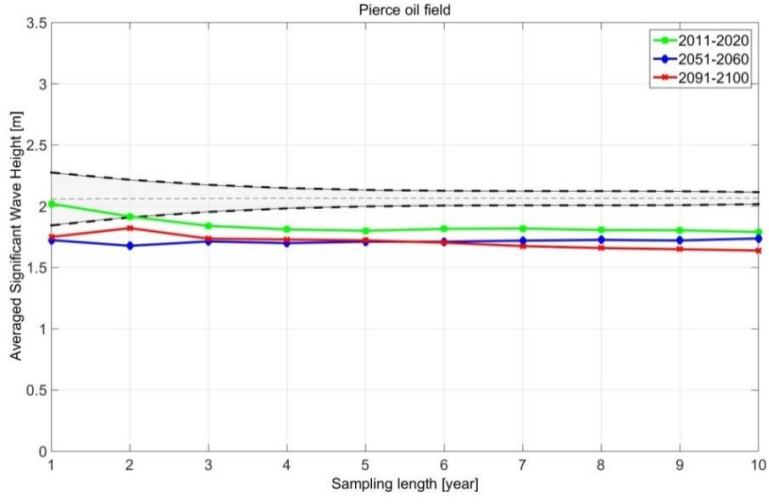

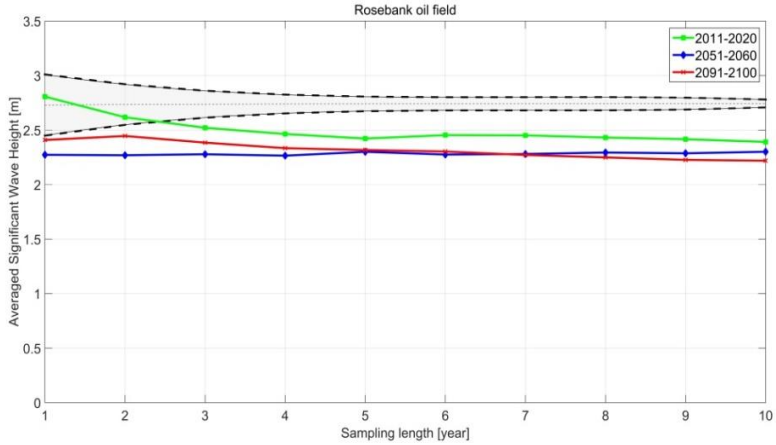

Figure 4.8: The natural variability of significant wave height with 6-hour time increment and the detection of human-induced climate change in the North Sea.

In section 4.3.2, I have compared the sampling results with different sampling time increments. They have very close μ and *SD*. Here I can plot the range of natural variability with 1-year time increment and compare it with the projected trajectories of H_s in Figs. 4.9 and 4.10. With the 1-year time increment, the range of natural variability was not significantly changed. The trajectories of projected wave height also exceed the boundary with the same detection periods (4 years for the Sable field, and 1 year for the North Sea). It indicates again that the change of time increment from 6 hours to 1 year would not significantly affect the detection of human-induced climate change. The detection period in all four oil fields is usually shorter than the detection period of other studies [5]. This difference could be explained by the fact that the present study focuses on a single location (four specific oil fields), whereas other studies focus on the average climate change over large areas. A decreasing trend at one location can be compensated by an increasing trend in other neighboring locations.

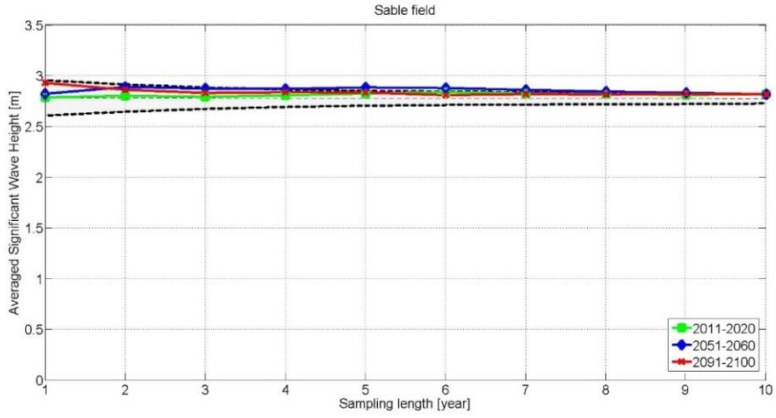

(a)

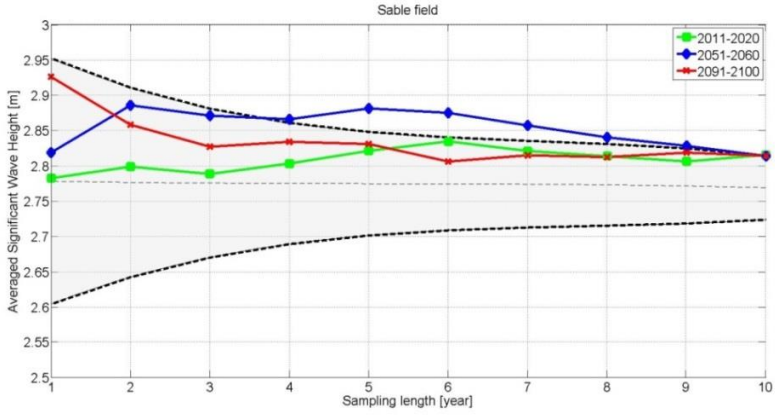

(b)

Figure 4.9: The natural variability of significant wave height with 1-year time increment and the detection of human-induced climate change in the Sable field. (b) is the zoomed-in plot of (a).

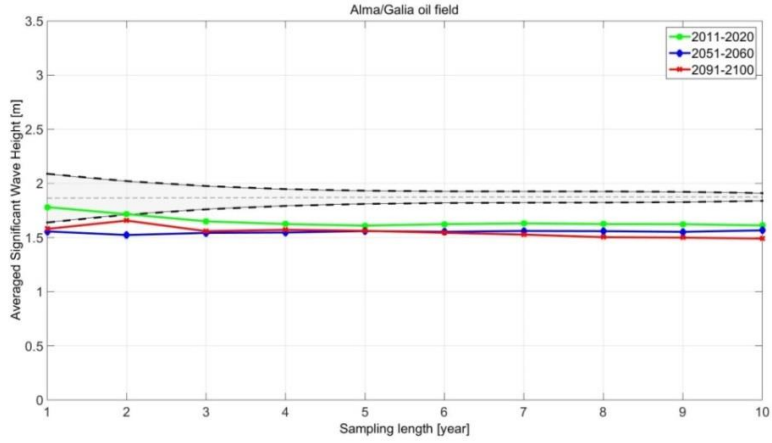
Alma/Galia oil field
2011-2020
2051-2060
2091-2100
Averaged Significant Wave Height [m]
Sampling length [year]

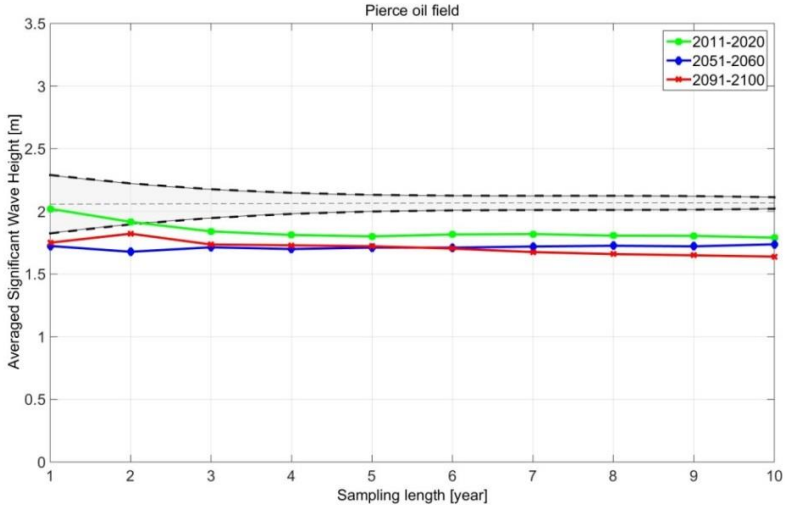
Pierce oil field
2011-2020
2051-2060
2091-2100
Averaged Significant Wave Height [m]
Sampling length [year]

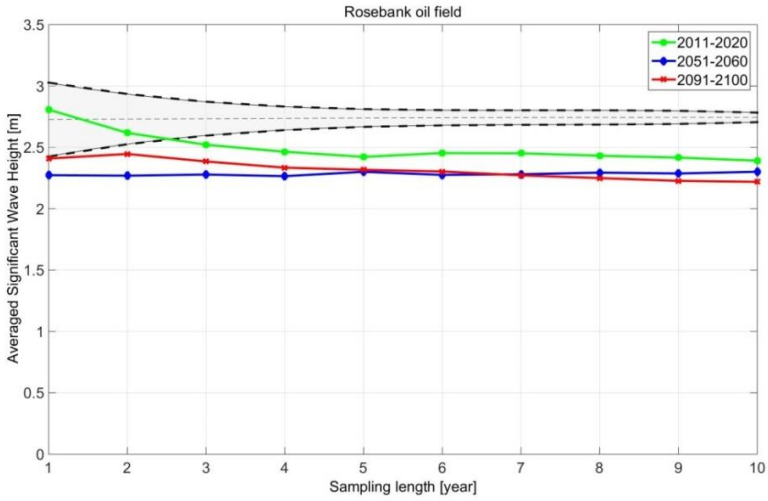

Figure 4.10: The natural variability of significant wave height with 1-year time increment and the detection of human-induced climate change in the North Sea.

4.4.2 Detection of human-induced climate change on cubic weighed wave height

S-N curves are often used to represent the fatigue resistance of materials. When the inverse slope of S-N curves is equal to 3, the fatigue damage is approximately proportional to third power of structural response. In this case, the effect of wave length is disregarded (i.e., RAO is constant), and the wave direction is unchanged. Besides, structural response in the hydro-structural linear model is proportional to significant wave height. Hence, cubic weighed value of significant wave height is usually used to roughly estimate fatigue damage of structures, which is defined as:

$$H_{cw} = \sqrt[3]{\frac{\Sigma_1^k {H_{si}}^3}{k}} \tag{4.6}$$

where:

H_{cw} : Cubic weighed significant wave height

H_{si} : Significant wave height of sea state i

k : Total number of sea state

The natural variability of H_{cw} was analyzed based on the control simulation just like we analyze the variability of H_s. The projected averaging cubic weighed significant wave height H_{cwa} for the three decades was calculated as Eqs. (4.2)-(4.5) and compared with the range of natural variability. The effect of human-induced climate change on H_{cw} was slightly detected in the Sable field with a low reliability, and the detection period is decreased to 2 years, which is further discussed in the following section 4.4.4, see Fig. 4.11. For the North Sea, the impact of human activities is detected with the same detection period as on H_s in the North Sea, see Fig. 4.12.

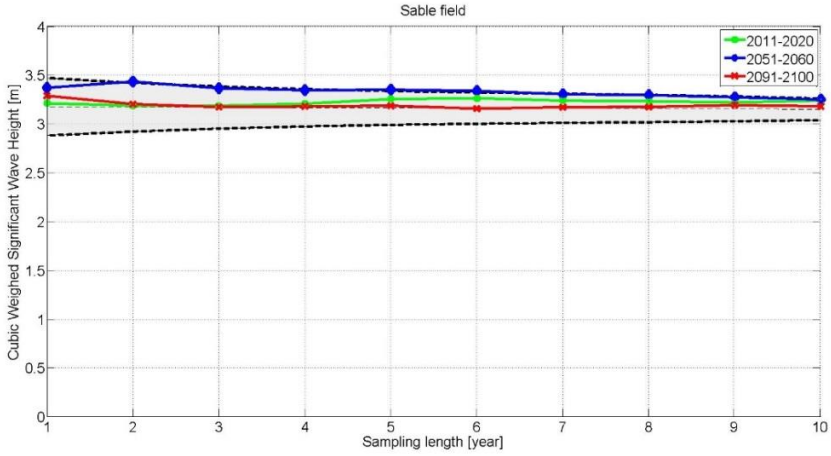

(a)

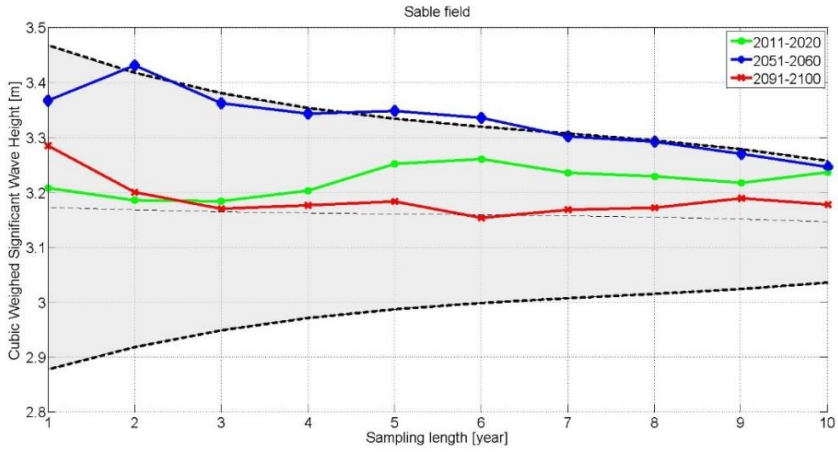

(b)

Figure 4.11: The natural variability of cubic weighed significant wave height with 1-year time increment and the detection of human-induced climate change in the Sable field. (b) is the zoomed-in plot of (a).

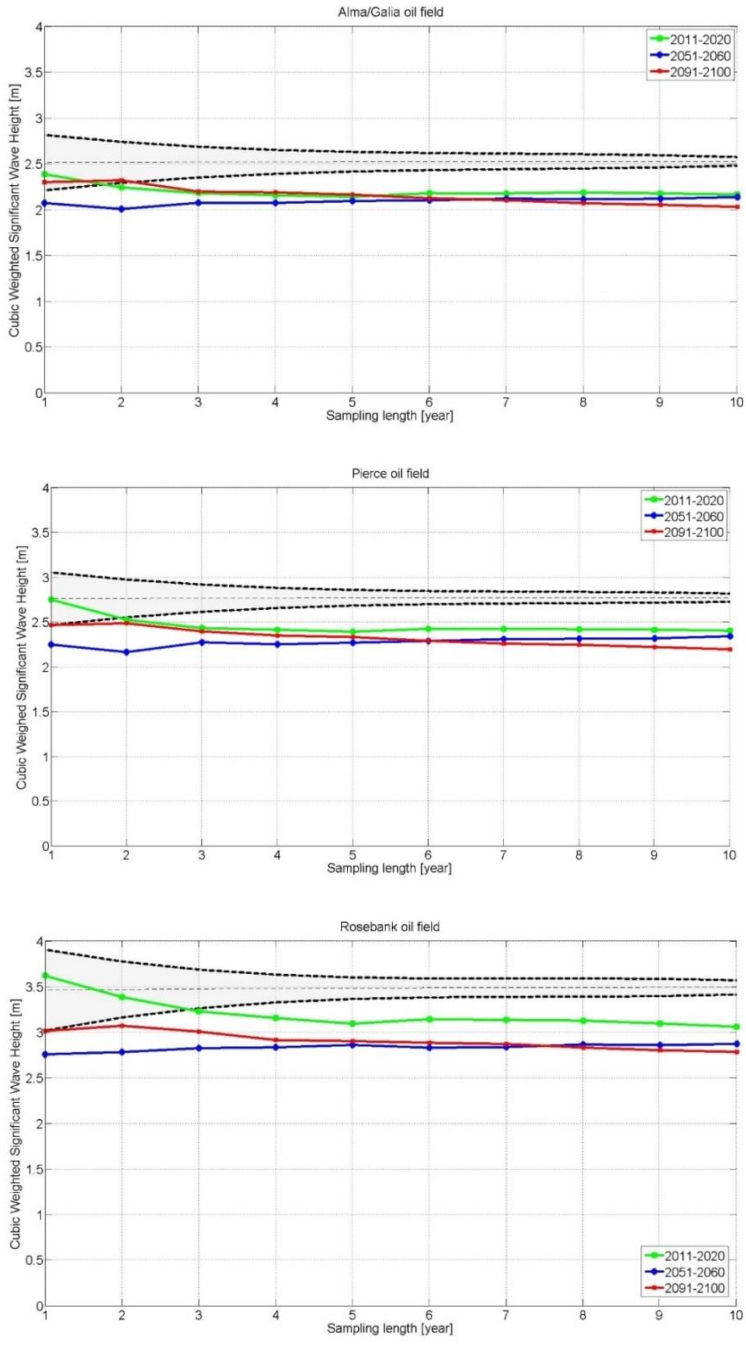

Figure 4.12: The natural variability of cubic weighed significant wave height with 1-year time increment and the detection of human-induced climate change in the North Sea.

4.4.3 Detection of human-induced climate change on fatigue damage

Although wave height is the dominant wave characteristic in fatigue calculations, wave period, wave direction and other wave characteristics may also affect fatigue damage. I have projected the annual fatigue damage for each oil field in section 3.6. This section aims to detect the impact of human activities on fatigue damage of offshore floating structures. The effect of natural variability on fatigue damage was evaluated in the same way as its effect on wave height, as described section 4.4.1. Based on the result of the control simulation, the fatigue damage was calculated under the time series of sea states simulated with the constant solar radiative level of 1850. The annual fatigue damages were subsampled with different sampling lengths and fitted by normal distributions. The confidence intervals of 0.05 and 0.95 were defined as the lower and upper limits of natural variability for each sampling length. The ranges of natural variability were compared with the averaging fatigue damages for the present, near-future and far-future decades in Fig. 4.13 (Sable field) and Fig. 4.14 (North Sea). The averaging fatigue damages were calculated in the same way to the averaging significant wave heights as in Eqs. (4.2)-(4.5).

Sable field offshore south Atlantic

The annual fatigue damage in the Sable field is increased over century time-scales, because the projected fatigue damages are basically above the averaged fatigue damage of control simulations (*i.g.,* the black dotted line in Fig. 4.13). Although the projected trajectory in 2011-2020 slightly exceeds the range of natural variability, the effect of human-induced climate change on fatigue damage is not so pronounced as its effect on wave height. The exceedance of the fatigue damages over the upper limit is so small, and all the three trajectories are basically within the range of natural variability. In addition, the annual fatigue damage is not increased significantly in the 30 years between the two neighboring projected periods. In other words, the upward trend of annual fatigue damage is not as significant as the trend of significant wave height, because fatigue damage is also affected by other factors, such as wave period, wave direction and the distribution of wave height. The change of wave height cannot entirely represent the change of fatigue damage.

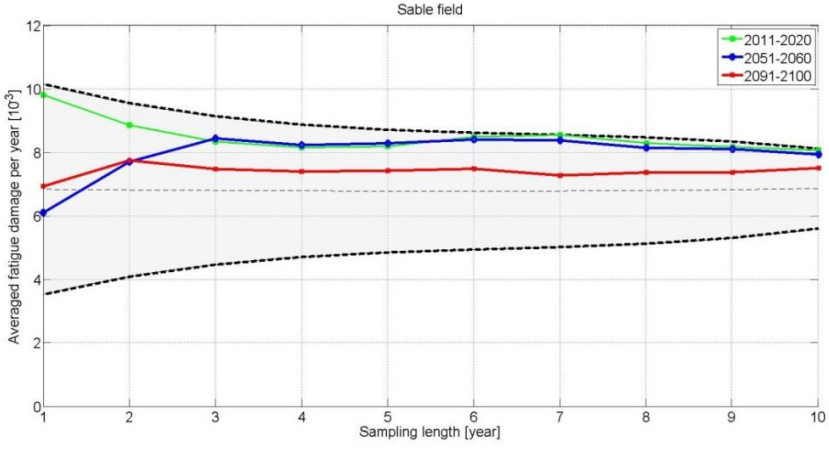

Figure 4.13: The natural variability of annual fatigue damage and the detection of human-induced climate change with 1-year time increment.

North Sea

All the projected trajectories of fatigue damage exceed the range of natural variability, as shown in Fig. 4.14. Hence, there is an obvious impact of human-induced climate change on annual fatigue damage in all three oil fields of the North Sea. In addition, all the trajectories are below the averaged annual fatigue damage of the control simulations, which reveals that the annual fatigue damage is decreasing with the emission of GHGs. The detection period is very short, only 1-2 years. It indicates the impact of human activities on the fatigue damage in the North Sea is considerable.

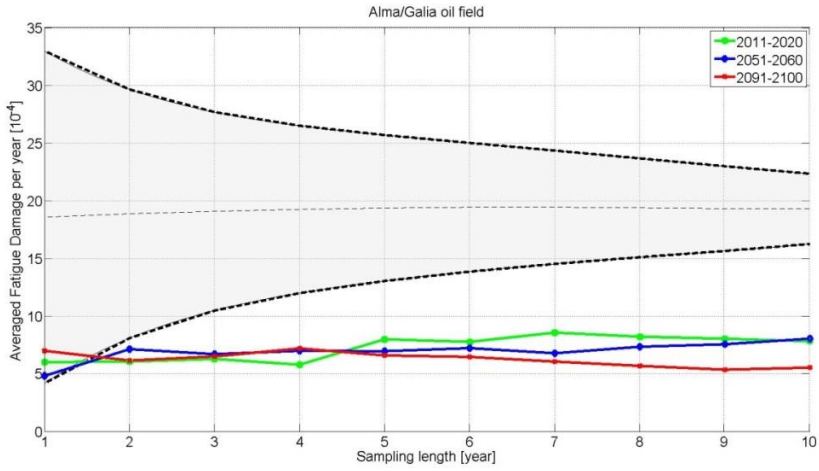

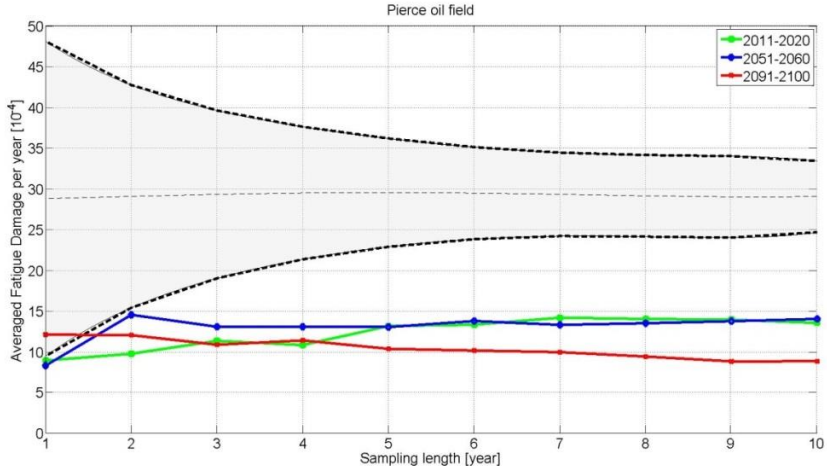

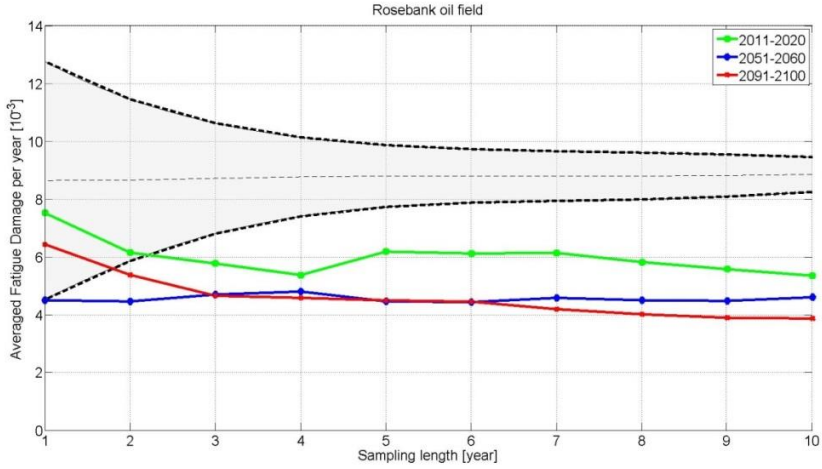

Figure 4.14: The natural variability of annual fatigue damage with 1-year time increment and the detection of human-induced climate change.

4.4.4 Comparison between the trends of wave height and fatigue damage

In this section, I compared the statistical properties of wave height and fatigue damage from the control simulations and projected simulations. The statistical characteristics of H_s, H_{cw} and fatigue damage are listed in Tables 4.4-4.6. Coefficient of variation (CV) expresses the extent of variability in relation to mean value. A higher CV stands for a higher variation. The bias has been defined as the ratio between the mean value from the projected simulations and the mean from the control simulations, which to some extent represents the effect of climate change.

Both H_s and H_{cw} are defined to describe wave height. Hence, they have very close variations and the effects of climate change on them are also similar which is reflected by bias, as listed in Tables 4.4 and 4.5. The fatigue damage is mainly induced by wave loadings, and it is more sensitive to climate change than wave height. In the Sable field, the bias of fatigue damage (1.10-1.18) is much higher than the bias of wave height (1.00-1.03). For the other three oil fields, the bias of fatigue damage (0.42-0.62) is much lower than the bias of wave height (0.79-0.88). It means the fatigue damage is changing faster than wave height in all these oil field. In addition, the change of fatigue damage is not only decided by wave height but also the other wave characteristics, such as wave periods, wave directions and their distributions. In the linear structural model, the fatigue damage is roughly proportional to the third power of wave height when m=3 in S-N curves. For instance, when the bias of wave height is ranging from 0.79 to 0.88, the bias of fatigue damage should be roughly ranging from 0.49 to 0.68 (0.79^3 to 0.88^3). The estimated bias of fatigue damage is higher than the calculated one in Table 4.6. It reveals that although wave height is the dominant wave characteristic in fatigue calculations, it is still necessary to consider the change of wave period and wave direction in fatigue calculations. Among all three oil fields in the North Sea, Rosebank has the highest bias of fatigue damage (0.45-0.62), which is also the closest to the estimated fatigue bias (0.49-0.68). It is because Rosebank has the highest wave height than the other two oil fields, and wave height is more dominant in fatigue calculations than the other

wave characteristics. The changes of wave periods and directions in Rosebank contribute less to the change of fatigue damage. If I compare the statistical characteristics of Sable field with the other three oil fields, it can be seen that the Sable field has a smaller *CV*, and its bias is closer to 1. The smaller *CV* indicates a smaller inter-annual variation, and the effect of natural variability is less dominant. Besides, if the bias is closer to 1, it means the impact of climate change (the combination of natural variability and human-induced climate change) is less pronounced. In other words, the North Sea is more sensitive to the effect of climate change than the Sable field in terms of wave height and fatigue damage.

Table 4.4: Comparison of significant wave height

Oil field	Simulation	Time	Mean	Standard deviation	CV	Bias
Unit	-	-	m	m	-	-
Sable	Control	1850-1879	2.78	0.09	0.03	-
	RCP85	2011-2020	2.82	0.07	0.02	1.01
		2051-2060	2.81	0.09	0.03	1.01
		2091-2100	2.81	0.07	0.02	1.01
Rosebank	Control	1850-1879	2.72	0.15	0.06	-
	RCP85	2011-2020	2.39	0.19	0.08	0.88
		2051-2060	2.30	0.09	0.04	0.84
		2091-2100	2.22	0.14	0.06	0.81
Alma/Galia	Control	1850-1879	1.86	0.12	0.06	-
	RCP85	2011-2020	1.61	0.09	0.06	0.86
		2051-2060	1.57	0.06	0.04	0.84
		2091-2100	1.49	0.12	0.08	0.80
Pierce	Control	1850-1879	2.06	0.12	0.06	-
	RCP85	2011-2020	1.79	0.11	0.06	0.87
		2051-2060	1.74	0.07	0.04	0.84
		2091-2100	1.64	0.12	0.07	0.80

Table 4.5: Comparison of cubic weighed wave height

Oil field	Simulation	Time	Mean	Standard deviation	CV	Bias
Unit	-	-	m	m	-	-
Sable	Control	1850-1879	3.17	0.15	0.05	-
	RCP85	2011-2020	3.24	0.12	0.04	1.02
		2051-2060	3.25	0.14	0.04	1.03
		2091-2100	3.18	0.10	0.03	1.00
Rosebank	Control	1850-1879	3.46	0.23	0.07	-
	RCP85	2011-2020	3.06	0.27	0.09	0.88
		2051-2060	2.87	0.12	0.04	0.83
		2091-2100	2.78	0.19	0.07	0.80
Alma/Galia	Control	1850-1879	2.51	0.16	0.06	-
	RCP85	2011-2020	2.16	0.13	0.06	0.86
		2051-2060	2.14	0.10	0.05	0.85
		2091-2100	2.03	0.18	0.09	0.81
Pierce	Control	1850-1879	2.76	0.15	0.05	-
	RCP85	2011-2020	2.40	0.15	0.06	0.87
		2051-2060	2.34	0.14	0.06	0.85
		2091-2100	2.19	0.18	0.08	0.79

In section 4.4.1, I defined a term “detection period”. It is a measure of climate change impact. A shorter detection period stands for a more significant climate change impact. By comparing the detection periods among four oil fields in Table 4.7, it can be confirmed that the effect of climate change on H_s in the North Sea is more pronounced that in the Sable field. In addition, the choice of time increment in sampling does not affect the detection time. The definition of H_{cw} is different from H_s, which leads to a different detection time in the Sable field. H_{cw} is defined to estimate fatigue damage. As a result, the impact of climate change on H_{cw} is very similar to the effect on fatigue damage. The impact of human-induced climate change on wave height and fatigue damage are both slightly detected in the Sable field. In the North Sea, however, the detection period of H_{cw} is not changed at all (as short as 1 or 2 years), because the effect of climate change on wave height is so significant here. It is the same to the detection period of fatigue damage. As mentioned above, fatigue damage is affected by many wave characteristics, which result in a longer detection period in the Sable field. The contribution to the fatigue change from the increase of wave height is compensated by the change of other wave characteristics. Whereas, the change of wave height in the North Sea is more pronounced than in the Sable field. As a result, the detection period of fatigue damage in the North Sea is not changed. The only exception is Alma/Galia oil field: the detection period of fatigue damage is slightly increased to 2 years. It can be concluded that when the dominant wave characteristic (wave height) has a significant change, the other wave properties can hardly affect the detection period.

Table 4.6: Comparison of annual fatigue damage

Oil field	Simulation	Time	Mean	Standard deviation	CV	Bias
Unit	-	-	10^{-3}	10^{-3}	-	-
Sable	Control	1850-1879	6.84	1.74	0.25	-
	RCP85	2011-2020	8.06	1.18	0.15	1.18
		2051-2060	7.93	1.3	0.16	1.16
		2091-2100	7.5	0.81	0.11	1.10
Rosebank	Control	1850-1879	8.64	2.1	0.24	-
	RCP85	2011-2020	5.35	1.95	0.36	0.62
		2051-2060	4.61	0.78	0.17	0.53
		2091-2100	3.88	1.12	0.29	0.45
Alma/Galia	Control	1850-1879	1.86	0.73	0.40	-
	RCP85	2011-2020	0.78	0.40	0.51	0.42
		2051-2060	0.81	0.27	0.33	0.43
		2091-2100	0.56	0.21	0.38	0.30
Pierce	Control	1850-1879	2.88	0.99	0.34	-
	RCP85	2011-2020	1.36	0.44	0.33	0.47
		2051-2060	1.40	0.38	0.27	0.49
		2091-2100	1.07	0.27	0.25	0.37

Table 4.7: Comparison of detection periods for all four oil fields

	H_s (6-hours increment) [year]	H_s (1-year increment) [year]	H_{CW} (1-year increment) [year]	Fatigue damage (1-year increment) [year]
Sable	4 (low reliability)	4 (low relaibility)	2 (low reliability)	7 (low reliability)
Rosebank	1	1	1	1
Alma/Galia	1	1	1	2
Pierce	1	1	1	1

4.5 Conclusions

In this Chapter, I further introduced the mechanics of natural variability and human-induced climate change. The natural variability is induced by the non-linear behaviors of climate system, and the human-induced climate change results from human activities (GHG emissions). They contain plenty of randomness, and they are hard to accurately predict. In order to investigate the effect of natural variability, 30-year control simulations were conducted under constant solar radiative forcing equivalent to the level in 1850. The range of

natural variability was estimated by confidence intervals. The averaging trajectories of wave height and fatigue damage were compared with the range of natural variability. Consequently, the effect of human-induced climate change was slightly detected in the Sable field and considerably detected in the three oil fields of the North Sea.

The result reveals that the wave height and annual fatigue damage are increasing in the Sable field due to the climate change, while they are decreasing in the North Sea. The rate of change is slower in the Sable field than in the North Sea, especially for fatigue damage. It has been detected that the human activities are making a considerable impact on wave height and fatigue damage over decade or century time-scale in the North Sea. Although the wave height is considered the dominant wave characteristic in fatigue calculations, fatigue damage is also affected by the change of other wave characteristics. Besides, the effect of human activities in the Sable field is not so pronounced as in the North Sea, and it is partially masked by the randomness of natural variability.

The control simulations are the key to investigating the randomness of natural variability in this study. It is designed to identify the possibilities of climate condition under constant radiative forcing, ignoring the effect of human activities. Due to the limit of computation power however, it is impossible to clarify all the possibilities. Hence, long-term (decades or centuries) simulations are recommended to estimate the confidence interval and to improve the reliability of control simulations. When sampling the result of control simulations, attention should be paid to the sampling time increment. In this Chapter, I compared the sampling results with different time increments (6 hours and 1 year). It turns out that 1-year time increment did not significantly affect the range of natural variability and has dramatically reduced the amount of fatigue calculations. But it does not mean the long-period sampling increment is always recommended, as it is dependent on the sample size and the length of sampling length.

All the wave characteristics may be changing due to climate change. This chapter only discussed the change of wave height. As I concluded above, the changes of other wave parameters are also important for fatigue calculations. In the next chapter, I will further investigate the contribution of other parameters to fatigue change, including wave characteristics, structural properties and other parameters in fatigue calculations, and analyze their sensitivities to the climate change.

References

[1] Zou T, Kaminski ML. Applicability of WaveWatch-III wave model to fatigue assessment of offshore floating structures. *Ocean Dynamics*. 2016; 66:1099-1108.

[2] Wu T, Song L, Li W, Wang Z, Zhang H, Xin X, et al. An overview of BCC climate system model development and application for climate change studies. *Acta Meteorologica Sinica*. 2014; 28:34-56.

[3] Andrew D. *Introduction to Modern Climate Change*. 2 ed: Cambridge University Press; 2012.

[4] Baehr J, Keller K, Marotzke J. Detecting potential changes in the meridional overturning circulation at 26˚N in the Atlantic. *Climatic Change*. 2008; 91:11-27.

[5] Dobrynin M, Murawski J, Baehr J, Ilyina T. Detection and attribution of climate change signal in ocean wind waves. *Journal of Climate*. 2015; 28:1578-1591.

5

SENSITIVITY ANALYSIS FOR OFFSHORE FLOATING STRUCTURES

In Chapter 3 and 4, I projected the future wave conditions, calculated the annual fatigue damage in a floating offshore structure and detected the effect of human-induced climate change on fatigue damage. The methodology basically includes two kinds of simulations: projected ones and controlled ones as discussed in sections 3.5 and 4.3. In numerical simulations, there are always a large number of uncertainties corresponding to different variables and physical schemes. The investigations and reductions of these uncertainties require the effort of scientists and engineers from different fields. Hence, this chapter focuses on the sensitivity analysis of some key variables. The sensitivity of each variable to fatigue damage is evaluated to find out the most sensitive parameters on which we can pay more attention to reduce the degree of uncertainty and to improve the reliability of methodology.

In section 5.1, the definitions of uncertainty and sensitivity analysis are introduced. Then, some key relevant variables are categorized and discussed in section 5.2. As last, the sensitivity analysis is performed on each variable.

5.1 Uncertainty and sensitivity analysis

The previous chapters demonstrated a methodology to project the future sea states and fatigue damage by coupling climate models to wave models. These models use numerical methods to simulate the physical behaviors in the atmosphere and ocean surface. They usually involve data assimilation, physical processes parameterization and governing equations which may induce a lot of uncertainties into the modelling [1]. These uncertainties originate from inaccuracy in the numerical modellings, as the physical processes in the climate system cannot be perfectly represented by the physical scheme in the numerical models. In addition, an uncertainty is not equivalent to an error. An error is a fixed number which represents the difference between the simulated value and the real value. Differently, an uncertainty factor is a statistical variable which represents all the possible values of the error.

There is a large number of variables involved in my methodology, and it is time-consuming to evaluate the uncertainties in all these variables. Fortunately, the contributions of these variables to the variation of fatigue damage are different. It is not necessary to evaluate the uncertainty in all variables. A sensitivity analysis is hence required to determine the most significant variables and how they influence fatigue damage.

Sensitivity analysis is defined as the study of how uncertainty in the output of a model can be attributed to different sources of uncertainty in the model input [2].

To be specific, the sensitivity in this study is the amount of fatigue damage changed when one of the independent variables in the modelling is varied. As mentioned above, the methodology is a comprehensive analysis which involves many variables, and all the effects of variables are combined. Therefore, this chapter conducts sensitivity analysis for some key variables with the purposes as summarized as follows:

- to detect the most important variables affecting fatigue damage;
- to reduce the number of random variables by neglecting the randomness in those less important variables;
- to reduce the computational effort and improve the time efficiency of computations.

5.2 Category of model input parameters

The variable factors in the sensitivity analysis are classified into three categories. The first category includes climate models [3]. Basically, all the state-of-the-art climate models are constructed by the same fundamental physical laws with many specific developments. In the meanwhile, they may differ in parametrizations and numerical formulations [4]. Climate models are complex comprehensive systems which can hindcast or forecast the surface wind field over the globe. However, it is difficult to quantify the reliability of climate modellings. It is basically recommended that the model simulations should be compared with the observations in order to identify the most appropriate climate model and ensemble for a specific sea area [5, 6].

The second category includes parameters in wave models. All the wave models are constructed based on energy or action conservations. They may have different parameters depending on the physical schemes. But there must be two parameters significant for all wave models and settings. They are spatial resolutions and time step settings. The spatial resolution is the distance between neighboring nodes, and the time step represents the time interval between which neighboring nodes exchange their information. A finer spatial resolution and a shorter time interval could improve the reliability of wave simulations, but they are also more time-expensive. Hence, the proper selection of spatial resolution and time step is depending on the purpose of simulations [7].

The last category of variable factors includes wave properties, such wave directions [8, 9]. In traditional scatter diagrams, all the waves are assumed to be equal for all directions. However, the response of offshore floating structures to waves is sensitive to relative wave directions [10]. In order to compare with wave directions, the sensitivities to significant wave height (H_s) and zero-crossing wave period (T_z) are also investigated.

5.3 Sensitivity analysis

In this chapter, sensitivity analysis was conducted for the fatigue damage in FPSO Glas Dowr. All the parameters in fatigue calculations are equal to those presented in the previous chapters including S-N curves and response amplitude operators (RAO). The FPSO is assumed to be operating in two oil fields of the North Sea. They are Rosebank and Alma/Galia. The time series of sea states were constructed by coupling wave models to climate models. The environmental wave spectrum was defined as JONSWAP spectrum. In order to analyse the sensitivities, at least one parameter is changed in the following numerical modelling and calculations. The other settings in the numerical simulations and fatigue calculations are equal to the settings in Chapter 3, if there is no specific explanation.

5.3.1 Climate models

In order to investigate the sensitivity to climate models, wave conditions in North Atlantic were simulated by coupling wave model WAM into five different climate models (GFDL-CM3, HADGEM2, IPS-CM5A-MR, MRI-GCG-CM3 and MIROC5, as introduced in Table 5.1). The ensemble r1i1p1[4] was selected which represents a combination of initial

[4] More information about ensembles in CMIP5 can be found in https://portal.enes.org/data/enes-model-data/cmip5/datastructure

conditions, initialization methods and perturb physics versions of climate models. The radiative forcing from 2081 to 2100 was projected based on the climate scenario RCP8.5. Then, the surface wind field data was obtained from different climate models and interpolated in 50 km grids to run WAM[5]. Then, the fatigue damage of FPSO Glas-Dowr within 2081-2100 was calculated based on the time series of sea states obtained from WAM. Each sea state was represented by JONSWAP spectrum with corresponding H_s and T_z. Absolute wave directions were defined to be equal to relative wave directions in order to simplify the calculations.

Table 5.1: Climate models in sensitivity analysis

Model Name	**Institute**
GFDL-CM3	NOAA Geophysical Fluid Dynamics Laboratory
HadGEM2-A	Met Office Hadley Centre
IPS-CM5A-MR	Laboratoire de M´et´eorologie Dynamique, Institut Pierre Simon Laplace
MRI-GCG-CM3	Meteorological Research Institute
MIROC5	University of Tokyo Center for Climate System Research, National Institute for Environmental Studies, Japan Agency for Marine-Earth Science and Technology Frontier Research Center for Global Change

The 3-hourly sea state data were analyzed and the averaged significant wave height are compared in Fig. 5.1. In Rosebank, the MRI-CGCM3 gives the highest wave height from 5th to 95th percentiles with the highest dispersion. In contrast, the wave height in IPS-CM5A-MR gives a slightly lower wave height at all the percentiles. The other three climate models result in very close significant wave heights at all the percentiles, and their dispersions are also similar. The differences in these three climate models are hence not large enough to make themselves distinguishable from each other. In Alma/Galia, the MRI-CGCM3 still gives the highest wave height with the highest dispersion, but the other four climate models have similar results. In Table 5.2 and Fig. 5.2, the maximum difference of averaged significant wave height among these models is up to 1.44m in Rosebank and 0.83m in Alma/Galia. The ratio between maximum and minimum is 1.67 and 1.56 respectively. It can be concluded that it is important to compare these climate models before making any wave simulations, because they may considerably underestimate or overestimate wave height. In addition, although these models may have a high performance for some other climate variables, they all show very similar abilities in projecting wave simulations except the model MRI-CGCM3 [11].

[5] These wave data were provided by DNV GL and simulated by the Norwegian Meteorological Institute.

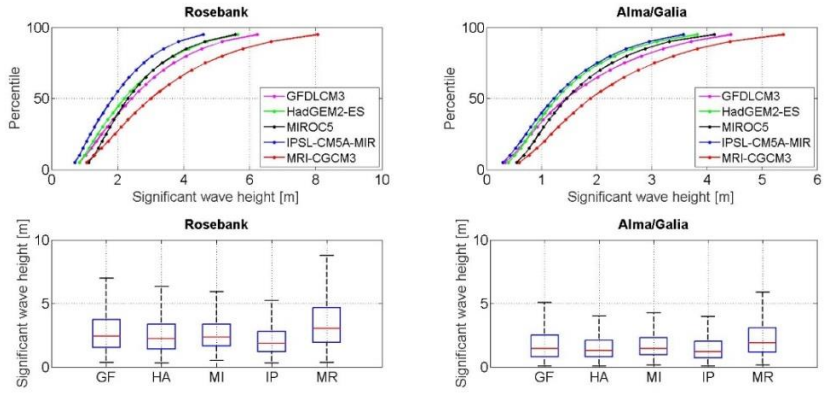

Figure 5.1: Percentiles and box plots of significant wave height with different climate models in Rosebank and Alma/Galia fields.

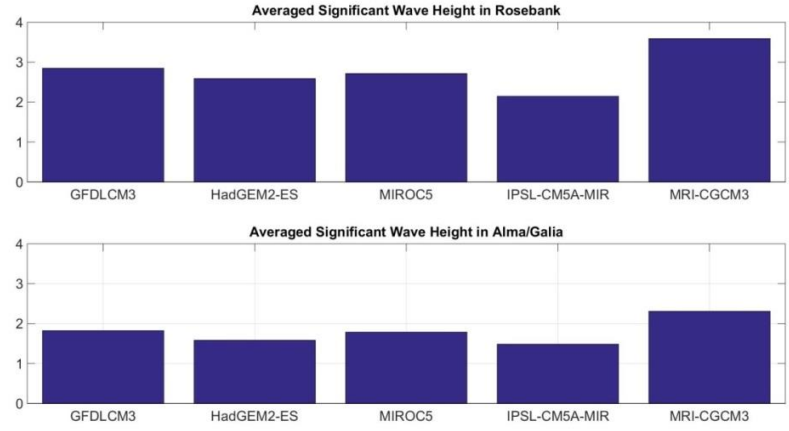

Figure 5.2: Comparisons of averaged significant wave height with different climate models in Rosebank and Alma/Galia fields.

Table 5.2: Comparisons of averaged significant wave height with different climate models in Rosebank and Alma/Galia fields

	GFDL-CM3	HADGEM2	MIROC 5	IPS-CM5A-MR	MRI-GCG-CM3	μ	*SD*	*CV*
	[m]	[m]	[m]	[m]	[m]	[m]	[m]	-
Rosebank	2.85	2.59	2.71	2.15	3.59	2.78	0.52	0.19
Alma/Galia	1.82	1.58	1.79	1.48	2.31	1.80	0.32	0.18

The fatigue damages were calculated based on these sea states, and their mean values are compared in Fig. 5.3 and Table 5.3. The maximum and minimum mean wave heights result from the sea states generated by MRI-GCG-CM3 and IPS-CM5A-MR, and the ratio of extreme values is enlarged up to 2.3 and 3.03. The *CVs* of fatigue damage in both oil fields (0.80 and 0.82) are much higher than the *CVs* of wave height (0.19 and 0.18). It indicates these five climate models result in very different fatigue damages. Although most climate models perform similarly in wave simulations, they may result in different fatigue damages, because the fatigue damage is very sensitive to the change of wave height. I will further discuss this point in section 5.3.3.

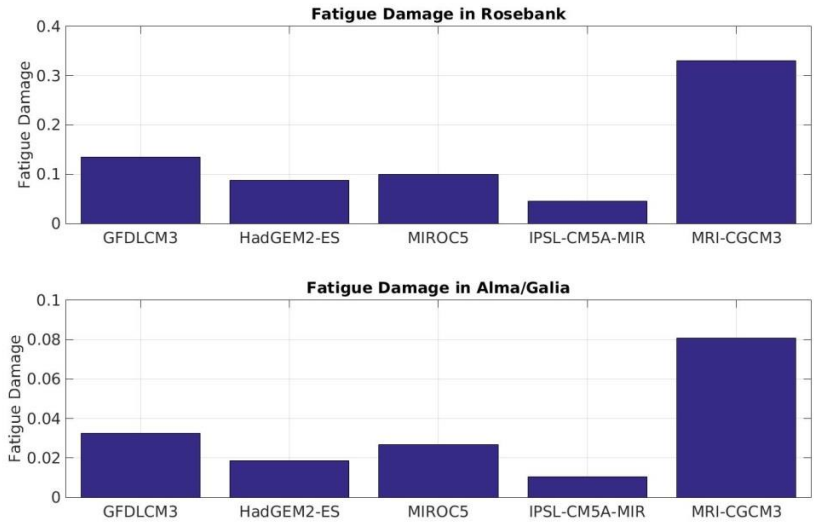

Figure 5.3: Comparisons of fatigue damage with different climate models in Rosebank and Alma/Galia fields.

Table 5.3: Comparisons of fatigue damage with different climate models in Rosebank and Alma/Galia fields

	GFDL-CM3	HADGEM2	MIROC5	IPS-CM5A-MR	MRI-GCG-CM3	μ	*SD*	*CV*
Rosebank $[\times 10^{-2}]$	13.52	8.81	9.99	4.54	33.00	13.89	11.11	0.80
Alma/Galia $[\times 10^{-2}]$	3.25	1.85	2.67	1.03	8.09	3.37	2.76	0.82

The sea states were also simulated by the climate model MIROC5 model with three different ensembles (r1i1p1, r2i1p1, r3i1p1), and the corresponding fatigue damage was calculated. The comparisons of H_s and fatigue damage are shown in Fig. 5.4 and 5.5. It can be seen that different ensembles made a very limited impact on H_s and fatigue damage. The wave heights only slightly differ at the 5th percentile, and the fatigue damages of these three ensembles are equal.

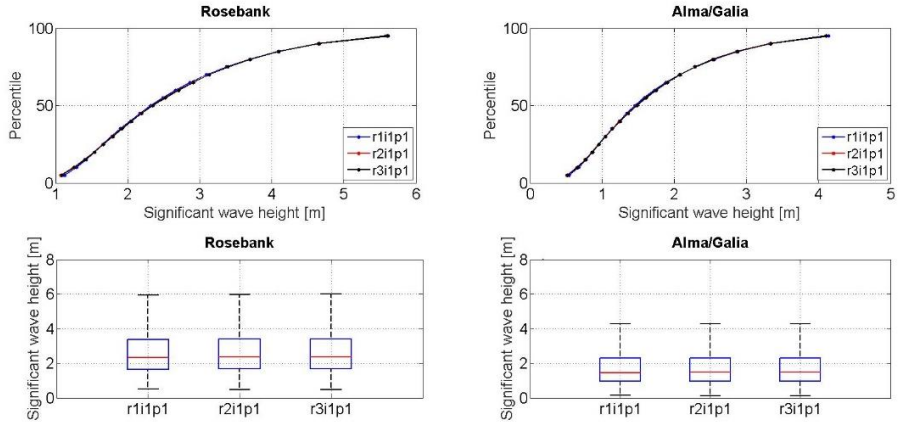

Figure 5.4: Percentiles and box plots of significant wave height with different ensembles in Rosebank and Alma/Galia fields.

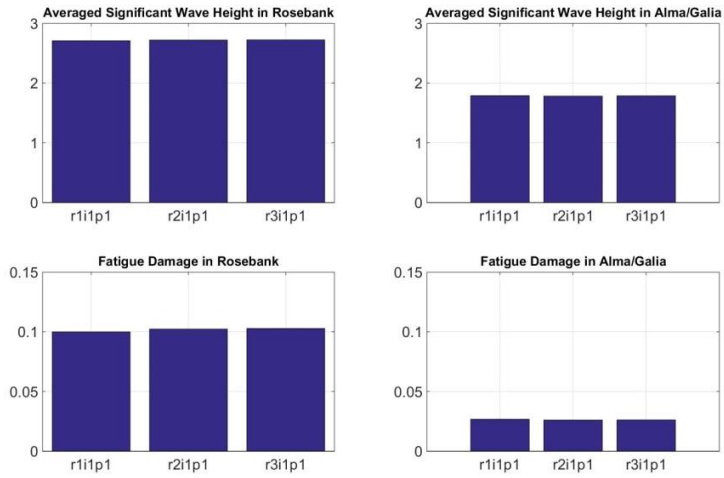

Figure 5.5: Comparisons of H_s and fatigue damage with different ensembles in Rosebank and Alma/Galia fields.

5.3.2 Wave model parameters

Spatial resolutions and time steps are two key parameters in wave model simulations. In order to investigate the sensitivity of fatigue damage to them, the time series of wave conditions in 2091 were generated by coupling WaveWatch-III wave model (WW3) to CMCC-CM with different grid sizes ($0.25° \times 0.25°, 0.75° \times 0.75°, 1.25° \times 1.25°, 1.50° \times 1.50°$ Lat/Lon) and different time step settings. There are four time-steps in each setting specifically for global wave propagations, spatial wave propagations, directional wave propagations and source term, as listed in Table 5.4.

Table 5.4: Time step settings. The number after setting is the global time step

Time step	Global [s]	Spatial [s]	Directional [s]	Source term [s]
Setting 450	450	225	225	15
Setting 900	900	450	450	75
Setting 1800	1800	600	60	150
Setting 3600	3600	1200	1800	300
Setting 7200	7200	2400	2400	600

1) The global time step is defined by which the entire solution is propagated in time and at which the input wind or currents are interpolated;
2) The second time step is for spatial wave propagations. If it is smaller than the global time step, the propagation is calculated grid by grid with a number of successive smaller time steps. This time step is also important for Currant-Friedrich's-Levy criterion.
3) The third one is for intra-spectral propagation. It is used to solve the Eq. (3.2) in the draft but without the spatial and source terms, as listed below.

$$\frac{\partial \mathrm{N}}{\partial \mathrm{t}} + \frac{\partial}{\partial \mathrm{k}} \dot{\mathrm{k}} \mathrm{N} + \frac{\partial}{\partial \theta} \dot{\theta} \mathrm{N} = 0 \tag{5.1}$$

   $\dot{\boldsymbol{k}}$ and $\dot{\boldsymbol{\theta}}$ are the wave number velocity and the directional objects which are defined in Eqs. (3.4) and (3.5).
4) In deep water, the source term includes three parts: wind-wave generation, nonlinear wave-wave interaction and dissipation by wave breaking. This time step is used to dynamically adjust the integration of the source term for each grid. When facing a rapidly changing source term, such as a rapidly changing wind force, the global time step may be too long to make an accurate calculation. Then, this source term time step is set as the minimum allowed value. When running WW3, a dynamic time step is calculated for each grid point separately for the information exchange between source terms and grids. The length of this dynamic time step is between the source term time step and the global time step. In this way, WW3 can make a more accurate calculations, and it minimizes the increased amount of calculations.

The climate scenario RCP8.5 is chosen to project the radiative forcing. The wave conditions based on different combinations of grid sizes and time step settings are compared in Table 5.5 and Figs. 5.5-5.6. There are some blanks in Table 5.5 due to Currant-Friedrich's-Levy criterion: the speed of fastest waves in the model must be less than or equal to the cell spacing (*i.g.,* the distance between neighboring nodes) divided by the time step.

Table 5.5 (a): Comparisons of H_s with different time step settings in Rosebank

	Global 450	Global 900	Global 1800	Global 3600	Global 7200	*SD*
	[m]	[m]	[m]	[m]	[m]	[m]
0.25° × 0.25°	2.34	-	-	-	-	-
0.75° × 0.75°	2.23	2.23	2.24	2.26	2.35	0.05
1.25° × 1.25°	2.13	2.13	2.14	2.15	2.19	0.02
1.50° × 1.50°	2.07	2.07	2.07	2.08	2.10	0.01
SD	0.12	0.08	0.09	0.09	0.13	-

Table 5.5 (b): Comparisons of H_s with different time step settings in Alma/Galia

	Global 450	Global 900	Global 1800	Global 3600	Global 7200	*SD*
	[m]	[m]	[m]	[m]	[m]	[m]
0.25° × 0.25°	1.29	-	-	-	-	-
0.75° × 0.75°	1.34	1.35	1.35	1.36	1.43	0.04
1.25° × 1.25°	1.31	1.31	1.31	1.32	1.34	0.01
1.50° × 1.50°	1.37	1.37	1.37	1.38	1.40	0.01
SD	0.04	0.03	0.03	0.03	0.05	-

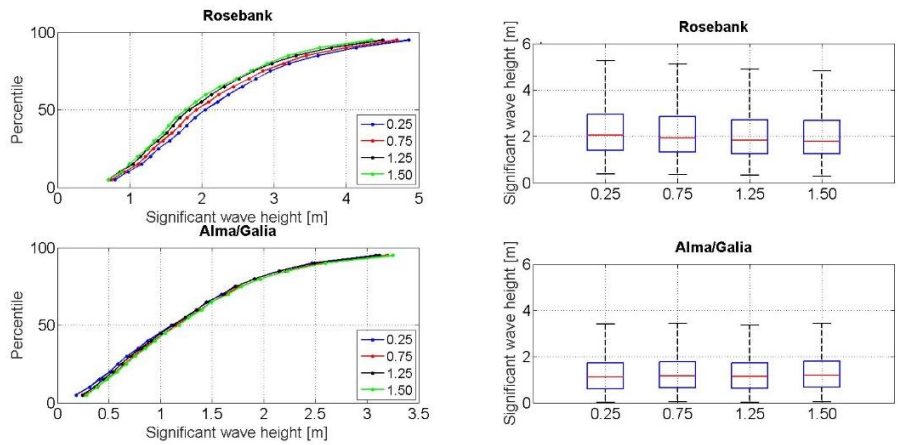

Figure 5.6: Percentiles and box plots of significant wave height under different grids in Rosebank and Alma/Galia fields.

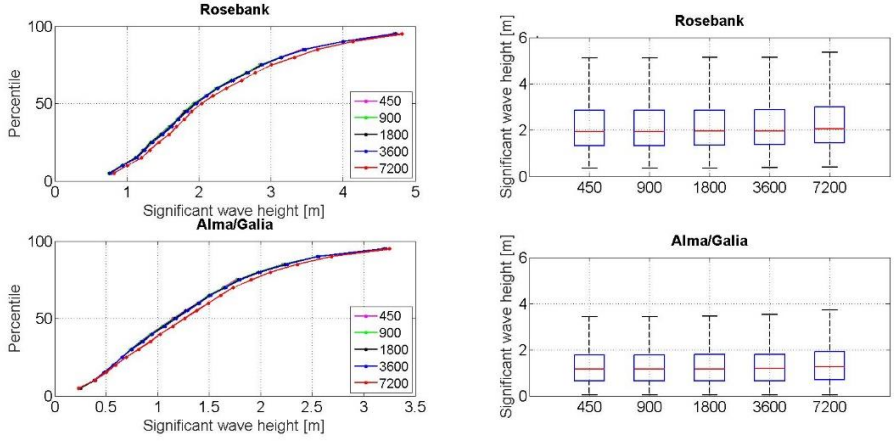

Figure 5.7: Percentiles and box plots of significant wave height under different time steps in Rosebank and Alma/Galia fields.

It can be concluded that the averaged significant wave height of Rosebank is rising up with the increase of time steps or with the decrease of cell size. For Alma/Galia oil field, a finer resolution (smaller grid sizes and shorter time steps) may result in lower wave height, except that H_s of $1.25° \times 1.25°$ is slightly lower than H_s of $0.75° \times 0.75°$. Their different trends may result from the oil fields' different locations. Alma/Galia is a windsea dominant sea area. In contrast, Rosebank is more vulnerable to waves from North Atlantic.

The standard deviation for both oil fields is very small. By changing the gird sizes and time steps, the averaged wave height may not significantly increase or decrease. As fatigue damage is, however, a long-term cumulative process, a small increase/decrease of wave height may result in a considerable change of fatigue damage. In addition, *SD* of each grid size is generally smaller than *SD* of each time step. It indicates that the wave height is more sensitive to the change of grid sizes than the change of time steps.

Fatigue damage of Glas-Dowr was calculated based on different time series of wave conditions. The first five time-series were generated with the same grid size ($0.75° \times 0.75°$ Lat/Lon) but different time step settings. Another four time-series were constructed with the same time step setting (*i.g.*, the global time step is 3600s) but different grid sizes. The results of fatigue calculations were compared in Fig. 5.8. It can be seen from the left two subfigures that the fatigue damage increases with longer time step in both oil fields.

In Table 5.6(a), *SD* and *CV* are relatively small. The fatigue life with different time steps can differ by 26 years (8%) in Rosebank and 157 years (13%) in Alma/Galia. Longer time steps in wave simulations would slightly underestimate the fatigue lifetime of offshore structures.

According to Table 5.6(b), fatigue damage in Rosebank is generally decreasing with coarser spatial resolutions. In Alma/Galia, there is no constant trend of fatigue damage with the change of spatial resolutions. *SD* and *CV* of fatigue damage are also small. The fatigue life with different spatial resolutions differs by 79 years (25%) in Rosebank and 157 years (19%) in Alma/Galia. Hence, it can be concluded that the sensitivity of fatigue damage to spatial resolutions is more significant than to time steps.

Table 5.6 (a): Comparisons of fatigue damage and fatigue life with different time step settings

	Global 450	Global 900	Global 1800	Global 3600	Global 7200	μ	*SD*	*CV*
Rosebank [$\times 10^{-3}$]	2.87	2.88	2.89	2.93	3.11	2.94	0.10	0.03
Fatigue life [year]	348	347	346	341	322	341	-	-
Alma/Galia [$\times 10^{-3}$]	0.75	0.76	0.77	0.79	0.85	0.78	0.04	0.05
Fatigue life [year]	1333	1316	1299	1266	1176	1278	-	-

Table 5.6 (b): Comparisons of fatigue damage and fatigue life with different spatial settings

	$0.25° \times 0.25°$	$0.75° \times 0.75°$	$1.25° \times 1.25°$	$1.50° \times 1.50°$	μ	*SD*	*CV*
Rosebank [$\times 10^{-3}$]	3.21	2.87	2.56	2.60	2.81	0.30	0.11
Fatigue life [year]	311	349	390	384	359	-	-
Alma/Galia [$\times 10^{-3}$]	0.68	0.75	0.70	0.82	0.74	0.06	0.08
Fatigue life [year]	1463	1332	1430	1225	1363	-	-

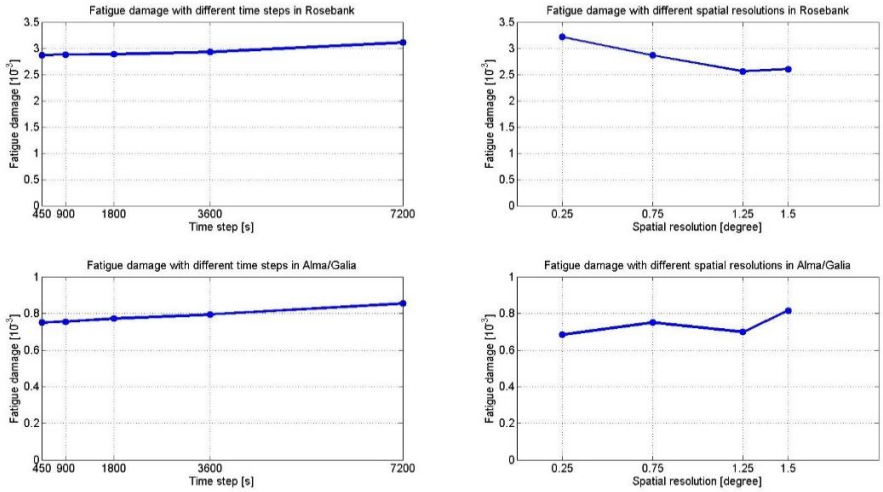

Figure 5.8: Comparisons of H_s and fatigue damage with different spatial resolutions and time step settings in Rosebank and Alma/Galia.

The calculation amount is increasing dramatically with finer spatial resolution and time steps. Hence, it is not recommended to extremely improve them due to the time efficiency of calculations. As can be seen from Table 5.6, when the time step is improved from Global 900 to Global 450, the fatigue life time is only changed by 1 year in Rosebank and 17 years in Alma/Galia. An extremely short time step is not necessary for wave simulations.

As for spatial resolution, multi-grid simulations are recommended [12-14]. The target sea area is meshed by finer grids, and the other neighbouring sea areas are meshed by a coarse resolution to reduce the calculation amount. In this study, three regular grids are nested for the simulations as shown in Fig. 5.9. The outermost grid is $0.75° \times 0.75°$ resolution over the North Atlantic; the second grid is $0.50° \times 0.50°$ over the North Sea and the innermost grid centred around Alma/Galia field with the resolution of $0.25° \times 0.25°$. The sea states from 2091 to 2100 were projected based on RCP8.5, and the result was compared with the simulations under one single grid ($0.25° \times 0.25°$), as shown in Fig. 5.10. The multi-grid does not significantly change the performance of wave modelling. The significant wave heights simulated under different grid settings have very similar statistical properties (*e.g.,* percentile, mean and distribution). The annual fatigue damages induced by these sea states are also as close as expected, see Table 5.7.

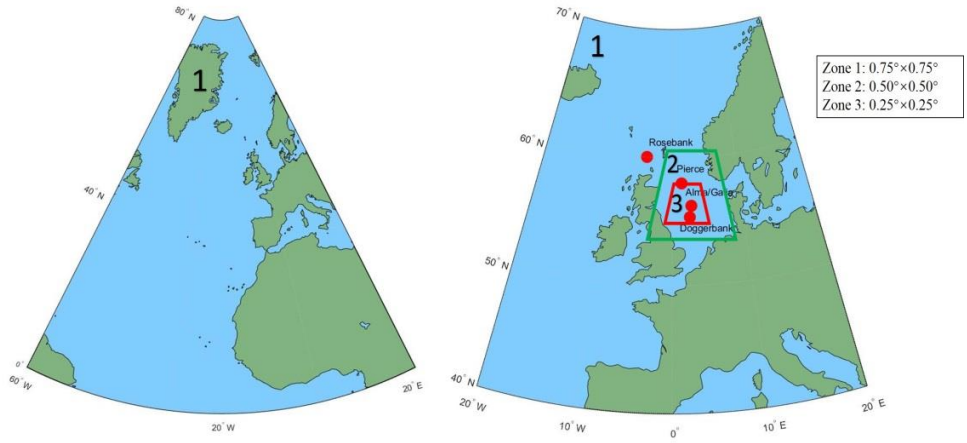

Figure 5.9: The three wave model grids. The outermost grid is $0.75° \times 0.75°$ resolution over the North Atlantic (0°-80°N/60°W-20°E); the second grid is $0.50° \times 0.50°$ over the North Sea (50°N-60°N/6°W-8°E) and the innermost grid centred around Alma/Galia field with the resolution of $0.25° \times 0.25°$ (53°N-58.5°N/0-7°E).

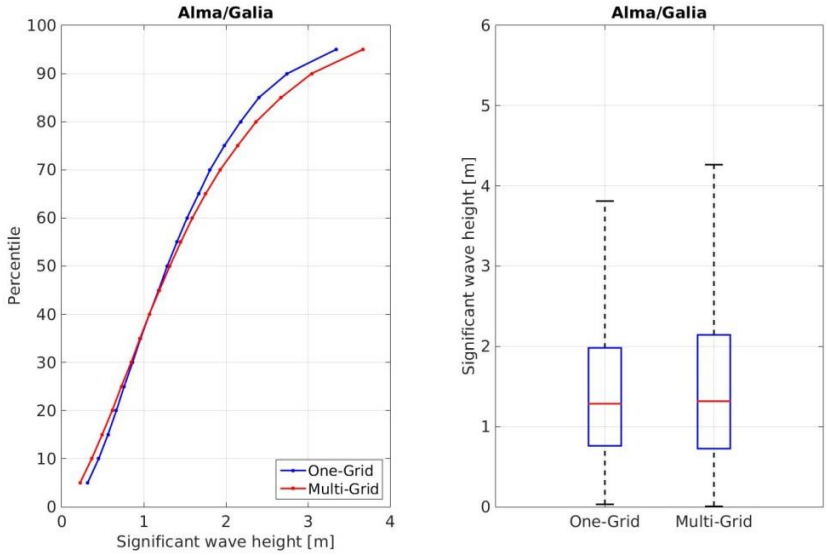

Figure 5.10: Percentiles and box plots of significant wave height under one-grid and multi-grid in the Alma/Galia field.

Table 5.7: Annual fatigue damages under one-grid and multi-grid in the Alma/Galia field

		2091	2092	2093	2094	2095	2096	2097	2098	2099	2100
Fatigue	One-grid	0.87	0.68	0.80	0.76	0.73	0.71	0.67	0.73	0.70	0.72
[$\times 10^{-3}$]	Multi-grid	0.90	0.70	0.86	0.78	0.71	0.74	0.69	0.77	0.75	0.74

5.3.3 Wave properties

In order to evaluate the sensitivities of fatigue damage to wave parameters, significant wave height (H_s) and zero-crossing wave period (T_z) and relative wave directions are taken into account. Based on RCP8.5, the sea states of Rosebank and Alma/Glia in 2091 were simulated by coupling WaveWatch-III to CMCC-CM. In this sea area, a joint distribution of H_s and T_z is constructed to represent the probability of all the sea states. Vanem and Bitner-Gregersen used a 3-paramenter Weibull distribution to describe the distribution of H_s and a log-normal distribttion to represent the conditional distribution of T_z, as shown in Eqs. (5.2)-(5.6) [15].

$$f_{H_s,T_z}(h,t) = f_{H_s}(h) f_{T_z|H_s}(t|h) \tag{5.2}$$

$$f(h) = \frac{\beta}{\alpha}\left(\frac{h-\gamma}{\alpha}\right)^{\beta-1} e^{-\left(\frac{h-\gamma}{\alpha}\right)^{\beta}}, h \geq \gamma \tag{5.3}$$

$$\mu_t = E[\ln T_z | H_s = h_s] = a_1 + a_2 h_s^{a_3} \tag{5.4}$$

$$\sigma_t = sd[\ln T_z | H_s = h_s] = b_1 + b_2 e^{b_3 h_s} \tag{5.5}$$

$$E(T_z) = \exp\left(\mu_t + \frac{{\sigma_t}^2}{2}\right) \tag{5.6}$$

where:

f_{H_s,T_z} : the joint distribution of H_s and T_z;

f_{H_s} : the marginal distribution of H_s (Weibull distribution);

$f_{T_z|H_s}$: the conditional distribution of T_z (log-normal distribution);

α, β and γ : the scale, shape and location parameters of Weibull distribution;

μ_t and σ_t : the parameters of log-normal distribution;

a_i and b_i : the empirical parameters to estimate μ_t and σ_t.

Then, the wave parameters in the sea states were assumed to be changed in the following conditions:

(1) H_s increases or decreases by 10% (±10%).

The significant wave height of each 6-hourly sea state increases or decreases by 10%. T_z is also changed based on the conditional distribution as Eqs. (5.4) and (5.5). Then, the mean zero-crossing wave period for each sea state is calculated by Eq. (5.6). The parameters for the originally-fitted and modified 3-paramenter Weibull distribution of H_s are listed in Table 5.8. By changing the wave height of sea states, the plot of the Weibull distribution is moving right and left as shown in Fig. 5.11. The parameters for the conditional distribution of T_z are assumed unchanged. This assumption is believed to be reasonable, because the marginal distribution of wave period will be correspondingly changing if the Weibull distribution of H_s is changed, even though the conditional distribution of wave period is unchanged [15].

(2) T_z is extended or reduced by 10% (±10%).

The mean zero-crossing wave period for each sea state is extended or reduced by 10%. H_s is also changed based on the conditional distribution. Basically, this condition is the reverse process of the first condition where H_s increases or decreases by 10%.

(3) The relative wave direction is changed clockwise and anticlockwise by 36° (±360°×10%).

Table 5.8: Parameters for the 3-paramenter Weibull distribution and the log-normal distribution

	α	β	γ
Fitted Weibull distribution	2.260	3.380	0.500
Modified Weibull distribution (+10%)	2.487	3.380	0.545
Modified Weibull distribution (-10%)	2.035	3.380	0.446
Log-normal distribution	a_1= 0.100	a_2= 1.489	a_3= 0.190
	b_1= 0.040	b_2= 0.175	b_3= -0.224

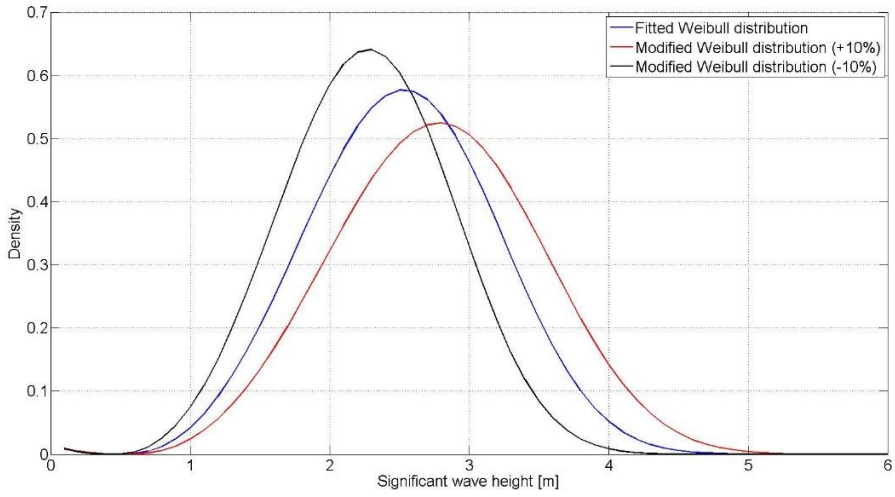

Figure 5.11: The originally-fitted and modified Weibull distributions for significant wave height.

For each condition, another two time-series of sea states were constructed. The fatigue damages based on these two time-series were boundary values. The tornado diagrams of fatigue damage associated with these wave parameters are plotted in Fig. 5.12. The result is discussed below:

(1) H_s increases or decreases by 10% (±10%).

The fatigue damages are increased by 29% and 41% in Rosebank and Alma/Galia, when the wave height rises by 10%. It indicates fatigue damage is very sensitive to the change of wave height.

(2) T_z is extended or reduced by 10% (±10%).

In this condition, the fatigue damage is changed significantly. The fatigue damages are increased by 74% and 80% in Rosebank and Alma/Galia, when the wave period is extended by 10%. It looks that the fatigue damage is more sensitive to the change of wave period than wave height. But this sensitivity is induced by the joint distribution between wave height and wave period. According to Eqs. (5.4) and (5.5), when the wave period is changed by 10%, the wave height of some sea states may also change by up to 25%, which results in such a big change of fatigue damage. If the wave height and period are assumed to be independent, the tornado diagram is shown in Fig. 5.13. As seen, the sensitivity to wave period is lower than to wave height.

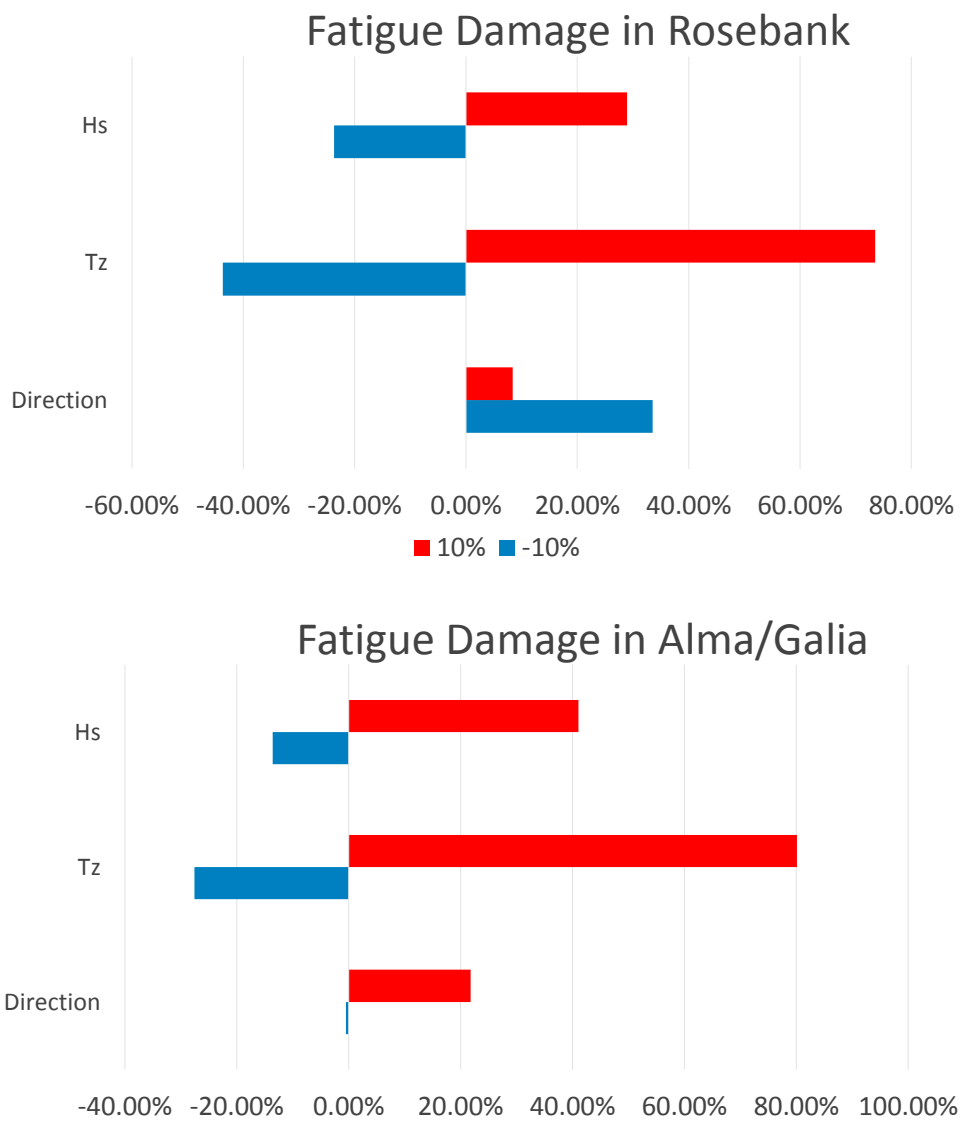

Figure 5.12: Tornado diagram showing the sensitivity of fatigue damage to each wave parameter in Rosebank and Alma/Galia. The significant wave height and zero-crossing wave period are correlated based on the joint distribution in Eq. (5.2).

(3) The relative wave direction is changed clockwise and anticlockwise by 36° (±360°×10%).

The boundary value associated with wave direction reached 22%. It indicates that the change of relative wave direction may result in a considerable impact on fatigue damage. The

extent of this impact is determined by the direction-dependant RAOs. Offshore structures respond differently to waves from different directions. Hence, for a turret moored FPSO, vessel heading analysis is very important in fatigue design, because it can alter vessel headings to get a different structural response to environmental loadings and significantly affect the design fatigue life of structures.

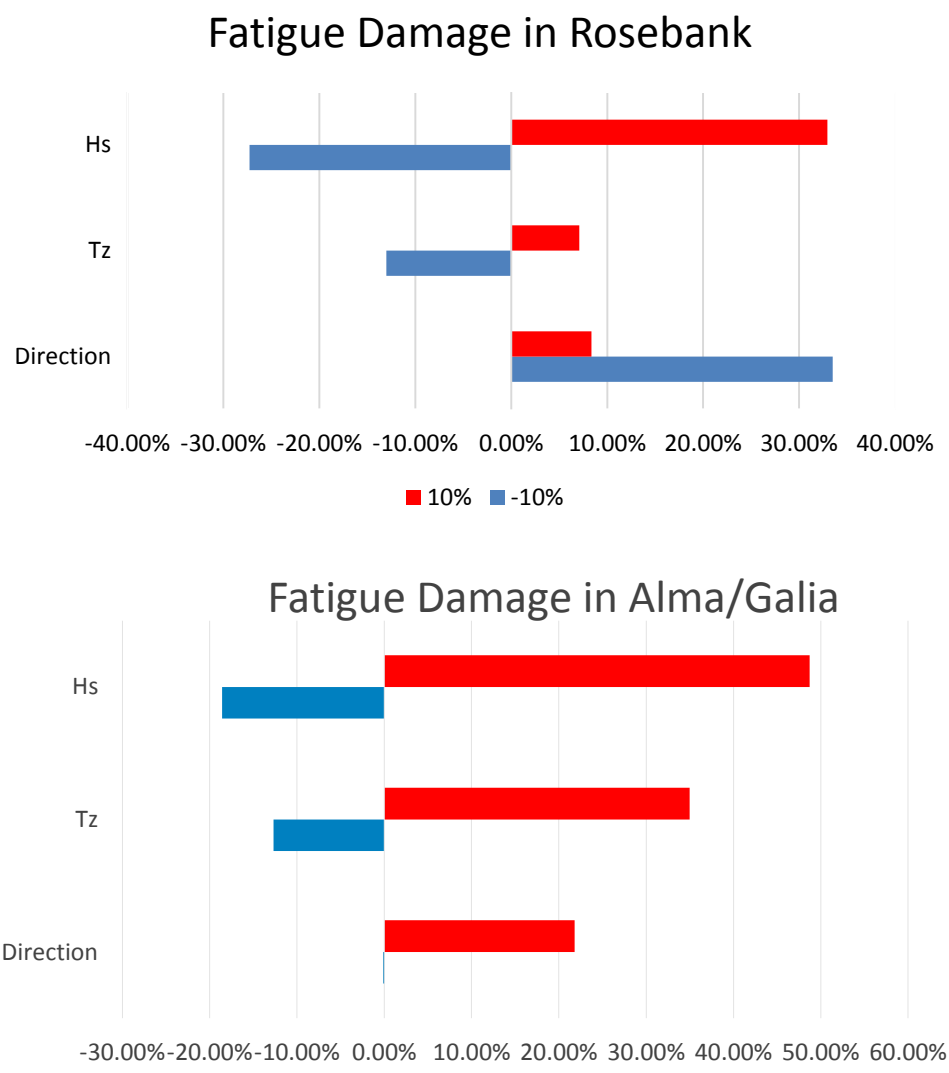

Figure 5.13: Tornado diagram showing the sensitivity of fatigue damage to each wave parameter in Rosebank and Alma/Galia. The significant wave height and zero-crossing wave period are assumed independent.

5.4 Conclusions

In this chapter, I investigated the sensitivity of offshore floating structures against several variable factors. The significance of variable factors to fatigue damage was evaluated. They are classified into three categories: climate models, spatial resolutions & time step settings, and wave parameters. Fatigue damage was calculated based on different time-series of wave conditions which were constructed with different variable factors.

The analysis indicates that most climate models show very similar abilities in projecting wave simulations, but it is still necessary to carefully select the climate models, because the fatigue damage is very sensitive to the change of wave height. An improper climate model can underestimate or overestimate fatigue damage. Hence, the climate model for a certain sea area requires validations by observations and measurements before projecting the impact of climate change on sea states and fatigue damage.

A finer spatial resolutions and time step settings will make more confidence on the simulations. But it is also very time-consuming. Modelling with longer time steps may overestimate the wave height and fatigue damage in the North Sea. The impact of grid sizes is rather region-dependant. As the coefficient of variation for fatigue damage over different spatial resolutions or time steps are quite small, it indicates their sensitivities are not so significant. Therefore, it is not recommended to simulate sea states with an extremely finer spatial resolution and time step. Instead, the multi-grid mesh may be a proper solution.

It is already widely accepted that wave height and wave period are key parameters in fatigue assessment. However, the traditional scatter diagrams provide limited information on wave directions. The tornado diagrams show that fatigue damage of FPSOs is also very sensitive to relative wave directions. Therefore, the directional time series of sea states constructed by wave modelling have another advantage, because wave models can generate information about the wave direction and wave spreading over all sea areas. For turreted FPSOs, vessel heading analysis can significantly improve the accuracy of fatigue calculations.

As stated above, the improvement of this methodology requires efforts from different fields, such as meteorology, oceanography and offshore engineering. This chapter has evaluated the significance of each variable and pointed out which variables need more attention to improve the reliability and reduce the uncertainties.

References

[1] Church JA, Clark PU, Cazenave A, Gregory JM, Jevrejeva S, Levermann A, et al. Sea Level Change. In: Stocker TF, Qin D, Plattner G-K, Tignor M, Allen SK, Boschung J, et al., editors. Climate Change 2013: The Physical Science Basis Contribution of Working Group I to the Fifth Assessment Report of the Intergovernmental Panel on Climate Change. Cambridge, United Kingdom and New York, NY, USA: Cambridge University Press; 2013; 1137–1216.

[2] Saltelli A, Ratto M, Andres T, Campolongo F, Cariboni J, Gatelli D, et al. *Global Sensitivity Analysis. The Primer.* 2008.

[3] Woollings T, Gregory JM, Pinto JG, Reyers M, Brayshaw DJ. Response of the North Atlantic storm track to climate change shaped by ocean-atmosphere coupling. *Nature Geoscience*. 2012; 5:313-7.

[4] Solomon S, Qin, D., Manning, M., Chen, Z., Marquis, M., Averyt, K.D., Tignor, M. & Miller, H.L. (eds). Contribution of Working Group I to the Fourth Assessment Report of the Intergovernmental Panel on Climate Change. Cambridge, United Kingdom and New York, NY, USA. 2007; 996.

[5] Donat MG, Leckebusch GC, Wild S, Ulbrich U. Benefits and limitations of regional multi-model ensembles for storm loss estimations. *Clim Res*. 2010; 44:211-25.

[6] Hemer MA, Katzfey J, Trenham CE. Global dynamical projections of surface ocean wave climate for a future high greenhouse gas emission scenario. *Ocean Modelling*. 2013; 70:221-245.

[7] Colle BA, Zhang ZH, Lombardo KA, Chang E, Liu P, Zhang MH. Historical Evaluation and Future Prediction of Eastern North American and Western Atlantic Extratropical Cyclones in the CMIP5 Models during the Cool Season. *Journal of Climate*. 2013; 26:6882-6903.

[8] Charles E, Idier D, Delecluse P, Deque M, Le Cozannet G. Climate change impact on waves in the Bay of Biscay, France. *Ocean Dynamics*. 2012; 62:831-848.

[9] Gallagher S, Tiron R, Dias F. A Detailed Investigation of the Nearshore Wave Climate and the Nearshore Wave Energy Resource on the West Coast of Ireland. *Proceedings of the Asme 32nd International Conference on Ocean, Offshore and Arctic Engineering - 2013 - Vol 8*. 2013.

[10] Wing DA, Johnson MC. Ship Operability Predicted from Long Term Directional Wave Records. *Int J Marit Eng*. 2011; 153:A105-A13.

[11] Hemer MA, Trenham CE. Evaluation of a CMIP5 derived dynamical global wind wave climate model ensemble. *Ocean Modelling*. 2016; 103:190-203.

[12] Gallagher S, Gleeson E, Tiron R, McGrath R, Dias F. Wave climate projections for Ireland for the end of the 21st century including analysis of EC-Earth winds over the North Atlantic Ocean. *Int J Climatol*. 2016; 36:4592-4607.

[13] Gallagher S, Gleeson E, Tiron R, McGrath R, Dias F. Twenty-first century wave climate projections for Ireland and surface winds in the North Atlantic Ocean. *Advances in Science and Research*. 2016; 13:75-80.

[14] Gleeson E, Gallagher S, Clancy C, Dias F. NAO and extreme ocean states in the Northeast Atlantic Ocean. *Advances in Science and Research*. 2017; 14:23-33.

[15] Vanem E, Bitner-Gregersen EM. Stochastic modelling of long-term trends in the wave climate and its potential impact on ship structural loads. *Applied Ocean Research*. 2012; 37:235-248.

6

CONCLUSIONS AND RECOMMENDATIONS

6.1 Overview of methodology

This thesis presented a methodology to project the effect of climate change on future fatigue damage in order to improve the fatigue design of floating offshore structures, as illustrated in Fig.6.1. Its key procedures are concluded as follows:

1. The projection of climate change impact starts with the construction of climate scenarios.
2. Global climate models are used to simulate the global surface wind field.
3. The wind-driven wave model simulates short-term wave conditions in terms of wave spectra and produces time series of sea states for fatigue calculations.
4. Stress analysis and fatigue assessment are conducted based on wave time series.
5. The effect of climate change is evaluated, and future fatigue damage is projected.

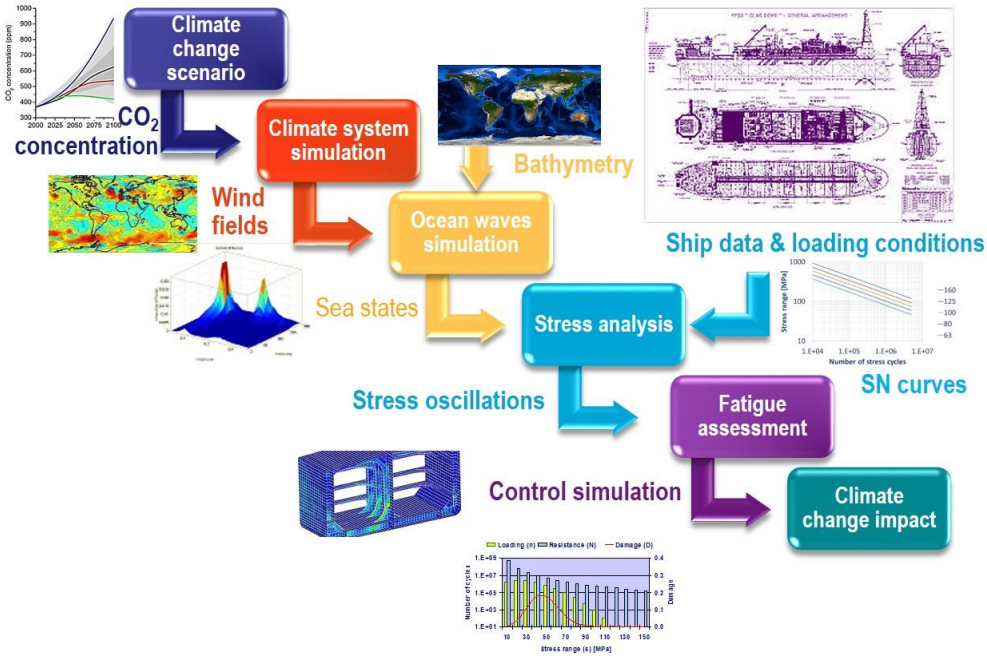

Figure 6.1: Procedures of fatigue assessment method with allowance for climate change

6.2 Main conclusions

The literature review in Chapter 1 has introduced the effect of climate change, especially on floating offshore structures. In order to project the climate change impact on fatigue damage, several important challenges were identified. First, the past climate trend should not necessarily be representative of the future climate trend, because the rate of climate change is affected by both human activities and random natural variability. Second, the statistical approach can hardly simulate all the relevant physical process in the climate circulation and the evolution of wave spectra. Third, the fatigue assessment requires the time series of sea

states including both wind waves and swells. The commonly-used assumption of a linear or quadratic trend in sea states is not appropriate for fatigue design, because the significant wave height of short-term sea states in reality does not change following a linear or quadratic trend.

In Chapter 2, I introduced the mechanics of climate change and its relationship with fatigue damage of offshore floating structures. Then, the first key question: "Why does the climate change affect wave conditions and consequently affect fatigue damage of offshore floating structures?" was answered. Similar to the climate change, fatigue failure is also a long-term cumulative process, and the main external source of fatigue damage for offshore floating structures is from wave loading. Due to the climate change, the wave climate in a specific sea area changes over time. More attention should hence be paid to the wave scatter diagrams or time series of sea states which have been constructed in the past, as they may not be totally representative of the sea states in the future. Otherwise, the fatigue design may overestimate or underestimate the fatigue life of floating structures.

Based on the mechanics of the climate system, the climate models were used to simulate the physical process of climate circulations, as discussed in Chapter 3. This chapter gave the answer to the second key question: "How can these physical processes in the climate system be numerically simulated?". The original driving force of climate system is solar radiation, and its radiative forcing trajectories were projected by the climate scenarios Representative Concentration Pathways (RCPs). The climate scenarios are not accurate prediction of future climate. Instead, each of them represents one possibility of future radiative forcing trajectory which is highly affected by human policies and activities. Then, climate models were used to simulate the circulation of atmosphere including the surface wind field. As the primary driving forcing of wave generation is the surface wind field, the wind-driven wave model WaveWatch-III was applied, based on the conservation of wave energy, to simulate the evolutions of wave spectra in the wave generation, wave-wave interaction, wave propagation, and wave dissipation. As a result, the sea states and annual fatigue damage of the Floating Production, Storage and Offloading unit (FPSO) in the Sable field and the North Sea were projected, based on the climate scenario RCP8.5.

Chapter 4 is the response to the last key question: "To what extent the climate change affects wave conditions and fatigue damage?". As the climate change results from both natural variability and human-induced climate change, the control simulations were carried out to evaluate the range of natural variability and to detect the impact of human activities. By controlling the radiative level, the effect of human-induced climate change was eliminated, and the range of natural variability was estimated as 0.05 and 0.95 confidence intervals. The trajectories of significant wave height and annual fatigue damage in each considered oil field were evaluated, and the effect of human-induced climate change was detected through the comparisons between control simulations and projected simulations. It is concluded that the effect of climate change is region-dependent. The annual fatigue damage in the Sable field is increasing, while it is decreasing in the North Sea. Besides, the effect of human-induced climate change on wave height and fatigue damage is significant in the North Sea, whereas it is less pronounced in the Sable field. At last, the trend of wave height is not individually representative of the trend of annual fatigue damage. The changes of other wave characteristics (such as wave period and wave direction) are also important to fatigue damage.

The accuracy of the proposed methodology in this dissertation is also dependent on the choices of climate models. These models involve many variables and parameters. These variables resulted in a high degree of uncertainty. In Chapter 5, a sensitivity analysis was

conducted to determine the most significant variables and to evaluate how they influence the calculated fatigue damage.

The methodology presented in the thesis has the following advantages:

- The effect of climate change on fatigue damage is projected based on the mechanics of climate change. The changes of all the relevant climate factors, such as GHG emissions, surface wind field or wave properties, are considered.
- Wave models can generate continuous time-series of wave conditions in either global or regional scale. The wave conditions from wave models are automatically partitioned to different wave systems (wind waves and swells), which are important for (multiaxial) fatigue analyses [1].
- Structural stresses and fatigue damage are sensitive to wave directions. The wave scatter diagrams in classification notes are assumed to be equal for all wave directions [2]. In contrast, both wave direction and directional spreading are considered in numerical wave models, which can improve the reliability of fatigue design.

By utilizing this methodology, it would be possible for designers and operators to:

1. identify the effect of climate change on long-term wave loading and consequently on fatigue life of offshore structures;
2. increase safety of structures during operational stage;
3. better justify service life extension of offshore structures;
4. improve fatigue design of future offshore structures.

6.3 Validations and development

As mentioned in section 3.2, climate models were constructed with many different specific developments [3]. These climate models can only meaningfully be evaluated relative to a specific purpose [4], because they were designed to simulate the circulation of climate system for different specific purposes and may differ in parametrizations and numerical formulations. The reliability of climate models is region-dependent. Since there is no widely-accepted universal climate models and wave models for all sea areas around the globe, for one specific sea area, these models are usually validated by measurement and observations. Unfortunately, the validations of these models for fatigue assessments are still not known to the author. For fatigue design, further validations of climate models and wave models are highly recommended to evaluate the reliability of their simulations on wave height, wave period and wave directions.

In fatigue assessment, the time-series of short-term sea states are required. The validation of climate and wave models is in the preliminary stage in terms of simulating short-term sea states. For now, it is too early to require each simulated sea state to fit the time series of observations. We should pay more attentions to their short-term statistical characteristics, including the average value and the variation which are essential for fatigue calculations.

6.4 Recommendation for future work

In this thesis, I presented a methodology which can projects the future fatigue damage of FPSOs. This methodology is applicable to all types of offshore structures, such as fixed platforms, semi-submersible, and offshore wind farms. As it is a multidisciplinary study, there are several recommendations to researchers from different fields listed as follows:

The traditional fatigue design of offshore structures is based on the results from uniaxial and constant amplitude fatigue tests in combination with the damage accumulation hypothesis. In reality however, the sea states consist of several wave systems (one wind wave and multiple swells), which may result in multiaxial stress states. In addition, the sequence of sea states or stress states also affects the amount of fatigue damage. For the future work, it is recommended to combine the proposed methodology in this thesis with the assessment of multiaxial fatigue to improve the accuracy of fatigue design.

The trajectories of radiative forcing and greenhouse gas concentrations from many widely-used climate scenarios were constructed discretely with a relatively long-time interval (normally one year). The interannual variation is mainly based on interpolations. The fatigue calculations of offshore structures however require the time series of wave conditions with a short-time interval (3 or 6 hours). It is hence recommended to improve the temporal resolution of climate scenarios based on the historical data and seasonal cycling. In addition, there are so many different climate models, because there is still no widely-accepted technique or scheme in climate and wave modelling. The accuracy of climate models may be highly dependent on the target location or variable. A universal climate model will definitely improve the efficiency of climate simulations. Otherwise, the comparison of climate models, as in section 3.4, will always be required for a specific oil field before applying the methodology presented in this thesis. Many of these climate models focus on the precipitation or other phenomenon in high atmospheric layers. When coupling wave models to climate models however, the quality of surface wind field would significantly affect the accuracy of wave models. If the ability of climate models in simulating surface wind states with 6-hours interval is further improved, it will significantly enhance the reliability of wave models.

Due to the development of wave modelling technology, the sea states over the globe can be simulated for both coastal and offshore sea areas. But their accuracy is believed to require further improvement, especially for those less popular sea areas. The length of FPSOs is normally around 200 meters. It requires that the wave models should simulate sea states with a finer spatial resolution. The multi-grid mesh (fine grids in the target sea areas and coarse girds in the boundary areas) could definitely improve the efficiency of calculations. But the finer mesh needs a higher spatial resolution for wind field data, which requires the improvement of climate scenarios and climate models.

References

[1] van Lieshout PS, den Besten JH, Kaminski ML. Comparative study of multiaxial fatigue methods applied to welded joints in marine structures. Fracture and Structural Integrity; No 37: 103221/IGF-ESIS3724. 2016.

[2] DNV GL AS. Fatigue Assessment of Ship Structures. 2014.

[3] Solomon S, Qin D, Manning M, Chen Z, Marquis M, Averyt KB, et al. Climate Change 2007: The Physical Science Basis. Contribution of Working Group I to the Fourth Assessment Report of the Intergovernmental Panel on Climate Change. IPCC; 2007.

[4] Notz D. How well must climate models agree with observations? Philos Trans A Math Phys Eng Sci. 2015; 373.

Acknowledgements

I would like to express my deepest gratitude to my promoter and supervisor Prof. Mirek Kaminski. Thanks to you, my PhD study became a fruitful, memorable and joyful journey. As a promotor, you offered me the opportunity to pursue my PhD in Delft; as a supervisor, you gave me practical advices on both research and social life. You are very patient in discussions, and always pinpoint the critical issues. You never pushed and gave me the full freedom to proceed the research on my own pace. You showed respect to my ideas and encouraged me to find out my way of doing research. You provided many opportunities to help me to grow in the academic society. Without you, I could not establish connections with those world-leading experts in offshore engineering. Your profound knowledge, strict attitude towards science and attractive personality are all the virtues I will pursue. In the private life, I deeply admire your love to your princess. Your passion in life significantly affects my attitude to my life. Very often, I feel you as a friend, a master and a father, with whom I can share my feelings and discuss about everything. The world is just like a Wonderland, and the discussions with you showed me how deep the rabbit-hole goes. Thanks to you, I have learned how to be a good researcher and a good engineer.

I'm very grateful to my daily supervisor during my Master's degree study — Prof. Defu Liu in Ocean University of China. Without your encouragement, I would never have had the confidence to continue my study as a PhD candidate abroad. Your greatly inspires me with his enthusiasm for offshore engineering.

I also thank all of the committee members for their valuable time in reviewing and attending my defense. Special thanks go to my Master promoter — Prof. Huajun Li. He is also one of the committee members. My heart was deeply moved when he agreed to attend my doctoral defense.

I would like to thank the Royal Netherlands Meteorological Institute (KNMI), BlueWater, MARIN and DNV GL for providing technical support used in this thesis. Andreas Sterl, Stefan Nienaber, Remco Hageman and Elzbieta Bitner-Gregersen all kindly helped me to step further on my academic work.

I appreciate the friendly and creative atmosphere created by my colleagues in Maritime and Transport Technology department. Menno van der Horst and BongJun Choi, you are my best office colleagues. I will never forget the valuable moment when we were discussing and exchanging our ideas. I'm grateful to my SHS and SOS colleagues who shared the same floor

with me. Henk den Besten, Paula van Lieshout, Reza Karimi, Xiaobo Zhang, Yanxin Qin, Long Wu, Pengpeng Xu, Reinier Bos, Gabriele Bufalari and Mark Tammer, thanks for all your help. It is my pleasure to work with all of you. Every lunch with you is memorable to me. Special thanks go to Pooria Pahlavan. I really appreciate his effort in improving the quality of my thesis.

I also want to thank my housemates and friends who are important to my private life in Netherlands. They are: Likun Ma, Yu Sun, Zilong Wei, Wuyuan Zhang, Lijian Qi and Xing Chang. They made my life so enjoyable and colourful. Without them, loneliness would fill my heart. Special thanks go to Xiuhan Chen. We shared our happiness and sadness; we encouraged each other to successfully complete our study. It means a lot to me.

Finally, I want to express my warmest gratitude to my mother, Li Ai. Her wisdom, encouragement and unconditional love really warmed my heart and touched my soul.

Tao Zou

July 2018, Delft

Curriculum Vitae

Tao Zou (邹涛) was born on March 11, 1987, in Fushun, Liaoning, China. From 2005 to 2009, he studied at Ocean University of China (OUC), Qingdao, China, specializing in Ships and Ocean Engineering for his Bachelor degree. From 2009 to 2012, he continued his study in the coastal and offshore engineering institute of OUC, and obtained his Master degree in Harbor, Coastal and offshore Engineering. Since 2012, he was supported by China Scholarship Council and started his PhD research at Delft University of Technology, Delft, the Netherlands.

From 2012 to 2018, Tao Zou worked as a PhD candidate of Ship and Offshore Structures at the Maritime and Transportation Technology department . His PhD topic is "the effect of climate change on fatigue assessment of offshore floating structures". This research developed and validated a methodology for projecting the effect of climate change on future wave climate and consequently on fatigue life of offshore structures. In this study, climate scenarios and climate models are utilized to simulate atmosphere of circulation. Wind-driven wave models (such as WaveWatch-III) are used to project the future sea states. Then, the fatigue damage of floating offshore structures is projected under these sea states.

List of Publications

- **T. Zou**, M.L. Kaminski, Applicability of WaveWatch-III wave model for investigation of climate change effects on fatigue lifetime of offshore floating structures', J Ocean Dynamics, 2016, DOI: 10.1007/s10236-016-0977-4.
- **T. Zou**, M.L. Kaminski, Detection and projection of climate change impact on fatigue damage of floating structures exemplified for an FPSO operating offshore South Africa, under review.

- **T. Zou**, M.L. Kaminski, X.L. Jiang, Application of wave models to fatigue assessment of offshore floating structures. Proceedings of the 5th International Conference on Marine Structures , MARSTRUCT 2015, Southampton, UK, 2015.
- **T. Zou**, X.L. Jiang, M.L. Kaminski, Possible Solutions for Climate Change Impact on Fatigue Assessment of Floating Structures. Proceedings of the 24th (2014) International Offshore and Polar Engineering Conference, ISOPE 2014, Busan, Korea, 2014.
- **T. Zou**, X.L. Jiang, M.L. Kaminski, Effects of Climate Change on Fatigue Life of Floating Offshore Structures. Proceedings of the 23rd (2013) International Offshore and Polar Engineering Conference, ISOPE 2013, Anchorage, Alaska, USA, 2013.